CHALMERS

Influence of bolted items on the results and consistency of Modal Analysis

Master's Thesis in the Master's programme in Sound and Vibration

MIGUEL COLOMO GONZÁLEZ

Department of Civil and Environmental Engineering
Division of Applied Acoustics
Vibroacoustics Group
CHALMERS UNIVERSITY OF TECHNOLOGY
Göteborg, Sweden 2007

Master's Thesis 2007:148

MASTER'S THESIS 2007:148

Influence of bolted items on the results and consistency of modal analysis

MIGUEL COLOMO GONZÁLEZ

Department of Civil and Environmental Engineering
Division of Applied Acoustics
Vibroacoustics Group
CHALMERS UNIVERSITY OF TECHNOLOGY
Göteborg, Sweden 2007

Influence of bolted items on the results and consistency of modal analysis

Master's Thesis 2007:148

Department of Civil and Environmental Engineering
Division of Applied Acoustics
Vibroacoustics Group
Chalmers University of Technology
SE-41296 Göteborg
Sweden

Tel. +46-(0)31 772 1000

Reproservice / Department of Civil and Environmental Engineering
Göteborg, Sweden 2007

INFLUENCE OF BOLTED ITEMS ON THE RESULTS AND CONSISTENCY OF MODAL ANALYSIS
Master's Thesis in the Master's programme in Sound and Vibration
MIGUEL COLOMO GONZÁLEZ
Department of Civil and Environmental Engineering
Division of Applied Acoustics
Vibroacoustics Group
Chalmers University of Technology

Abstract

Modal analysis testing is commonly performed on Body in Greys (BIGs), which are automobile structures in the designing/manufacturing stage where the body is formed by assembled metal sheets, and the main components as chassis, powertrain, doors, seats, etc. are not still mounted. Some bolted items are included in the BIG to better take into account their influence on body stiffness. However, their contribution to the stiffness is not important in the frequency range accessible for modal analysis (usually up to 70 Hz on a BIG). Moreover, they increase the dispersion in modal parameters obtained for nominally identical test objects. The questions that arises are whether the items should be included in the BIG definition when performing modal analysis or not, and, in this case, how the items in detail influence the results? Multi-input-multi-output (MIMO) measurements of inertances were carried out on three Volvo S80 BIGs. Several configurations were measured for each BIG, starting from the complete body, the bolted items were progressively removed. A modal analysis Matlab programme, MACOL, was developed following the poly-reference Least-Squares Frequency Domain (p-LSCF) method, well-known as PolyMAX. Modal analysis results have proved bolted items influence. The biggest bolted item, the grill-overhanging-reinforcement (GOR) has standed out as the major source of the results inconsistency. It introduces modes highly affected by coupling. High coupling yields unreliability of the estimated modal parameters. The GOR removal has been suggested to improve the accuracy of modal analysis results. Comparison of MACOL results with PolyMAX ones has validated the developed programme.

Keywords: Modal analysis, Body-in-grey, Body-in-white, PolyMAX, p-LSCF, Least-squares, MIMO, FRF, Mode shape, MAC

Contents

Acknowledgements

First of all, I would like to express my deepest gratitude to my supervisor Andrzej Pietrzyk from Volvo Car Corporation (VCC), for his unconditional support and his efforts to be there whenever it was needed.

I am very grateful to my supervisor at Chalmers University, Wolfgang Kropp, for his contribution to important aspects as thesis organization and programme development.

Many thanks to all members of Chalmers Applied Acoustics division for creating the best working (and non-working) enviroment I have ever experienced. Special thanks to Patrik Andersson for the interest shown in my work, it has encouraged me to keep on track with programming. My special thanks also goes to Börje Wijk, I cannot find enough words to express how helpful and kind he has been.

Muchas gracias, thanks a lot, to all my friends. To those who have been essential in my life, always making me feel appreciated and necessary. To those who have made Sweden my home for this year and a half. To the one beyond friendship, for understanding my departure and heartening me overseas.

Lastly, the most important acknowledgement, to my parents. They have led me to become everything I am. They have sacrificed many things for their sons and daughter. They have given me all, support, love and life. Gracias.

Acronyms

BIG	Body In Grey
BIG*n*	Body In Grey number *n*
BIW	Body In White
EMA	Experimental Modal Analysis
FBM	Flexible Body Mode
FEM	Finite Element Method
FRF	Frequency Response Function
GOR	Grill Overhanging Reinforcement
MAC	Modal Assurance Criterion
MACOL	Modal Analysis Colomo
MIF	Mode Indicator Function
MIMO	Multi Input Multi Output
MISO	Multi Input Single Output
MMIF	Multivariate Mode Indicator Function
MPC	Modal Phase Collinearity
MPE	Modal Parameters Extraction
p-LSCF	Poly reference Least-Squares Frequency Domain
RB	Radiator Beam
RBM	Rigid Body Mode
SDOF	Single Degree Of Freedom
SIMO	Single Input Multi Output

SISO	Single Input Single Output
TB	Tunnel Brace
VCC	Volvo Car Corporation
VTF	Vibrational Transfer Function

Symbols and Notation

Matrix symbols

[ ]: Matrix

{ }: Column vector

< >: Row vector

$_{a\times b}$: Dimensions (a rows, b columns)

$^{-1}$: Inverse

^{T}: Transpose

tr(A): Trace

$\otimes$: Kronecker product

Complex operators

Abs(x): x absolute value

Re(x): x real value

Im(x): x imaginary value

$\|x\|$: x norm

x^*: x conjugate

x^H: x hermitian

General notation

$[0]$: Zeroes matrix

$[A]$: Numerator matrix

$[A_c]$: Companion matrix

$[B]$: Denominator matrix

A_r: Modal constant of r^{th} mode

C: Correlation

$\mathbb{C}$: Complex number

E: Normalized error

f: Frequency

f_p: Frequency of p^{th} pole

$\{F(f)\}$: Force frequency spectrum

$[G_{AA}(f)]$: Autopower spectrum of A signal

$[G_{AB}(f)]$: Crosspower spectrum between A and B signals

H_1: FRF estimation for uncorrelated input forces and noise

$\widehat{H}$: Measured FRFs

H_{sum}: FRFs sum

$H^{synt}(f)$: Synthesized FRFs

$[I]$: Identity matrix

j: Complex number unit

L_p: p^{th} modal participation factor

LR_{oi}: Lower residual for o^{th} output and i^{th} input

$[M]$: Reduced normal equations matrix

n: Number of resonance modes

N_a: Number of averages

N_i: Number of inputs

N_o: Number of outputs

p: Numerator/denominator matrix polynomial order

$\mathbb{R}$: Real number

UR_{oi}: Upper residual for o^{th} output and i^{th} input

w: Weighting function

$X(f)$: Displacement frequency spectrum

$\ddot{X}$: Displacement second derivative (acceleration) frequency spectrum

z: z-value

$[\alpha_r](f)$: Denominator polynomial coefficient for r^{th} power

$< \beta_{or} > (f)$: Numerator polynomial coefficient for r^{th} power and o^{th} output

ϵ_o: Error between measured and modelled FRF for o^{th} output

$[m\gamma_o^2](f)$: Multi-coherence of o^{th} output

η_p: Damping ratio of p^{th} pole

λ_r: r^{th} system pole (in Laplace-domain)

Δt: Samping time

θ: Matrix containing all polynomial coefficients

ψ_{or}: Mode shape for o^{th} output and r^{th} mode

σ: Standard deviation

$[\Psi]$: Mode shapes matrix

Chapter 1

Introduction

Modal analysis is a powerful tool to characterize the dynamic properties of a vibrating structure. Data quality and limitations of the used method have been generally established as the main factors determining modal analysis accuracy. However, in some cases the inherent differences between supposedly identical structures could be an important factor as well. In such cases modal models have to be built up from testing a set of nominal objects in order to diminish models inaccuracy. In addition, it is of convenience to determine the dispersion of the modal parameters due to the differences between structures.

A Body In White (BIW) is the automobile designing/manufacturing stage where the body is formed by assembled metal sheets, and the main components as chassis, powertrain, doors... are not still mounted. A Body In Grey (BIG) is plainly a BIW containing front and rear window. BIGs will be the test objects along the thesis.

The designers aim of performing modal analysis on a BIG is avoiding resonances in the frequency range excited by the engine when idling, which is 15-30 Hz. By combining Modal Analysis and Finite Element Method (FEM) techniques one can redesign the car in order to shift in frequency a disturbing mode or modify its damping. This is an advantageous solution as it spares money in prototypes.

1.1 Thesis background

During GPDS project at Volvo Car Corporation (VCC) three Volvo S80 BIGs were measured without fixing the Grill Overhanging Reinforcement (GOR) by mistake. When system response was studied, a significant peak around 20 Hz was discovered. This resonance had not appeared in previous tests (done with fixed GOR). Moreover some resonance frequencies were shifted, their damping factors were changed or/and some modes were split. Interest about the influence of bolted items on modal analysis results was aroused. Besides GOR, two other bolted items had potential to be decisive in the results, the radiator beam (RB) and the tunnel brace (TB). The three bolted items can be observed in figure 1.1:

Figure 1.1: Bolted items: *Grill Over-hanging Reinforcement* (polygon), *Radiator Beam* (dash-line) and *Tunnel Brace* (elipse)

The three items are included in modal testing to better take into account their influence on body stiffness. However, their contribution to the stiffness might not be important in the frequency range accessible for modal analysis (usually up to 70 Hz on a BIG).

Every structure has its own resonance modes (self-modes). Joining a sub-structure to an original one (base structure) yields the appearance of new modes in the base object and the modification of its self-modes. Coupling between each structure self-modes is the cause for modification of the original ones. Same phenomenon is observed when bolted items are attached to the BIG. Furthermore, these bolted items increase the dispersion between results obtained for nominally identical BIGs.

1.2 Objectives

Section 1.1 introduces the consequences of using bolted items when modal analysis is performed. The objectives of the master's thesis were set according the analysis of their influence:

- Investigate the dispersion produced by the bolted items.
- Recommend the best option for further measurements: Including or excluding the bolted items from the BIG concept.
- Determine how high in frequency body modes can be consistently identified.

As a beginner in modal analysis one has secondary goals. On the one hand, getting acquainted on modal analysis testing, on the other hand gaining a deep insight into the newest modal analysis algorithm, the p-LSCF method. With this last aim on mind, a Matlab programme is developed following p-LSCF algorithm, it is called MACOL (Modal Analysis Colomo). One more goal is set, MACOL's validation by cross-checking its results with a "professional"software, the well-known LMS PolyMAX.

1.3 Overview

The thesis has been structured following the chronological order of the work done:

- Chapter 2 gives the overall theoretical foundation of modal analysis. Its phases are presented. Special attention is paid to the system identification stage as it is key to better understand theory behind Modal Parameters Extraction (MPE).
- The third chapter covers all aspects referring modal analysis programme development. Firstly, p-LSCF method steps are described. Secondly, MACOL use is explained. Lastly, tests are run in order to validate MACOL by PolyMAX software.
- Chapter 4 deals with all facets related to measurements. Measurements planning reveals the tests performed to decide the final measurements set-up. Additionally, measurements procedure can be found.

- The fifth chapter shows the results obtained during the thesis. They are divided in five sections: the frequency limit of modal analysis on BIGs, results from studying MACOL ins and outs, the brackets effect on modal analysis, the dispersion introduced by the bolted items, and their influence on body modes.

- Chapter 6 discusses results. Conclusions are summarized.

- The seventh chapter proposes future work.

Chapter 2

Modal Analysis Theory

Modal Analysis is an experimetal technique to characterize the dynamic properties of a vibrating system. The properties, known as modal parameters, are estimated from measured Frequency Response Functions (FRFs). The most important modal parameters are presented below:

- **Resonance frequency:** Frequencies at which the system tends to vibrate at maximum amplitude.

- **Mode shapes:** Form adopted by the system when it is excited at the resonance frequency.

- **Damping ratio:** Actual damping over the amount of damping required to reach critical damping. The critical damping can be interpreted as the minimum damping that results in non-periodic motion, i.e. simple decay.

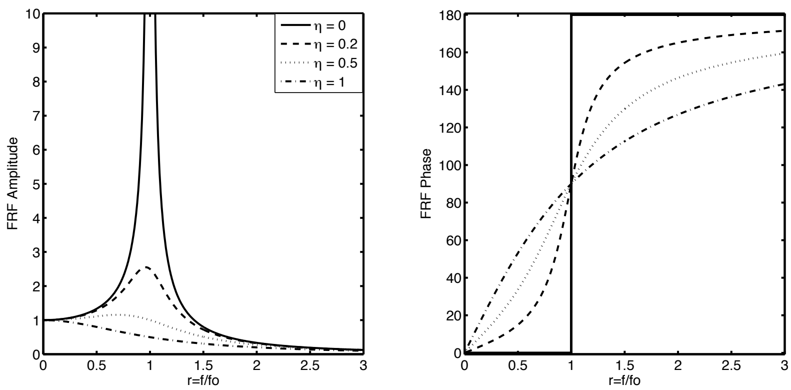

Figure 2.1: *FRF* for a SDOF: Amplitude and Phase

Figure 2.1 shows the damping effect on the amplitude and the phase of a resonance mode (f_0). The figure corresponds to the FRF of a vibrating SDOF (Single Degree Of Freedom) structure. The extreme cases are damping ratio equal to zero and equal to one (critical damping). Damping ratio equal to zero yields an infinite amplitude at the resonance frequency whereas damping greater than or equal to critical damping yields permanent decay.

2.1 Experimental Modal Analysis phases

Modal Analysis is known as Experimental Modal Analysis (EMA) in more precise terms when input forces can be measured. EMA comprises multiple fields of engineering as reflected in the characteristics of its phases:

1. **Set-up:** Preliminary studies are done to decide the excitation source, the test object suspension, the output points location...etc. A wrong set-up could derive in missing some modes, nonlinearities appearance...

2. **Data acquisition:** Optimal signal processing is essential to assure the suitability and quality of the data. Measurements data allows estimating FRFs and coherence functions.

3. **System identification:** Procedure whereby measured FRFs are analyzed to find the theoretical model which mostly resembles the behavior of the actual test object [1]. The modal model leads to modal parameter estimation.

4. **Validation:** Results reliability is evaluated. Parameters, as Modal Assurance Criterion (MAC) or Mode Phase Collinearity (MPC), quantify the rightness of the selected modes.

5. **Application:** Modal analysis can be used for prediction purposes. The aim is improving the structural dynamic behavior. Nowadays the main tool to apply EMA results are Finite Element Method (FEM) techniques.

System identification phase is actually the one covered by the developed modal analysis programme MACOL. Hence, this phase is of high interest to the thesis. Section 2.2 provides more information about system identification in order to introduce the basics of modal analysis methods. Further explanations about the other phases are given in [2].

2.2 System identification phase

The Vibrational Transfer Functions (VTFs) are FRFs which describe the system response to vibrations. The use of Fourier transform creates a VTF easy to handle. The well-known VTFs are: inertance (output acceleration over input force), mobility (output velocity over input force) and receptance (output displacement over input force). The results of the thesis are based on inertance VTFs. From now onwards, FRFs are used to referred to inertance VTFs.

A FRF is a function over frequency which has different dimensions depending on the number of inputs and outputs. A test can be classified according to its inputs and outputs: SISO, SIMO, MISO, and MIMO (where: I = input, O = output, S = single, M = multi). The extreme cases are SISO where the FRF is unidimensional and MIMO where the FRF at a certain frequency is a matrix $[H(f)]$ which has as many rows as outputs (N_o) and as many columns as inputs (N_i):

$$
\begin{aligned}
\left\{ \begin{array}{c} \ddot{X}_1(f) \\ \vdots \\ \ddot{X}_{N_o}(f) \end{array} \right\} &= \left[\begin{array}{ccc} H_{1,1}(f) & \dots & H_{1,N_i}(f) \\ \vdots & \ddots & \vdots \\ H_{N_o,1}(f) & \dots & H_{N_o,N_i}(f) \end{array} \right] \left\{ \begin{array}{c} F_1(f) \\ \vdots \\ F_{N_i}(f) \end{array} \right\} \\
\{\ddot{X}(f)\} &= [H(f)]\{F(f)\}
\end{aligned} \tag{2.1}
$$

The equation 2.1 shows the transfer matrix of a MIMO system at a certain frequency. $F(f)$ and $\ddot{X}(f)$ vectors are the frequency spectrum of the force and the acceleration, respectively. There are different approaches to estimate the FRF matrix. The approach followed along the thesis assumes no noise on the input forces and uncorrelated noise on the outputs. The notation commonly used for this FRF estimation is H_1.

$$
[H(f)]_{N_o \times N_i} = [G_{XF}(f)]_{N_o \times N_i} [G_{FF}(f)]^{-1}_{N_i \times N_i} \tag{2.2}
$$

In equation 2.2 the transfer matrix is calculated by the "H_1 estimation". Crosspower spectrum between force and acceleration signals ($[G_{XF}(f)]$) and autopower spectrum of force signal ($[G_{FF}(f)]$) are involved in the estimation.

When performing measurements is it of interest to have an indicator of data quality. The coherence function indicates the degree of consistent linear relationship between output and input signals during the averaging process for each frequency [3]. The coherence varies between 0 and 1, in other words no consistent linear relation and perfect consistent linear relation, respectively. When there is more than one input, the coherence of an output signal is related to all the outputs and it is called multiple coherence ($[m\gamma_o^2](f)$) [4]:

$$[m\gamma_o^2](f) = \sum_{s=1}^{Ni}\sum_{t=1}^{Ni} \frac{H_{os}(f)G_{F_sF_t}(f)H_{ot}^*(f)}{G_{oo}(f)} \tag{2.3}$$

Where $G_{F_sF_t}$ is the crosspower spectrum between forces s^{th} and t^{th} and G_{oo} is the autopower spectrum of the o^{th} output.

Once the transfer matrix has been estimated, it is studied to better select the appropriate model, which is finally curve-fitted to the measured FRFs. There are several models but they share the same principle, a vibrating system response can be determined by the summation of the contribution of each mode. The principle comes along with the main limitation of modal analysis, modal models cannot accurately reflect the effect of modes out of the frequency range where modal analysis is performed. Each mode is dominating around its own resonance frequency, therefore inaccuracy is mainly noticeable between resonances.

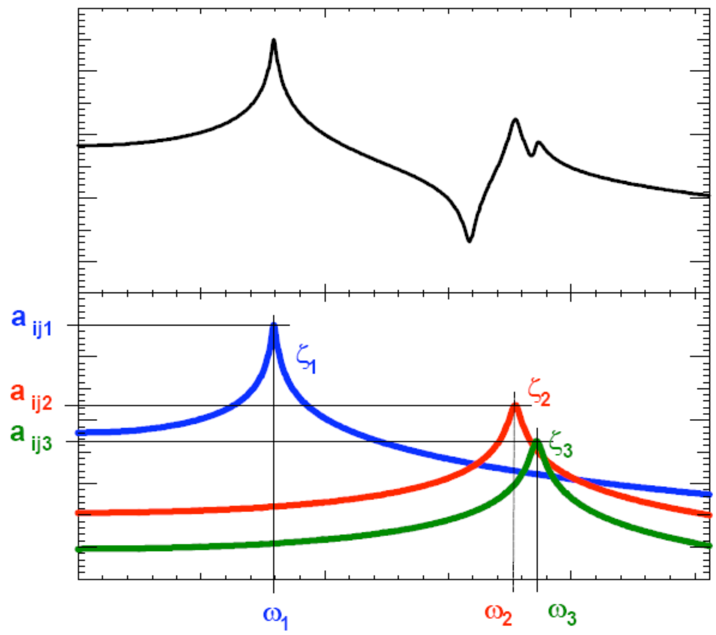

Figure 2.2: FRF breakdown into single modes contribution

Figure 2.2 illustrates the base of modal models [5]. The top curve shows the FRF of a system which has three resonance modes in the considered frequency range. The lower curves show the contribution of each mode to the system response. The modes dominance in the frequency range nearby their resonance frequencies is significant. In addition, the antiresonances

(FRFs minima) can be observed. They appear at the modes contribution intersection.

The general form of the FRFs model is a consequence of the principle. As one can observe in equation (2.4), modeled transfer function (for o^{th} output,i^{th} input) is formed by adding each mode contribution:

$$H_{oi}(f) = \frac{\ddot{X}_o}{F_i} = \sum_{r=1}^{n} \frac{A_{r,oi}}{\lambda_r^2 - (2\pi f)^2} \tag{2.4}$$

Where λ_r is the Laplace pole corresponding to the r^{th} mode and $A_{r,oi}$ is its modal constant for o^{th} output and i^{th} input, whereas n represents the number of modes. Modal models can be more complex as shown in equation 3.16.

Chapter 3

Modal Analysis Programme

The poly-reference Least Squares Complex Frequency-Domain Method (p-LSCF) is the latest algorithm proposed for performing modal analysis. It has successfully settled among the industry world as the most effective modal analysis technique thanks to the programme LMS Test.Lab, developed by LMS International. LMS Test.Lab contains a p-LSCF module called PolyMAX.

Research work done at thesis beginning revealed p-LSCF as most powerful modal analysis method. Hence, it was decided to develop and implement a code based on this theory in Matlab. The resulting modal analysis programme is called MACOL (Modal Analysis COLomo) with reference to the author's family name.

To understand the advantages of p-LSCF method is key to be aware of the difficulties involved in Modal Analysis, according to [6]:

- High order systems are problematic due to their high modal overlapping.
- The damping of fully trimmed structures is not properly estimated.
- Difficulty to avoid mathematical poles.
- Uncertainty about the optimal poles selection.
- Inconsistencies of the measured data.
- Inconsistency of the modal participation factors obtained from different analysis.

The main strength of p-LSCF method is being able to handle with the "rough"cases, i.e. high order or trimmed systems. Its very stable poles identification is the reason why it can overcome these cases. In addition, modal parameters are precisely extracted via short operational time.

3.1 The p-LSFD method

The p-LSFD method is explained following the description provided by [7]. Nevertheless research from other sources was needed as well.

3.1.1 Right matrix-fraction model

The right matrix-fraction model expresses the FRFs matrix as the division of two matrices. In order to simplify method presentation, the o^{th} row of FRFs matrix is taken. It represents the o^{th} output over all inputs:

$$\begin{aligned} [H(f)]_{N_o \times N_i} &= [B(f)]_{N_o \times N_i} [A(f)]^{-1}_{N_i \times N_i} \\ < H_o(f) >_{1 \times N_i} &= < B_o(f) >_{1 \times N_i} [A(f)]^{-1}_{N_i \times N_i} \end{aligned} \tag{3.1}$$

Both, $A(f)$ and $B(f)$, are matrices built by polynomials. The polynomials variable is z (from z-domain):

$$z(f) = e^{-j2\pi f \Delta t} \tag{3.2}$$

In equation 3.2 Δt is the sampling time. Polynomials are presented as follows:

$$\begin{aligned} < B_o(f) > &= \sum_{r=0}^{p} < \beta_{or} > z^r(f) \in \mathbb{C}^{1 \times N_i} \\ [A(f)] &= \sum_{r=0}^{p} [\alpha_r] z^r(f) \in \mathbb{C}^{N_i \times N_i} \end{aligned} \tag{3.3}$$

The denominator matrix ($A(f)$) roots are actually the structure poles. The polynomial order p is a key parameter in curve fitting. Its importance is highlighted in sections 3.1.3 and 5.2. The polynomial coefficients shown in equation 3.3 are not the standard ones but a vector (in the case of the numerator) and a matrix (in the case of the denominator). Polynomial coefficients can be assembled in matrices (equation 3.4):

$$\begin{aligned} \beta_o &= \begin{bmatrix} \beta_{o0} \\ \beta_{o1} \\ \vdots \\ \beta_{op} \end{bmatrix} \in \mathbb{R}^{(p+1) \times N_i} \qquad \alpha = \begin{bmatrix} \alpha_0 \\ \alpha_1 \\ \vdots \\ \alpha_p \end{bmatrix} \in \mathbb{R}^{N_i(p+1) \times Ni} \\ \theta &= \begin{bmatrix} \beta_1 \\ \vdots \\ \beta_{N_o} \\ \alpha \end{bmatrix} \in \mathbb{R}^{(N_o+N_i)(p+1) \times N_i} \end{aligned} \tag{3.4}$$

Where matrix θ includes all the polynomial coefficients which must be calculated to curve-fit the measured FRFs matrix.

3.1.2 System poles calculation

The curve-fitting is performed by least-squares means. The error between the measured FRFs ($\widehat{H}$) and the right matrix-fraction modeled FRFs (H) is taken in a way which linearizes the problem:

$$\epsilon_o(f,\theta) = w_o(f)\left(B_o(f,\beta_o) - \widehat{H}_o(f)A(f,\alpha)\right) \tag{3.5}$$

The error (ϵ_o) in equation 3.5 can be weighted by a function w for each frequency and output. The weighting function for each FRF matrix row can be determined by the FRF variance [8]. Statistical error serves for estimating variance [2]:

$$w_o(f) = \frac{1}{\sqrt{\mathrm{var}(\widehat{H}_o(f))}} = \frac{1}{\sqrt{\frac{1-m\gamma_o^2(f)}{2N_a m\gamma_o^2(f)}}} \tag{3.6}$$

The equation 3.6 illustrates the weighting function dependency on the coherence ($m\gamma_o^2$) and the number of averages over each measurement (N_a). The cost function all over the frequency points and FRFs can be derived from equation 3.7, where tr refers to matrix trace.

$$ł(\theta) = \sum_{o=0}^{N_o}\sum_{k=1}^{N_f} \mathrm{tr}((\epsilon_o(f_k,\theta))^H \epsilon_o(f_k,\theta)) \tag{3.7}$$

The values participating in the cost function are gathered in a special system, the so-called reduced normal equations. Matrices used to build the system are defined in equation 3.8. Symbol $\otimes$ denotes Kronecker product.

$$\begin{aligned}
X_o &= \begin{bmatrix} w_o(f_1)(1\, z(f_1)\ldots z^p(f_1)) \\ \vdots \\ w_o(f_{N_f})(1\, z(f_{N_f})\ldots z^p(f_{N_f})) \end{bmatrix} \in \mathbb{C}^{N_f\times(p+1)} \\
Y_o &= \begin{bmatrix} -w_o(f_1)(1\, z(f_1)\ldots z^p(f_1)) \otimes \widehat{H}_o(f_1) \\ \vdots \\ -w_o(f_{N_f})(1\, z(f_{N_f})\ldots z^p(f_{N_f})) \otimes \widehat{H}_o(f_{N_f}) \end{bmatrix} \in \mathbb{C}^{N_f\times N_i(p+1)} \\
R_o &= Re(X_o^H X_o) \in \mathbb{R}^{(p+1)\times(p+1)} \\
S_o &= Re(X_o^H Y_o) \in \mathbb{R}^{(p+1)\times N_i(p+1)} \\
T_o &= Re(Y_o^H Y_o) \in \mathbb{R}^{N_i(p+1)\times N_i(p+1)}
\end{aligned} \tag{3.8}$$

Least-squares solution is found by equaling the cost function derivative to zero. Matrices defined in equation 3.8 simplify the expression:

$$\begin{aligned}
\frac{\partial l(\theta)}{\partial \beta_o} &= 2(R_o\beta_o + S_o\alpha) = 0, \forall o = 1, \ldots, N_o \\
\frac{\partial l(\theta)}{\partial \alpha} &= 2\sum_{o=1}^{N_f}(S_o^T\beta_o + T_o\alpha) = 0 \qquad (3.9)
\end{aligned}$$

First equation from 3.9 allows expressing the numerator coefficients as a function of the denominator coefficients:

$$\beta_o = -R_o^{-1}S_o\alpha \qquad (3.10)$$

The reduced normal equations are gathered by a matrix, M, by applying the equation 3.10 on the second equation from 3.9:

$$\left(2\sum_{o=1}^{N_f}\left(T_o - S_o^T R_o^{-1} S_o\right)\right)\alpha = 0 \Leftrightarrow M\alpha = 0 \qquad (3.11)$$

Where $M \in \mathbb{R}^{N_i(p+1)\times N_i(p+1)}$ is the reduced normal equations matrix. Last α coefficient is imposed to avoid the trivial solution and parameters redundancy in the right matrix-fraction model: $\alpha_p = I_{N_i\times N_i}$. The rest of the α coefficients are derived from equation 3.12:

$$\begin{bmatrix} \alpha_0 \\ \alpha_1 \\ \vdots \\ \alpha_{p-1} \end{bmatrix} = -M(1:N_ip, 1:N_ip)^{-1}M(1:N_ip, N_ip+1:N_i(p+1)) \qquad (3.12)$$

Once the denominator coefficients are obtained, system poles can be found. The suggested method to calculate them is solving the eigenvalue problem of the denominator polynomial companion matrix (A_c) [9]:

$$A_c = \begin{bmatrix} 0_{N_ixN_i} & I_{N_ixN_I} & 0_{N_ixN_i} & \cdots & 0_{N_ixN_i} & 0_{N_ixN_i} \\ 0_{N_ixN_i} & 0_{N_ixN_i} & I_{N_ixN_I} & \cdots & 0_{N_ixN_i} & 0_{N_ixN_i} \\ \vdots & \vdots & \vdots & \ddots & \vdots & \vdots \\ 0_{N_ixN_i} & 0_{N_ixN_i} & 0_{N_ixN_I} & \cdots & 0_{N_ixN_i} & I_{N_ixN_i} \\ -[\alpha_0^T] & -[\alpha_1^T] & -[\alpha_2^T] & \cdots & [-\alpha_{p-2}^T] & [-\alpha_{p-1}^T] \end{bmatrix} \qquad (3.13)$$

The eigenvalue problem solution also provides the modal participation factors L. Each modal participation factor is a vector which corresponds to a system pole. Taking for instance the r^{th} pole, the modal participation factor is the r^{th} column and the last N_i rows of the eigenvectors matrix.

Modal participation factors relate to system inputs and they are proportional to mode shapes. In section 3.1.4 more information is given about modal participation factors. In addition, equation 3.16 presents the role of modal participation factors in a modal model.

The poles are obtained in z-domain (z_p). Then, they are converted to Laplace domain (λ_p) in order to calculate the resonance frequencies (f_p) and the damping ratios (η_p):

$$z = e^{-\lambda \Delta t} \Rightarrow \lambda_p = \frac{-\ln z_p}{\Delta t} \tag{3.14}$$

Resonance frequency and the damping ratio formulas (3.2.1) are straight forward when deriving them from poles in Laplace domain [11]:

$$f_p = \frac{\mathrm{Abs}(\mathrm{Im}(\lambda_p))}{2\pi} \qquad \eta_p = -\frac{\mathrm{Re}(\lambda_p)}{\mathrm{Abs}(\lambda_p)} \tag{3.15}$$

3.1.3 Physical poles selection. Stabilization diagrams

Years of research in Modal Analysis have not found yet a modal analysis algorithm capable to calculate only physical poles. Non-physical poles appear in calculations as a result of the over-estimation of the polynomial order necessary to find all the physical poles. They are called spurious or mathematical poles as well.

The tool used to discriminate physical poles from the spurious ones is the stabilization diagram. It is obtained by repeating the poles calculation for decreasing model order. The Laplace poles which are not stable, according to Laplace stability criterion (Re$(\lambda_p) < 0$), are not shown in the stabilization diagram. Each set of poles calculated for a certain model order is compared with the set of poles calculated for the lower modal order. If r^{th} pole at p^{th} modal order is not found for the order below (p-1) is labeled as new or unstable pole in the stabilization diagram. A pole is considered not found when there is no pole in a 1% frequency margin for the lower order. In MACOL the symbol used is a red circle (o). When the pole is found there are different stability cases:

Table 3.1: Stability borders of damping ratios (η) and modal partipation factors ($< L >$) for Stabilization Diagrams

$\frac{\eta_{r,p}-\eta_{r,p-1}}{\eta_{r,p-1}} < 5\%$	$\frac{\left\| <L_{r,p}> - <L_{r,p-1}> \right\|}{\left\| <L_{r,p-1}> \right\|} < 2\%$	**Symbol**
no	no	blue square
yes	no	blue diamond
no	yes	blue triangle
yes	yes	black cross
$\Delta\eta_r$	$\Delta \left\| < L_r > \right\|$	

The default background of MACOL stabilization diagram is the summation of FRFs (equation 3.21). The summation is scaled in order to have similar dimensions to the stabilization diagram ones. The last case in table 3.1 will be from now onwards referred as a stable pole. After plotting the stabilization diagram the next step is selecting the physical poles. Further comments about poles selection are given in section 3.2.1. In addition a stabilization diagram example is shown in figure 3.4.

3.1.4 Modal Parameters Extraction. LSFD method

The poles and the modal participation factors are the modal parameters already obtained at this point. The rest of the modal parameters can be estimated by identifying the FRFs with a modal model. In equation 2.4 a simple modal model was shown. When the poles and the modal participation factors of a MIMO system are known the following modal model is of convenience:

$$H_{oi}^{synt}(f) = \sum_{r=1}^{n} \left(\frac{\psi_{or} L_{ir}^{T}}{j2\pi f - \lambda_r} + \frac{\psi_{or}^{*} L_{ir}^{H}}{j2\pi f - \lambda_r^{*}} \right) - \frac{LR_{oi}}{(2\pi f)^2} + UR_{oi} \qquad (3.16)$$

The FRF built from the estimated modal parameters is called synthesized FRF (H^{synt}). Equation 3.16 shows the synthesized FRFs dependence on modal parameters. The stable poles appear as conjugate couples. Setting the modes in conjugate couples reduces to the half the quantity of modal parameters to calculate. The modal parameters included in the modal model are:

- **System poles(λ):** The poles of the system in Laplace domain. Damping ratios and frequencies can be obtained from poles by using equation 3.2.1.

- **Modal participation factors (L):** Modal participation factors relate to system inputs and they are proportional to mode shapes. There is a modal participation factor for each mode (r) and input (i).

- **Mode shapes (ψ):** A mode shape is the specific pattern of vibration adopted by the system at a resonance frequency. There is a mode shape for each output (o) at each resonance mode (r).

- **Upper residual (UR):** The upper residual is a term introduced to compensate the modes above the analyzed frequency range. It is a constant term defined for each transfer function (one per input-output combination). In MACOL the UR is implemented as a real value but could be taken as complex value as well.

- **Lower residual (LR):** The lower residual is a term introduced to compensate the modes below the analyzed frequency range. Assuming proportional damping one can estimate the lower residual by a constant term over the squared frequency (in $\frac{rad}{s}$) of the considered point. There is a lower residual term for each transfer function (one per input-output combination). In MACOL the LR is implemented as a real value but could be taken as complex value as well.

The residual terms (UR and LR) formulation is done for receptance FRFs, i.e. for output displacements over input forces.

The equality of the measured FRFs and the modal model yields a linear system of equations where the unknowns are the mode shapes and the residuals. The number of equations is higher than the number of unknowns, therefore least-squares technique is once more needed. This step of modal analysis is commonly called LSFD method.

3.1.5 Modal Validation

The modal validation phase intends to verify the results obtained in the Modal Parameter Extraction (MPE) stage. There have been developed several parameters to perform modal validation. A complete description of them can be found in [2]. In this section the parameters calculated by MACOL are presented.

Normalized Error and Correlation between measured and synthesized FRFs

The synthesized FRFs comparison with the measured FRFs is the first verification to be done in modal analysis. The selection of a spurious pole as a stable one can be easily observed at first sight. The accuracy of the synthesis is quantized by the normalized error (3.17) and the correlation (3.18):

$$E_{H_{oi}} = \frac{\sum\limits_{nf=1}^{N_f} \left| \widehat{H}_{oi}(f_{nf}) - H_{oi}^{synt}(f_{nf}) \right|^2}{\sum\limits_{nf=1}^{N_f} \left| H_{oi}^{synt}(f_{nf}) \right|^2} \tag{3.17}$$

$$C_{H_{oi}} = \frac{\left| \sum\limits_{nf=1}^{N_f} \widehat{H}_{oi}(f_{nf}) H^{*}{}_{oi}^{synt}(f_{nf}) \right|^2}{\left(\sum\limits_{nf=1}^{N_f} \widehat{H}_{oi}(f_{nf}) \widehat{H}_{oi}^{*}(f_{nf})\right)\left(\sum\limits_{nf=1}^{N_f} H_{oi}^{synt}(f_{nf}) H^{*}{}_{oi}^{synt}(f_{nf})\right)} \tag{3.18}$$

A proper modal analysis should not expect less than a 0.85 of correlation and more than a 0.1 of error.

Modal Assurance Criterion (MAC)

The Modal Assurance Criterion (MAC) compares different sets of estimated mode shapes. MAC is plainly the correlation between mode shape vectors. It can be used to check the relation between modes within the same set [2] as well, then it is called auto-MAC. It is based on the theoretical orthogonality between different physical modes. Ideally two equal modes would have a MAC of 1 (or 100%) and two different physical modes would have a MAC of 0.

$$MAC([\Psi_1],[\Psi_2]) = \frac{\left|[\Psi_1^H][\Psi_2]\right|^2}{([\Psi_1^H][\Psi_1])([\Psi_2^H][\Psi_2])} \tag{3.19}$$

Equation 3.19 allows the calculation of the MAC-matrix. The MAC matrix contains the MAC values between all possible pairs between the modes of the two sets. $\Psi_1 \in \mathbb{C}^{N_o \times n_1}$ and $\Psi_2 \in \mathbb{C}^{N_o \times n_2}$ are matrices formed by all the mode shapes from first and second set respectively.

The MAC value between two estimates of the same physical mode should be above 90% and the MAC value of two different modes should be below 10%. Other phenomena are explained below [2]:

- MAC<90% between estimates of the same physical pole: At least one of the estimates is poor. This could be due to a poorly excited mode or a low amplitude mode.

- MAC>35% between estimates of different modes at close frequencies: The modes are similar. It might be that they are the same modes but one part of the system is vibrating in phase. Small frequency shifts during measurements might have happened as well.

- MAC>35% between estimates of different modes at distant frequencies: Measurements set-up error. An insufficient number of outputs or an erroneus setting of them could cause this phenomenon.

Modal Phase Collinearity (MPC)

The Modal Phase Collinearity (MPC) is a measure of the complexity degree of a mode. It quantizes the linear relation between real and imaginary parts of the mode shape coefficients. Its derivation is shown in equation 3.20.

$$\begin{aligned}
\widetilde{\psi}_{or} &= \psi_{or} - \frac{\sum_{s=1}^{N_o} \psi_{sr}}{N_o} \\
\epsilon &= \frac{\left\|Im\{\widetilde{\psi}\}_r\right\|^2 - \left\|Re\{\widetilde{\psi}\}_r\right\|^2}{2\left(Re\{\widetilde{\psi}\}_r^T \cdot Im\{\widetilde{\psi}\}_r\right)} \\
\theta &= \arctan\left(|\epsilon| + sign(\epsilon)\sqrt{1+\epsilon^2}\right) \\
MPC_r &= \frac{\left\|Re\{\widetilde{\psi}\}_r\right\|^2 + \frac{\left(Re\{\widetilde{\psi}\}_r^T \cdot Im\{\widetilde{\psi}\}_r\right)\left(2(\epsilon^2+1)\sin^2\theta - 1\right)}{\epsilon}}{\left(\left\|Im\{\widetilde{\psi}\}_r\right\|^2 + \left\|Re\{\widetilde{\psi}\}_r\right\|^2\right)}
\end{aligned} \tag{3.20}$$

The physical modes have a MPC close to 1. If the mode has a low MPC is either a mathematical or a noisy pole. The MPC is a valid tool when the modes are normal, i.e. when the damping is proportional.

3.2 Matlab p-LSCF version: MACOL

The literature study done at the start of this master thesis revealed p-LSFD method as the most advanced and capable for cases of high modal overlapping. This is the case of the thesis test object, the Volvo S80 BIG. The programming of a Matlab version became a challenge although initially it was not one of the thesis objectives. Due to its secondary role it has not been possible to complete the programme and, what is more important, to test it for other test objects than the 3 BIGs.

Fortunately the modal analysis performed during the thesis has allowed testing MACOL capabilities. In addition, some cross-checking has been performed using PolyMAX from LMS Test.Lab, the software which introduced p-LSCF method in industry.

In section 3.2.1 MACOL use is explained and some details are given about the programme development. Section 3.2.2 presents the tests done to validate MACOL results by PolyMAX ones.

3.2.1 MACOL use

The structure of the programme is found in appendix A and can serve as a reference to follow this chapter. The programme needs a data file to be started. The file contains the following inputs:

- **Frequency vector (fa)**: It is a vector containing all measured frequency points. It is highly recommended to have enough frequency resolution otherwise modal analysis algorithms fail.

- **Transfer matrix (H)**: Matrix containing the inertance FRFs of a system. It is a three-dimensional matrix, where the first dimension relates to the frequency components, the second one to the input signals and the third one to the output signals.

- **Coherence**: Matrix containing the coherence between the ouput signals and the contribution over all system inputs. It is a two-dimensional matrix, where the first dimension relates to the frequency components and the second one to the output, as it is defined in equation 2.3. Section 3.1.2 explains the use of the coherence in FRFs weighting. It is not a necessary input because programme default settings establish no weighting, i.e. all the components of the coherence matrix are one.

MACOL steps are described in following points:

Frequency range selection

Modal analysis is seldom performed over all the measured frequency range. The standard action is dividing it into smaller frequency ranges which are independently analyzed. MACOL must be run for each range. The division leads to improvement on the results accuracy. Two suggestions are given [2]:

- Each partition of the measured frequency range should have less than ten resonance modes.

- Frequency limits are recommended to have low levels. Adittionally, resonance slopes should be avoided in order to diminish out-of-band modes influence.

The influence of frequency range width on poles estimation has been observed. Checks performed discovered that using very narrow frequency ranges implies overlooking stable poles. Figures 3.1 and 3.2 illustrate this phenomenon. Narrowing the frequency range entitles the lost of frequency points, i.e. number of equations is reduced. This could be improved increasing the polynomial order (MACOL intends to find more poles) although increasing frequency range has proved to be more effective.

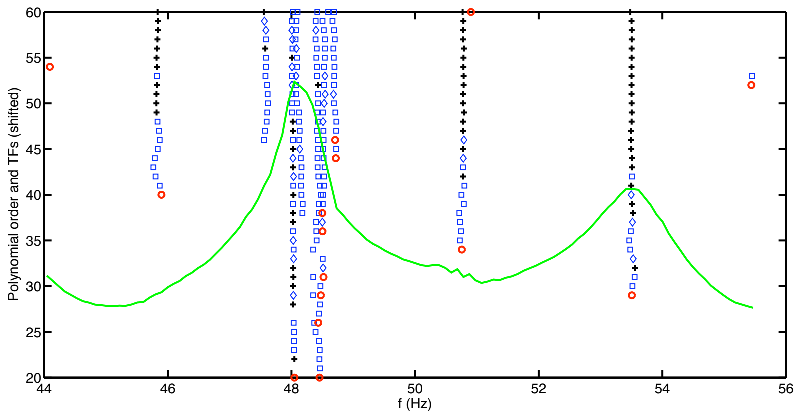

Figure 3.1: *Stabilization diagram* for the standard configuration of BIG1 *wider range*

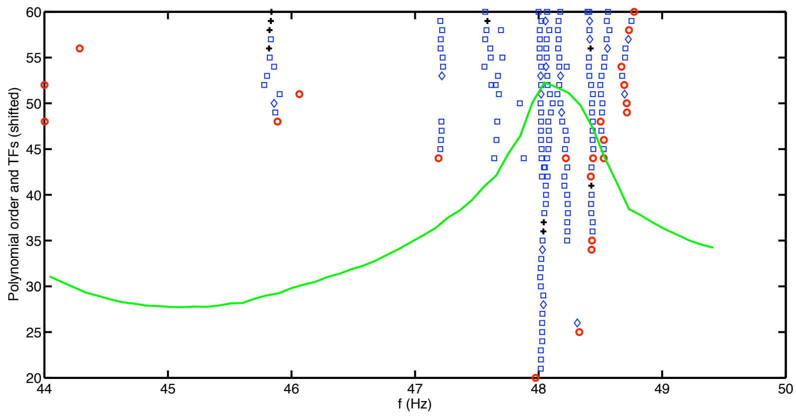

Figure 3.2: *Stabilization diagram* for the standard configuration of BIG1 *narrower range*

In order to select a proper frequency range, measured data can be studied in three different forms:

- **SDOF**: The most of the modes can be clearly found by checking one of the system FRFs although a few modes could be overlooked.
- **FRFs Sum**: According to one's experience it is the best tool when choosing the frequency range although local modes or highly coupled modes could be hard to identify. The summation of FRFs is done separately in real and complex terms (3.21):

$$H_{sum} = \sum_{o=1}^{N_o} \sum_{i=1}^{N_i} |Re(H_{oi})| + j \sum_{o=1}^{N_o} \sum_{i=1}^{N_i} |Im(H_{oi})| \qquad (3.21)$$

- **Multivariate Mode Indicator Function (MMIF)**: It is a derivation of the common Mode Indicator Function (MIF). The difference is that it takes into account all inputs. The MIF expresses the ratio of the kinetic energies of in-phase response to total response. It is a value from 0 to 1. The minimum of this function indicates the presence of modes that can be excited as real normal modes [10]. The MMIF is the minimum of the eigenvalues in equation 3.22.

$$\lambda \left(Re(H)^T Re(H) + Im(H)^T Im(H) \right) v = Im(H)^T Im(H) v \qquad (3.22)$$

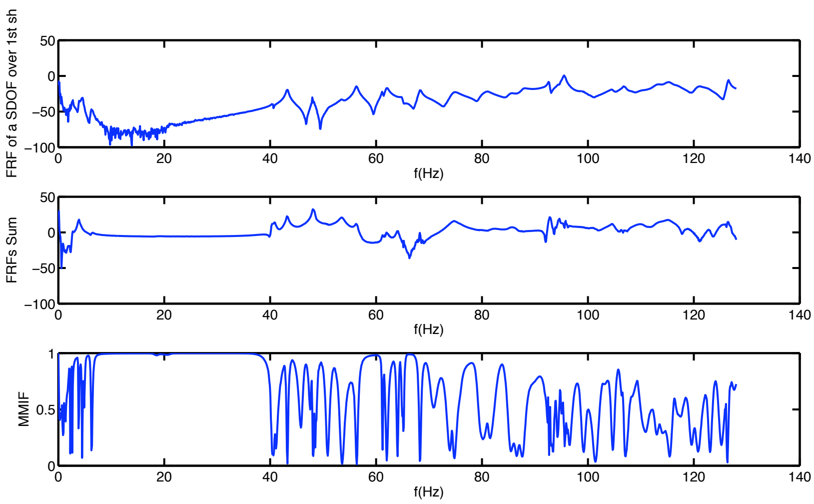

Figure 3.3: *Measured data representations*: Inertance SDOF FRF, Inertance FRFs Sum, MMIF

The use of any of this indicators is acceptable. The three possibilities are shown in figure 3.3.

System poles calculation. Polynomial orders selection

The system poles are calculated in z-domain and then converted into Laplace-domain. Poles are found for different polynomial orders as explained in section 3.1.3. MACOL allows choosing the minimum and maximum polynomial order (p) to create stabilization diagrams.

The poles are found by solving the companion matrix eigenvalue problem (3.13), where the matrix dimension is $N_i \times p$. Therefore the operational time is approximately proportional to p^2, which means that it is advisable avoiding very high polynomial orders.

A reasonable maximum polynomial order is 50 but this is dependent on the frequency range width, the number of FRFs and the measurements quality. Hence, it is worth to do some testing when performing modal analysis on a data set for the first time. The lower polynomial orders do not contend all the poles as many of the ones found are unstable in laplace terms. Therefore, the minimum can be usually set from 10 to 20.

In short, a proper selection of the frequency range and polynomial order limits is based on experience, engineer judgment and trial and error.

System poles identification. Stabilization diagrams

The system poles identification is the key step in modal analysis. Indeed, this is the only stage which needs of human intervention. Programs are able to find system poles for different polynomial orders but only mankind, through experience, is capable of selecting the physical poles among the ones found as stable.

Table 3.1 contains the different poles one can find in a stabilization diagram according to MACOL notation. One physical pole is easy to identify when it appears for the most of the polynomial orders. In this case, a vertical line of black crosses can be seen.

When two poles are close in frequency or the modal overlapping is too high, the vertical line is not seen. Instead, few stable poles appear in between blue marks (either squares, diamonds or triangles). The coupling between close-in-frequency modes hinders the stabilization of modal parameters in calculations. From now onwards, the modes which are not clearly identifiable will be called “unclear modes“.

The selection of a stable pole for an unclear mode can still be done but its reliability is doubtful. A discontinuity of pure stable poles (black crosses) appears for these poles. From one stable pole (black cross) to the next one, poles unstable in damping factor and/or modal participation factor are found.

The discontinuity entitles that the extracted modal parameters are significantly different depending on the polynomial order selected. Section 5.2 compares the results consistency of the unclear modes and the “easy-to-identify“ones.

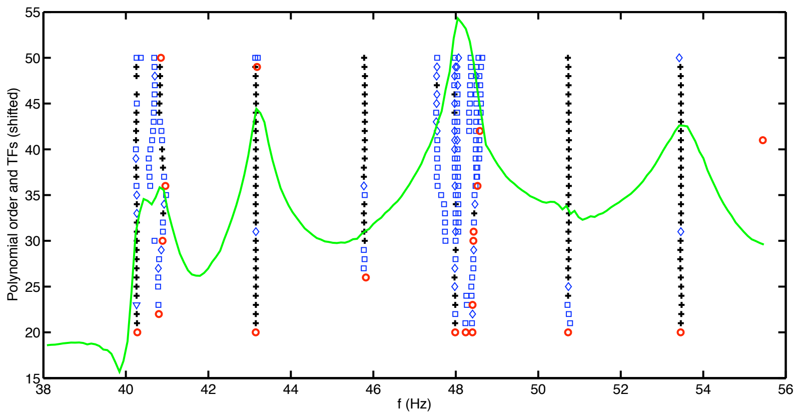

Figure 3.4: *Stabilization diagram*. BIG1 standard configuration (f:38-55.5)

In Figure 3.4 the two kind of modes can be found: easy-to-identify modes (at 40.26, 43.15, 45.79, 50.74 and 53.46 Hz) and unclear ones (at 40.83 and 48 Hz).

Figure 3.5, on next page, shows how poles are selected. MACOL poles selection works by introducing, in the Matlab Command Window, the poles one by one. Firstly, the pole frequency, and then the polynomial order used to calculate it (figure 3.5).

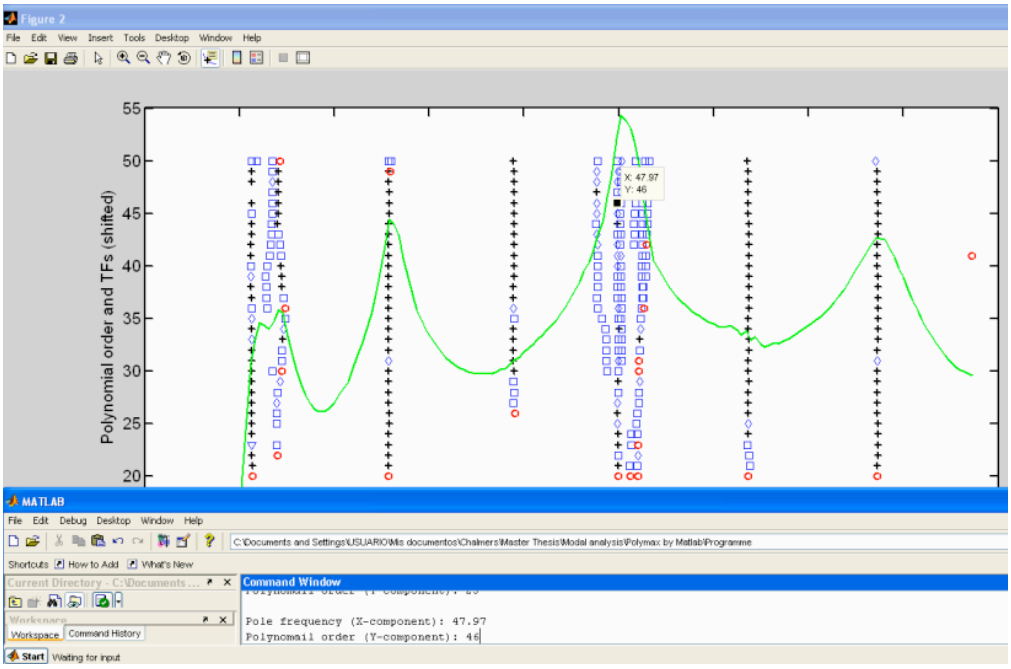

Figure 3.5: *MACOL* selection of stable poles

MACOL's modal parameters extraction

Modal participation factors and poles are extracted from the stabilization diagram. The frequency and damping factor of each pole can be estimated as explained in equations and .

The residuals and the mode shapes are the modal parameters left to estimate. Equation 3.16 can be used to create a linear equations system where these modal parameters are the unknowns. The measured transfer functions are the system constant terms. As the modal model is formulated for receptance FRFs, MACOL converts the inertance FRFs to receptance FRFs in order to solve the system.

MACOL operates the system to speed the solving process up. The diagram in figure 3.6 explains the procedure followed. It starts from the initial situation, where there is one equation for each frequency point, input and output. The number of unknowns is related to the mode shapes (one per output for each of the resonance modes) and the residuals (one per output for each of the inputs).

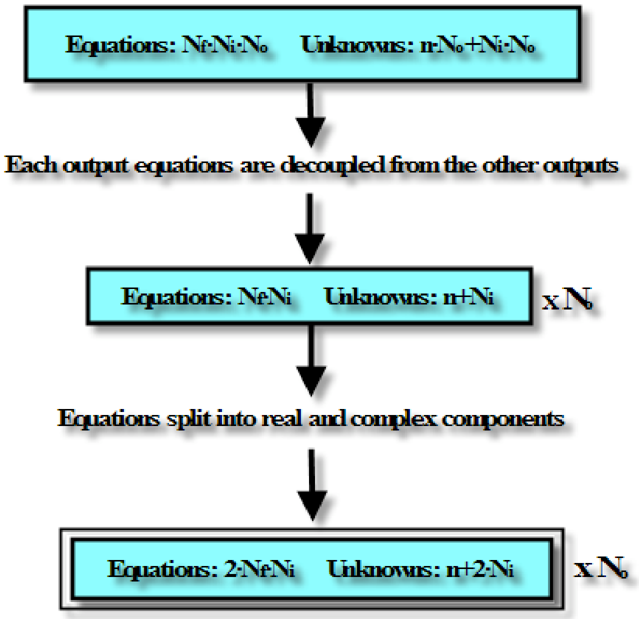

Figure 3.6: *Equations system operation diagram*

As Matlab is not able to handle matrices over a certain size is wise to shorten the number of equations by separately solving the equations for each output. It can be done because the equations generated by each output can be decoupled from the equations generated by the others. Moreover, Matlab is proved to be faster when solving a real system instead of a complex one.

Hence MACOL splits the equation system. Each equation becomes two, one from the real components and another one from the complex components.

Modal Validation

A complete description of the modal validation is given in section 3.1.5. When the MPE is done, MACOL offers checking the synthesized FRFs in comparison to the measured ones (figure 3.7). The modal parameters calculation is highly dependent on fitting accuracy at resonance frequencies, and surroundings. Therefore, it is the most important feature to analyze when comparing measured and synthesized FRFs. This modal validation step provides the operator a first view of the results quality and, specially, which modes are not well identified. In addition, MACOL calculates the FRFs normalized error and their correlation according to equations 3.17 and 3.18.

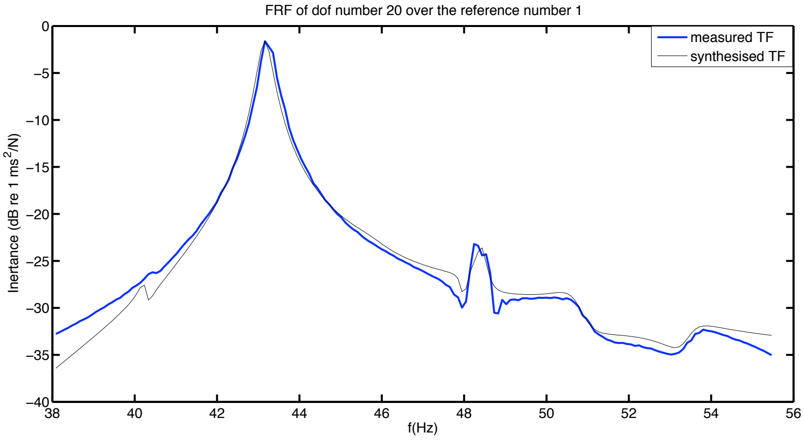

Figure 3.7: *Synthesized and Measured FRF* for a single DOF

The second step of MACOL's modal validation is the auto-MAC matrix study. All the elements contained in the matrix diagonal equal 100% (they are the auto-correlation of each mode shape). Coupling phenomena can be studied from auto-MAC values. The coupling between modes close in frequency yields a MACs over 10% although it should not be higher than 40-50%. A MAC over 50% between two close-in-frequency modes is a sign of having selected twice the same mode. Hence, one of them should be removed from analysis. Another issue to be checked is the high MAC values between far in frequency modes. In this case a MAC over 35% indicates an inappropriate measurement set-up, as commented in section 3.1.5.

Figure 3.8 shows an example of MACOL's modal validation. The modes under validation are the ones selected from figure 3.4. The study of the MAC values and the synthesized FRFs could suggest the modification of certain poles. MACOL allows the user to remove or modify poles, for instance by taking another polynomial order. When none of the options leads to a satisfactory accuracy level for a certain pole, a zooming of the pole is advised. However, the frequency range width cannot be extremely reduced as explained in section 3.2.1.

The correlation and the normalized error can be observed at the bottom of figure 3.8. The fitting accuracy of synthesized FRFs is high (correlation: 92.6%, normalized error: 7.6%) as expected. At Command Window's top, the modes frequencies and damping ratios are listed. The mode index corresponds to the number of row/column in the auto-MAC matrix. The MAC values study reveals a strong coupling between the 1^{st} and 2^{nd} modes (MAC=28.52%), and between the 5^{th} and 6^{th} modes (MAC=38.92%). MAC values (around 30%) between the 5^{th} and 9^{th} modes, and between the 6^{th} and 9^{th} modes are of relevance as well. The 9^{th} mode shape is similar to two other mode shapes. The cause might be the lack of output signals to totally capture body movement for the 9^{th} mode.

```
Command Window
LIST OF POLES

    Index      f(Hz)     Damping(%)

    1.0000    40.2554     0.2131
    2.0000    40.8298     1.3254
    3.0000    43.1572     0.4248
    4.0000    45.7930     1.2173
    5.0000    47.5401     0.7964
    6.0000    47.9964     0.2251
    7.0000    48.4460     0.2982
    8.0000    50.7246     0.8667
    9.0000    53.4472     0.7672


MAC =

  100.0000    28.5216     0.2289     2.3521     0.0534     0.1297     1.7661     0.3329     0.9135
   28.5216   100.0000     0.6121     2.1359     3.1280     0.3676     0.8544     0.1714     1.3394
    0.2289     0.6121   100.0000     1.4380     0.8055     4.9660     5.6509    34.6682     0.1397
    2.3521     2.1359     1.4380   100.0000     1.1288     3.9837     3.2469     0.6503     3.4122
    0.0534     3.1280     0.8055     1.1288   100.0000    38.9192    20.9484     3.9319    27.2568
    0.1297     0.3676     4.9660     3.9837    38.9192   100.0000    31.7252    16.6749    35.8561
    1.7661     0.8544     5.6509     3.2469    20.9484    31.7252   100.0000     4.5784    25.5139
    0.3329     0.1714    34.6682     0.6503     3.9319    16.6749     4.5784   100.0000     1.8599
    0.9135     1.3394     0.1397     3.4122    27.2568    35.8561    25.5139     1.8599   100.0000


---------------------------------------------------------------------------------------------
ACCURACY OF THE SYNTHESIZED VTF

Correlation: 0.9256
Normalized error: 0.076044
```

Figure 3.8: *Modal Validation by MACOL*

3.2.2 MACOL validation by LMS PolyMAX

MACOL could not be completely finished by the end of the thesis although the most important modal analysis features can be performed except for modes animation. In programmes development is mandatory the verification of the results. PolyMAX from LMS Test.Lab is well-known in industry as a reliable modal analysis software. As PolyMAX and MACOL come from same method (p-LSCF), PolyMAX was chosen as benchmark in order to assure MACOL's correct operation.

Stabilization diagrams comparison

Figures 3.9 and 3.10 show an example of stabilization diagrams from PolyMAX and MACOL, respectively. The example was taken for same body and configuration. The notation in PolyMAX diagram is different. The red *s* means stable pole and is the equivalent to the black cross in MACOL.

Same modes are found from both diagrams. Therefore MACOL search of poles works correctly. However, other differences between MACOL and PolyMAX operation have been observed.

For instance, MACOL needs a higher polynomial order to find all the poles PolyMAX does. The consequence is reflected in operational time, which is higher for MACOL. Additionally, PolyMAX shows the damping ratio and the scattering to facilitate poles selection. More diagrams were investigated to reassure the reliability of MACOL diagrams.

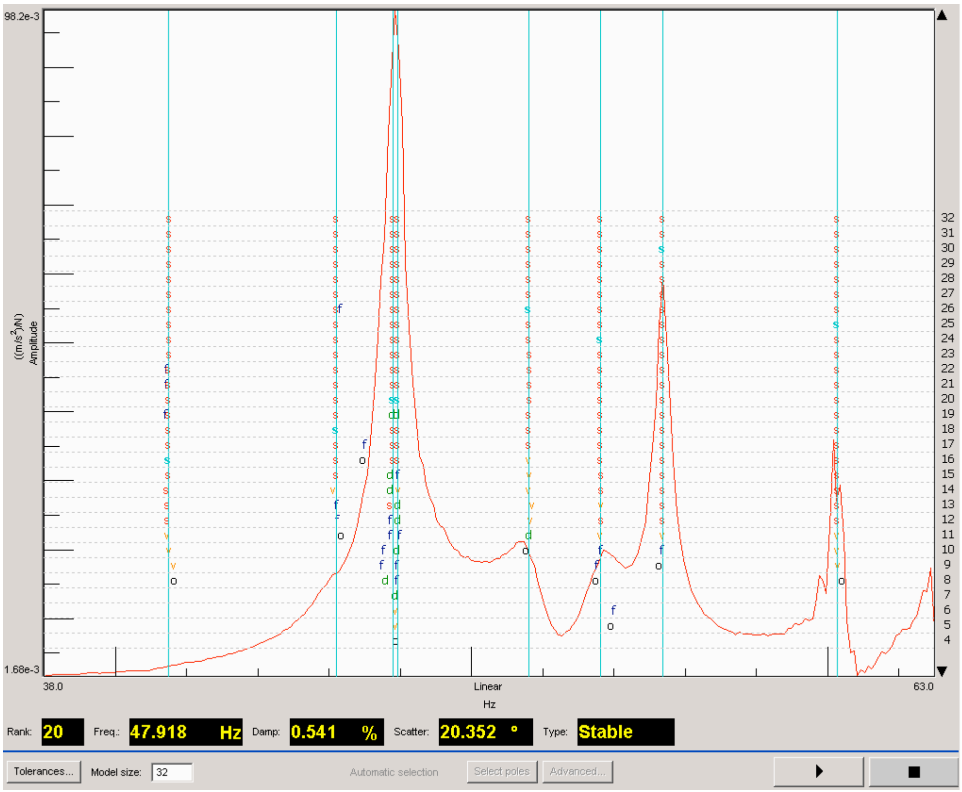

Figure 3.9: *BIG3 without GOR&RB Stabilization diagram by PolyMAX*

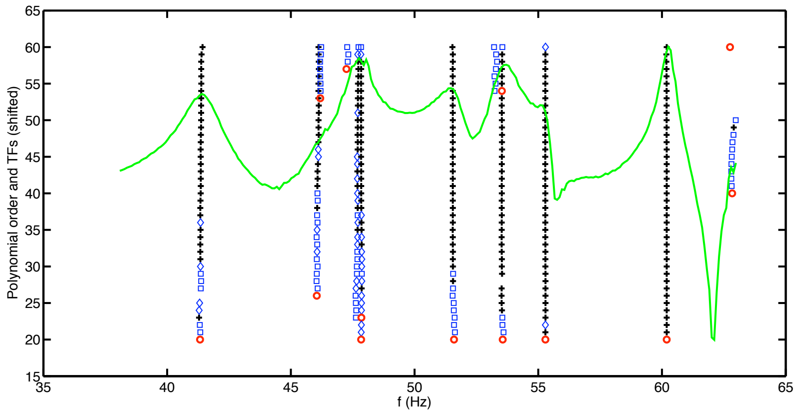

Figure 3.10: *BIG3 without GOR&RB Stabilization diagram by MACOL*

Estimated poles validation

The stabilization diagrams checking was somehow visual. The comparison between resonance frequencies and damping factors allows making a more solid judgment about the calculations validity up to this point.

Table 3.2 compares the modes selected from the stabilization diagrams in figures 3.9 and 3.10. MACOL shows slightly lower values than PolyMAX for both resonance frequencies and damping ratios. The low differences between results certify MACOL's capability for finding the correct physical poles.

Table 3.2: f_r and η_r for *PolyMAX* and *MACOL*

$f_r(LMS)$	$f_r(MACOL)$	Δf_r	$\eta_r(LMS)$	$\eta_r(MACOL)$	$\Delta\eta_r$
41.48	41.34	**0.13**	1.49	1.37	**0.12**
46.21	46.08	**0.13**	1.33	1.11	**0.22**
47.79	47.69	**0.11**	0.87	0.92	**0.05**
47.92	47.84	**0.08**	0.54	0.55	**0.01**
51.62	51.55	**0.07**	1.04	0.95	**0.09**
53.62	53.53	**0.09**	0.94	0.90	**0.04**
55.38	55.29	**0.09**	0.34	0.35	**0.01**
60.28	60.19	**0.09**	0.32	0.31	**0.01**

Modal Parameters Extraction (MPE) checkings

The MPE leads to the estimation of the residuals and the mode shapes. MACOL calculates real residuals and PolyMAX complex residuals. Therefore residuals cannot be numerically compared. Moreover, residuals are terms meant to compensate out of band modes, therefore they do not have an absolute value.

The residuals aim is improving the fitting in the lower frequencies and the ranges between resonances. Synthesized FRFs provide information about residuals contribution. Reader can use figure 3.7 to check residuals effect on synthesize FRFs. MACOL shows a reasonable fitting although it could be improved by using complex residuals.

The mode shapes are vectors which have different magnitudes depending on the weighting system used. The weighting (scaling) is done depending on the system information one has. For instance, the mass associated to each output. PolyMAX can perform weighting whereas MACOL does not. However, weighting is not necessary to animate system mode shapes.

The comparison between animations would be the best tool to validate MACOL mode shapes. Unfortunately, MACOL modes animation is not implemented yet. Therefore, the comparison of mode shapes magnitudes is the only possibility. Mode shapes amplitude have been compared for several cases. One of them is shown in appendix B.

A reasonable approximation is observed for most of FRFs, although few of them (16 DOFs out of 279) present significant errors (over 40%). Moreover, two FRFs cannot be taken into account because their error is over 1000%. If they are excluded, the averaged normalized error is less than 20%.

The DOFs which have high errors might have a very low level of movement, or they might be poorly excited. As a result mode shapes are innacuratedly estimated for these DOFs. In spite of them, MACOL overall results are considered acceptable although further studies are left to be done whenever animations are available.

Modal validation comparison

Section 3.2.1 highlighted the importance of an accurate fitting at the resonance peaks when considering synthesized FRFs. There is no parameter to quantify the fitting quality around the resonance peaks. Therefore the study has to be reduced to general results, i.e. the correlation and the normalized error.

Table 3.3 gives a comparison between programmes for a single case, BIG3 without GOR and RB. Results are slightly in favor of MACOL, specially if one looks at the normalized error. Once again MACOL results are validated.

Table 3.3: *Coherence* and *Normalized Error* by *PolyMAX* and *MACOL*

	LMS	*MACOL*
Correlation (%)	91.66	89.07
Normalized Error (%)	17.91	11.13

The auto-MAC values are compared as well. Values from figure 3.12 are cross-checked with the ones from LMS PolyMAX (figure 3.11). It cannot be expected to have same MACs as mode shapes correspond to different poles selections done by different programmes. Still values should be close, specially the ones having a high magnitude. For instance the MAC values between the 6^{th} mode and 7^{th} one ($MAC_{MACOL} = 64.99\%$,$MAC_{LMS} = 61.04\%$) or the 7^{th} mode and the 8^{th} one ($MAC_{MACOL} = 16.52\%$,$MAC_{LMS} = 20.78\%$). These values are a coupling sign. The resemblance is acceptable. Hence, PolyMAX results support MACOL ones.

Auto-MAC	**41,478**	**46,205**	**47,787**	**47,918**	**51,615**	**53,623**	**55,379**	**60,279**
41,478	100	2,445	1,331	0,273	0,146	0,634	0,021	0,178
46,205	2,445	100	3,8	0,276	1,213	2,805	2,856	0,081
47,787	1,331	3,8	100	47,692	1,236	9,96	1,527	2,268
47,918	0,273	0,276	47,692	100	0,758	2,443	0,397	0,856
51,615	0,146	1,213	1,236	0,758	100	0,469	0,04	0,148
53,623	0,634	2,805	9,96	2,443	0,469	100	61,039	2,361
55,379	0,021	2,856	1,527	0,397	0,04	61,039	100	20,776
60,279	0,178	0,081	2,268	0,856	0,148	2,361	20,776	100

Figure 3.11: *Auto-MAC values extracted from LMS Test.Lab*

```
MAC =

  100.0000    4.9127    6.9648    1.9359    0.0702    0.7360    0.1039    0.9056
    4.9127  100.0000    2.0175    0.0362    1.1661    1.1664    0.7452    0.2006
    6.9648    2.0175  100.0000   36.8573    2.0904    9.0979    1.3454    4.9057
    1.9359    0.0362   36.8573  100.0000    0.7777    2.2468    0.4367    1.1133
    0.0702    1.1661    2.0904    0.7777  100.0000    2.7277    0.6152    0.1184
    0.7360    1.1664    9.0979    2.2468    2.7277  100.0000   64.9856    2.8579
    0.1039    0.7452    1.3454    0.4367    0.6152   64.9856  100.0000   16.5207
    0.9056    0.2006    4.9057    1.1133    0.1184    2.8579   16.5207  100.0000
```

Figure 3.12: *Auto-MAC values extracted from MACOL*

The poly-reference least squares frequency-domain method, p-LSFD, and its Matlab implementation, MACOL, have been explained along this chapter. Further comments and suggestions about MACOL will be given in section 5.2 in order to provide modal analysis operators a deeper understanding of the method and help them to improve their use of programmes.

Chapter 4

Measurements

4.1 Measurements planning

Any modal analysis test entails an extensive planning phase in which important decisions have to be taken. The concerns related to this thesis were:

- **Test subjects:** Sufficient quantity to ensure the characterisation of the bolted items influence.

- **Supports configuration:** Minimisation of external influences.

- **Excitation system:** Effective excitation of modes.

- **Response points:** Positioned to capture all body modes and clarify their identification.

4.1.1 Test subjects

The main goal of the thesis is studying the influence of three bolted items on the results and consistency of modal analysis performed on a Volvo S80 BIG. In order to observe their influence, modal analysis must be run over different body configurations. These configurations shall reveal the items contribution to body modes. Ideally, all possible configurations (sixteen) should be tested although it is not time-feasible. Therefore, it was decided to measure the configurations resulting from a progressive removal of the bolted items:

- Standard BIG (all bolted items on).

- Standard BIG without grill overhanging reinforcement (radiator beam and tunnel brace on).

- Standard BIG without grill overhanging reinforcement and radiator beam (tunnel brace on).

- Standard BIG without grill overhanging reinforcement, radiator beam and tunnel brace (all bolted items off).

An additional configuration was measured to study the effect of fixing the GOR with brackets. The bolted items on the body are shown in figure 1.1. Figures 4.1, 4.2, 4.3 and 4.4 offer an image of them when they are not attached to the body:

Figure 4.1: *Grill Overhanging Reinforcement: GOR*

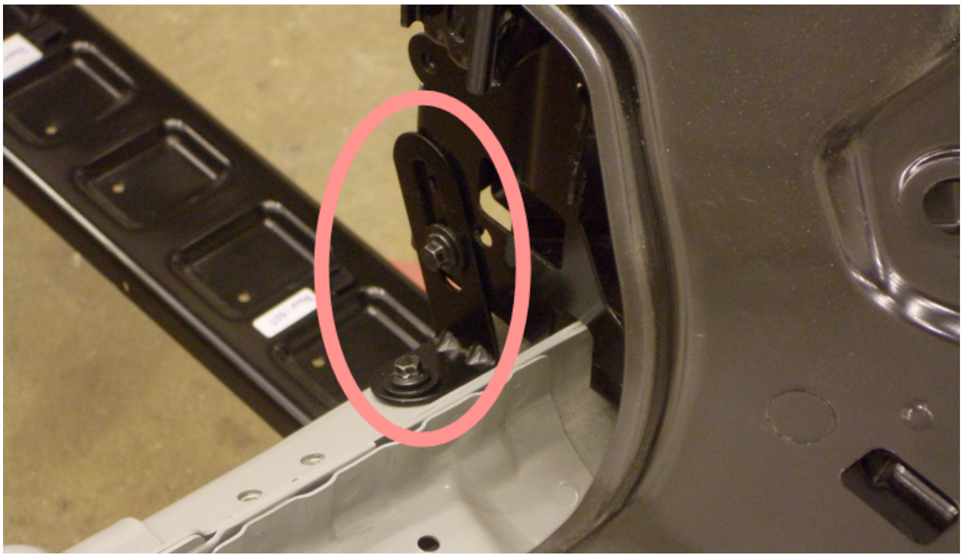

Figure 4.2: *Brackets fixing GOR*

Figure 4.3: *Radiator Beam: RB*

Figure 4.4: *Tunnel Brace: TB*

Modal Analysis tests on BIGs have dispersion added by the differences between nominally identical car bodies. Such differences come from manufacturing process of the structure components and their assembling. During Volvo GPDS project bolted items were identified as a source of dispersion as well. In order to discern the bolted items dispersion from the one coming from the structure, it seems advisable to measure more than one body. In addition, the thesis aims for a general conclusion which could be extrapolated to any Volvo S80 BIG. The bigger the number of measured bodies is, the better the results generalization is. Once again the ideal case, measuring a huge number of bodies, it is not feasible. Time restrictions derived in the measurement of three bodies: BIG1, BIG2 and BIG3.

4.1.2 Support configurations

An inappropiate support configuration could lead to high noise levels, in other words to a poor estimation of the modal parameters, specially for the first flexible mode. The ideal support condition is free-free, i.e. structure freely suspended in space. In this case the structure would not be affected by any external forces or noise. The free-free support is not viable. In practice very soft springs are used to approach the free-free supporting.

The standard way to check the supports configuration quality is finding the Rigid Body Modes (RBMs) frequency. Every system has 6 RBMs. Each of them corresponds to the movement in one of the natural space DOFs (3 translations and 3 rotations). The main characteristic of a RBM is that the hole body moves as a rigid structure. The RBMs of a structure are determined solely by its mass and inertia properties. When having free-free support conditions the resonance frequencies of the RBMs are coincident at 0 Hz. The use of soft springs yields RBMs over 0 Hz. If the highest RBM in frequency is less than 10 to 20% the frequency of the lowest Flexible Body Mode (FBM), one can still derive the mass and inertia properties of the body [1].

Modal analysis performed on automotive industry uses air-mounts to support car bodies due to their heavy weight. The air-mounts are air-filled balloons. They have a very low stiffness and are capable of supporting heavy structures. Figure 4.5 shows one of the air-mounts used during the thesis. The air-mount appears attached to a wood structure to stabilize its contact with the floor and the body.

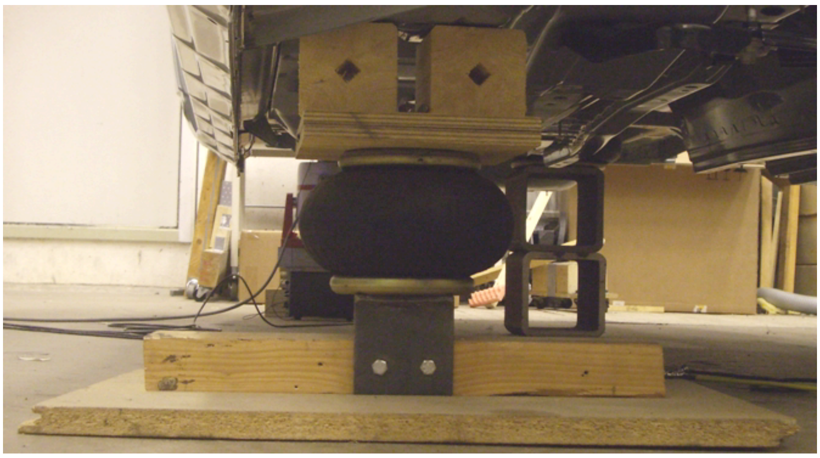

Figure 4.5: *Air-mount*

Preliminary tests were done to assure a correct supporting system. The standard configuration was measured supported by three air-mounts (triangle-positioning) and four air-mounts (rectangle-positioning). The goal was testing whether three air-mounts would be sufficient to approach free-free supporting conditions or an extra air-mount would be needed.

Figure 4.6 shows the 3 air-mounts configuration, which is 2 air-mounts at the front and one at the rear. The 4 air-mounts configuration was built replacing the centered rear air-mount by two air-mounts placed where the arrows mark.

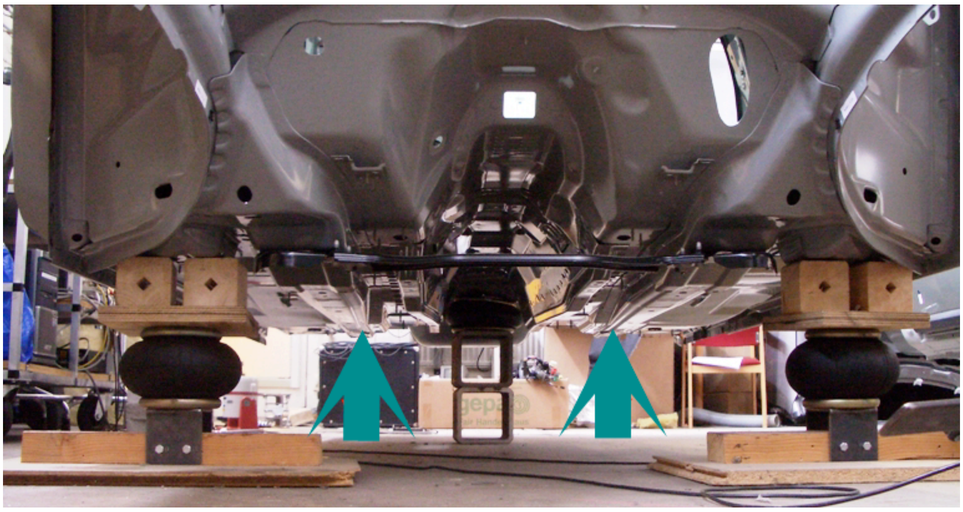

Figure 4.6: *Supports configuration*

The test was performed using two electrodynamic shakers exciting in vertical direction. They were placed on the right side, one at the front and the other one at the rear. Attention must be paid to figure 4.7. The shakers are on two height-adjustable supports. When modal analysis was performed using these supports unexpected resonances were found from 15-20 Hz. The body is actually designed not to have resonances below 35 Hz, except for the RBMs.

The resonance peaks were significantly stronger for the FRFs over the front shaker. Therefore, unexpected resonances investigation was directed towards the shakers set-up. Firstly, repeteability was tested confirming results. In the next step, shaker supports were exchanged observing that resonances were then appearing at the rear shaker. Hence, it was concluded that an internal resonance from the front shaker support was causing the unexpected resonances. Measuring experts were consulted about this behaviour. They advised using rigid supports for shakers, therefore height-adjustable supports must be avoided. Figure 4.9 shows the shakers on the rigid supports used for the "production"measurements. The unexpected resonances disappeared when these supports were used.

Figure 4.7: *Preliminary test shakers set-up* (left: rear shaker, right: front shaker). Shakers on *height-adjustable supports*

Unexpected resonances were not considered as flexible modes in the RBMs study. Table 4.1 presents the results from modal analysis performed on this preliminary test. The table contains the six RBMs and the first Flexible Body Mode (FBM).

Table 4.1: *RBMs for 3 and 4 air-mounts* & 1^{st} *FBM* frequencies (Hz)

$Air - mounts$	RBM_1	RBM_2	RBM_3	RBM_4	RBM_5	RBM_6	FBM_1
3	2.10	2.63	3.86	4.16	4.35	6.03	39.03
4	2.04	2.53	3.17	4.03	4.50	6.12	39.03

A closer look to the table leads to the following conclusions:

a) 3 air-mounts are enough to guarantee free-free conditions. Last RBM represents 15.4% (<20%) of the first FBM.

b) An extra air-mounts does not improve the system behaviour. Last RBM is the one setting the quality of the supporting system. Actually, it can be observed that is slightly higher when 4 air-mounts are used.

4.1.3 Excitation system

Once the number of air-mounts was decided, the aim was finding the best excitation system among the possible ones. Impact hammer or electrodynamic shakers are the two methods to excite systems for EMA. The use of shakers was determined by the need of having enough energy density over a wide frequency range. Two different points suggested the use of more than one shaker:

a) All modes of interest cannot be excited from a single reference or shaker.

b) The structure has highly coupled modes. Hence, more references help for identifying them [12].

The laboratory where the thesis was done counted on two electrodynamic shakers. Therefore, excitation systems were limited to a maximum of two shakers.

The criterions to follow when selecting the best excitation system are:

- All modes sufficiently excited $\Rightarrow$ No mode is missed.

- Low correlation between input signals $\Rightarrow$ Higher linearity of the system response.

- High coherence between output and input signals $\Rightarrow$ Less noise.

According to the criterions and the number of shakers one counted on, the following excitation systems were tested (pictures are found in figure 4.8):

1º **One shaker excitation:** One shaker at right rear with vertical excitation.

2º **Right side excitation:** One shaker at right rear and another one at right front with vertical excitation.

3º **Diagonal excitation:** One shaker at right rear and another one at left front with vertical excitation.

4º **45-degrees excitation:** One shaker at right rear and another at left front with 45º excitation (direction $\in \Pi_{yz}$ and 45$\angle$ to y and z).

The use of a single shaker was meant to study the goodness of having a single input in terms of coherence. Moreover, the 45º excitation was of high educational interest to observe the structural behaviour in comparison to the vertical excitation. One could think that having excitation in two different directions (y and z) would derive in having modes better excited.

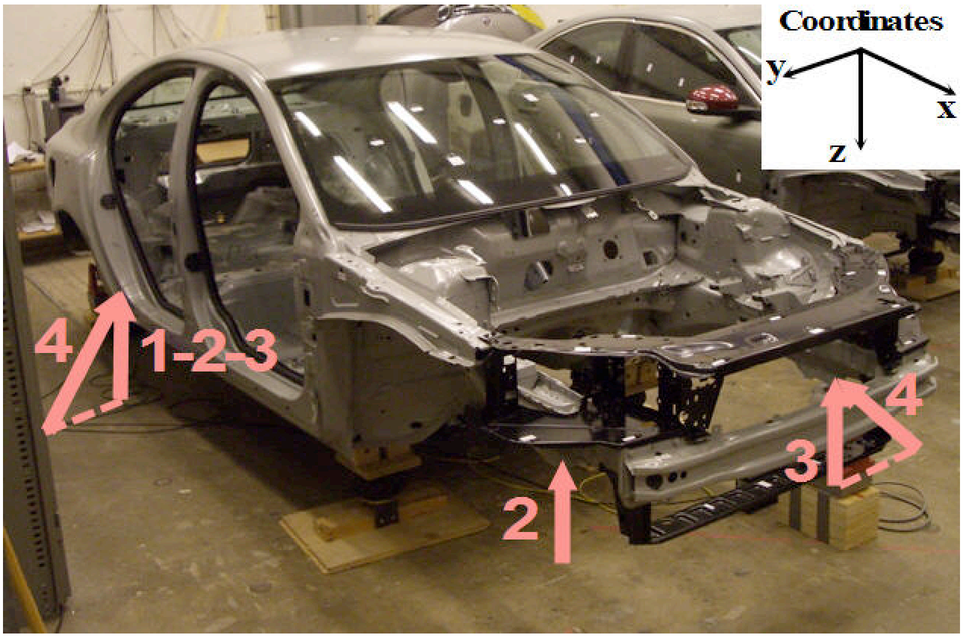

Figure 4.8: *Excitation systems tested:* 1º One shaker 2º Right side 3º Diagonal 4º 45-degrees

Figure 4.9 shows the shakers for vertical excitation. They are set on rigid supports which are formed by a heavy iron block and some wooden boards on the top.

Figure 4.9: *Preliminary test shakers set-up* for vertical excitation (left: rear shaker, right: front shaker)

The first tests performed on the 45-degree excitation system were not succesful. Unexpected resonances were found in the frequency range between RBMs and first FBM again. The experience obtained during the supports configuration study draw the attention to shakers supports.

Modifications done to improve the stability of the shaker supports are reflected in the FRF of a single DOF (figure 4.10).

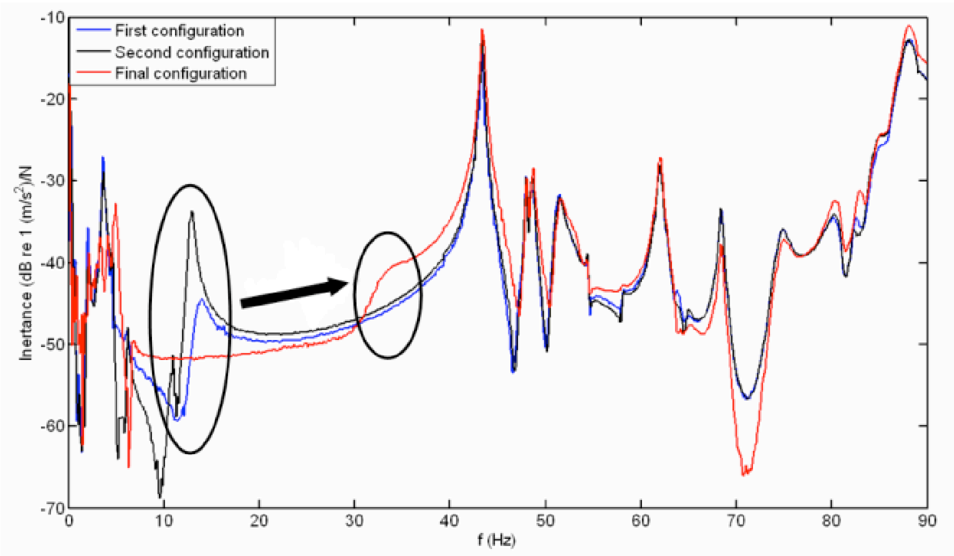

Figure 4.10: *Single DOF inertance for different 45^o-excitation set-ups*

Initially, the shaker supports used were the ones shown in figure 4.9 for vertical excitation (first configuration in figure 4.10). First hypothesis was that resonances were generated by boards sliding, therefore boards were glueded and clamped in vertical direction (z-direction) (second configuration). This modification actually made results worse, unexpected resonances were amplified.

Second hypothesis was that shaker supports were not capable to firmly hold shakers in y-direction. Hence, two heavy iron blocks were clamped in y-direction to the initial support (final configuration). The unexpected resonances dissapeared althought higher levels were found around 30 Hz. The improvement was considered sufficient. Therefore, the final configuration (figure 4.11) was the one used to be compared with the other excitation systems.

Figure 4.11: *Preliminary test shakers set-up* for 45-degrees excitation (left: rear shaker, right: front shaker)

The four excitation systems were measured on the standard configuration of the BIG3. The study was based on the criterions presented in this section:

Modes proper excitation

Modal analysis was performed by MACOL yielding the results shown in table 4.2. The aim was checking the first requirement for the excitation system, missing no mode. The modes in bold could hardly be identified, i.e. modal analysis had to be done for a narrow frequency range and higher polynomial orders to find them.

All excitation systems were able to excite modes, although it was observed that 45-degrees excitation (number 4) did not excite properly three modes. Surprisingly having excitation in two directions is not a guarantee to better excite modes. No clear indication could be extracted from these results to decide the best excitation system.

Table 4.2: f_r and η_r for excitation systems

Index	f_1	η_1	f_2	η_2	f_3	η_3	f_4	η_4
1	38.97	0.204	39.03	0.253	39.03	0.205	39.01	0.190
2	41.19	1.471	41.24	1.452	41.26	1.506	41.24	1.452
3	43.32	0.512	43.34	0.433	43.38	0.446	43.33	0.425
4	46.07	1.288	46.07	1.182	46.11	1.361	46.10	1.187
5	47.54	0.392	47.63	0.598	47.68	0.685	**47.89**	**0.270**
6	47.93	0.179	48.04	0.158	48.02	0.204	**48.04**	**0.149**
7	48.43	0.226	48.53	0.256	48.53	0.246	48.35	0.237

8	51.15	0.959	51.20	0.944	51.23	0.976	51.28	1.012
9	53.20	0.912	53.25	0.855	53.29	0.883	53.33	0.935
10	54.37	0.260	54.41	0.233	54.44	0.247	54.38	0.220
11	57.96	0.396	58.01	0.388	58.03	0.377	57.98	0.373
12	61.93	0.503	61.92	0.485	61.93	0.450	61.95	0.428
13	63.59	0.346	63.59	0.344	63.57	0.343	63.58	0.319
14	65.00	0.150	65.00	0.212	64.84	0.188	64.98	0.149
15	68.32	0.359	68.31	0.344	68.33	0.341	68.39	0.366
16	70.60	1.272	**70.60**	**1.196**	70.59	1.236	70.63	1.234
17	73.92	1.064	74.01	0.855	73.96	1.015	73.99	1.077
18	74.60	0.908	74.61	0.762	74.62	0.896	74.70	0.863
19	75.92	0.706	75.99	0.637	**75.95**	**0.712**	**75.80**	**0.769**

Input signals correlation

In Figure 4.12 the coherence (correlation) between the measured forces of the two shakers, for each system, is shown. Obviously the excitation system with a single shaker is missing. The high coherence up to 10 Hz is explained by the shakers signal offset and the fact that the shakers produce a strong response at each other when RBMs are excited. The shakers correlation is very low for all systems except for the 45-degrees excitation one which has strong peaks at certain frequencies (some of them coincident with resonance modes).

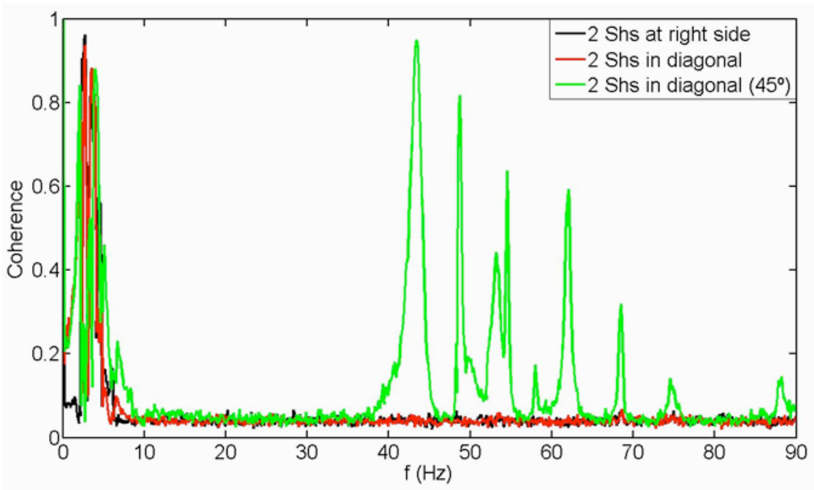

Figure 4.12: *Shaker signals correlation* for each excitation system

The high correlation between shakers worsens the FRFs estimation which loses linearity. Therefore, the 45-degrees excitation system should be avoided. The shakers correlation do not point out any of the other three systems as better than the others.

Output-inputs signals coherence

The output-input coherence is the last element of comparison left to analyze. The average over all outputs and both inputs appears in figure 4.13. The coherence of all configurations resembles except for the frequency range between RBMs and FBMs. One could think beforehand that having just a single input would induce better coherence. It turns out that the single shaker system is the worst in terms of coherence. This might be due to insufficient input power applied to the structure when using just one shaker.

The 45-degrees excitation is the most coherent but it was discarded by the forces correlation criterion. The second one is the diagonal system. No excitation system was highlighted by the other criterions. Hence, the diagonal excitation system was considered as the best among the available options and it has been the one used for the "production"measurements.

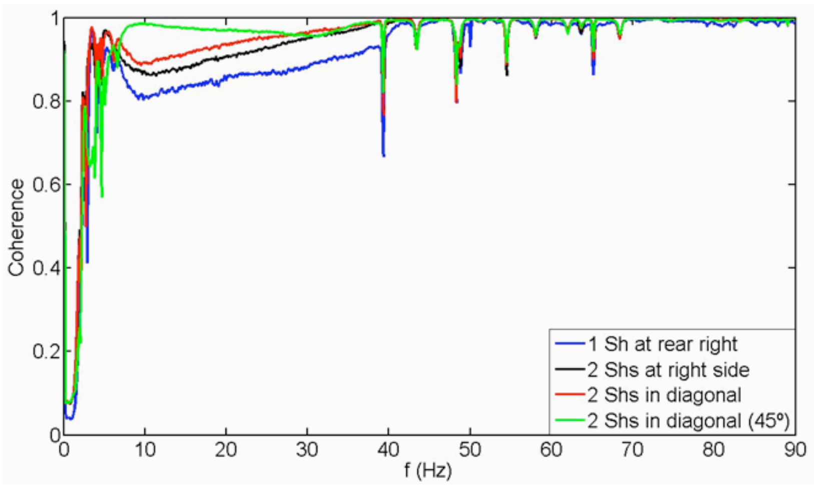

Figure 4.13: *Averaged acceleration-force coherence* for each excitation system

4.1.4 Response points

Response points must be set in order to cover all structure and register all body modes. During GPDS Volvo project, 101 points were measured on BIGs. The animations obtained from measurements did not perfectly defined the body movement at certain frequencies. Before the thesis "production"measurements, a study was done to add extra points. It was based on the observation of resonance modes animations. Points were added at the following sub-structures: grill-overhanging-reinforcement (GOR), radiatior beam (RB), roof beams, beams between doors and trunk. In total 126 points were measured. Pictures showing all measured points are shown in appendix D and coordinates are given in table C.1.

4.2 Measurements set-up

Previous section (4.1) described the process followed to take the main decisions related to measurements set-up. This section presents the equipment used and its arrengement in order to perform measurements.

In [13], reader can found a complete description of the equipment necessary for carrying out vibroacoustic measurements and the explanation about how to mount it.

Figure 4.14, on next page, is a sketch of the measurements set-up used for the "production"measurements. The numbers appearing in the figure relates to table 4.3, a list of the set-up equipment. Equipment pictures are shown in appendix E.

Table 4.3: *Equipment*

Index	**Manufact.**	**Item**	**Num.**	**Serial num.**
1	FireStone	Air-mount	3	W01-M58-6008
2	B&K	Triaxial accelerometer Type 4524B	4	30231 30234 30284 30285
3	B&K	Mounting clips UA 1564	126	n/o
4	Agilent	E8408 Acquisition system VXI	1	n/o
5	Acer	Computer VXI2 station	1	n/o
6	LDS	Power amplifier	2	PA100E
7	LDS	V406 Electrodynamic shaker	2	57835/2 57835/3
8	B&K	Force transducer Type 8200	2	1948760 2071279
9	B&K	Charge amplifier Type 2635	2	872470 986722

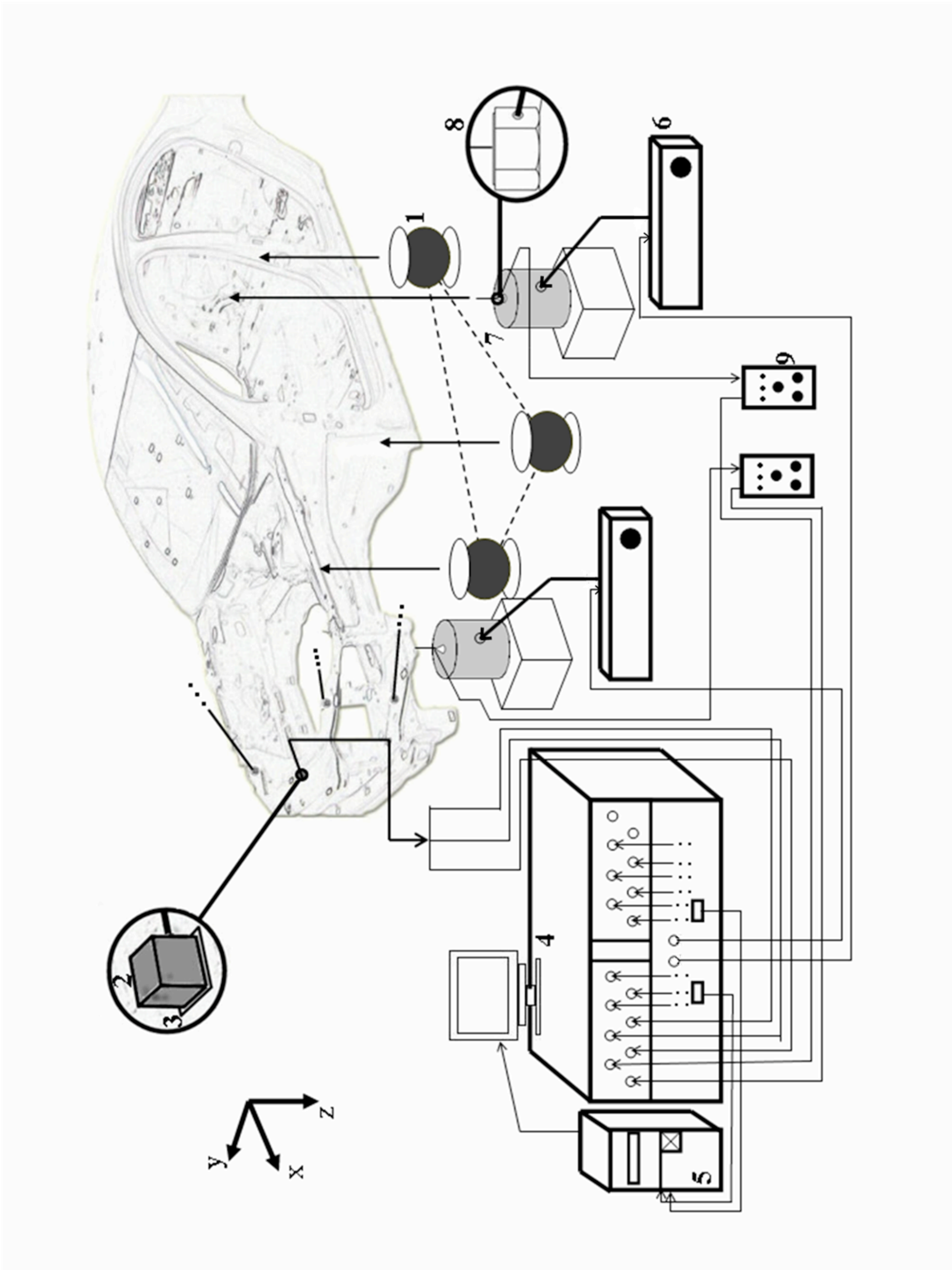

Figure 4.14: *Measurements set-up*

4.3 Measurements procedure

Measurements were performed by the author of the thesis, although one counted on Chalmers Acoustics Department members, specially when mounting the set-up.

The signal analysis software used is a programme developed in Matlab, the Trigger Happy software which was programmed at the Applied Acoustics department of Chalmers University. During this Thesis an update of Trigger Happy was done to implement MIMO transfer function and coherence using equations 2.2 and 2.3. The Trigger Happy code update is presented in appendix F. Further details about this software can be found in [13]. The signal analysis settings used are listed in table 4.4. Two different sets of measurements were done. The one at lower frequencies for modal analysis (up to 625 Hz) and the other one at higher frequencies for Volvo GPDS project (up to 1250 Hz).

The study of the different excitation signals proposed in [2] derived in the use of pure random signal to excite BIGs. The pure random signal is a non-periodic stochastic signal with a Gaussian probability distribution. The stochastic property implies the necessity of data averaging. The advantage of using this signal is that it has a low peak to RMS ratio. Therefore, it yields the best linear approximation of non-linear systems, as BIGs. Its main drawback is leakage. Hanning window is performed by Trigger Happy software to diminish it. Sygnal analysis settings are presented in table 4.4.

Table 4.4: *Signal analysis settings*

	Blocksize	***f* range**	**Samping *f***	***f* resolution**
Modal Analysis	16384	625	1600	0.0977
Volvo GPDS	4096	1250	3200	0.7813

32 measurement sets were performed to cover the 126 points of the standard configuration and the one without brackets. The channels correspondance is provided in appendix G. Configurations not having all bolted items have less points: 114 points for configuration without GOR, 109 points for configurations without GOR and RB and without both and the TB. When less points were measured, the accelerometers and sets order in figure G were kept. In addition, the points belonging to the same set were not separated into different sets when one of the points was removed.

Chapter 5

Results and Analysis

The results obtained during the thesis are presented in this chapter. Firstly, frequency limit is set. It defines the boundary up to which results can be considered as reliable. Secondly, a study of MACOL's poles identification is done to find the most consistent way to perform it. Afterwards, brackets results are analyzed to better understand their function.

Sections 5.4 and 5.5 contain the key results in order to achieve the thesis objectives. The dispersion introduced by each bolted item is studied. Then, the modes evolution is derived, from the configuration without bolted items to the standard one. It illustrates the effect of having each bolted item on and their contribution to unclear modes.

5.1 Frequency limit of Modal Analysis on BIGs

Modal analysis essence is characterizing the system dynamic response by the contribution of each resonance mode. Modal analysis methods intend to isolate each mode contribution and determined its characteristics (modal parameters). Nevertheless algorithms do not always succeed. The difficulties they have to overcome were presented in chapter 3. Among difficulties it stands out the results inconsistency when having high modal over-lapping. A high modal over-lapping, i.e. a high modal density, entitles modes coupling.

The frequency limit when performing modal analysis is actually related to modal over-lapping. More modes are found when frequency is increased. Hence, modal density is higher as one moves up in frequency. At certain point, modes coupling is too strong and modes contribution cannot be clearly identified. Stable poles can still be found although modal parameters extracted are not reliable.

No analytical calculations can be done to set a modal analysis frequency limit. It is a common-sense matter which relies on the operator experience. When a clear trend of unclear modes is observed, one can considered that the limit has been exceeded.

A study has been done to define the limit of the modal analysis tests performed in this thesis. The study was based on BIG3. Stabilization diagrams of its five possible configurations were analyzed. The stabilization diagrams of the standard configuration are shown in figures 5.1 and 5.2. The rest of the stabilization diagrams can be found in appendix H.

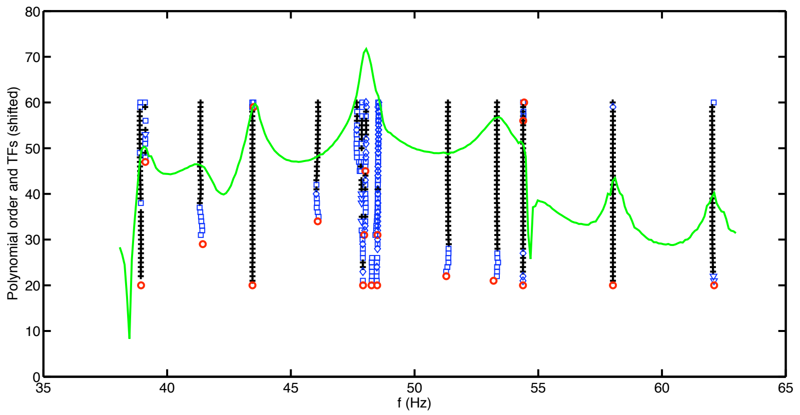

Figure 5.1: *Stabilization diagram* for BIG3 at “middle“frequencies

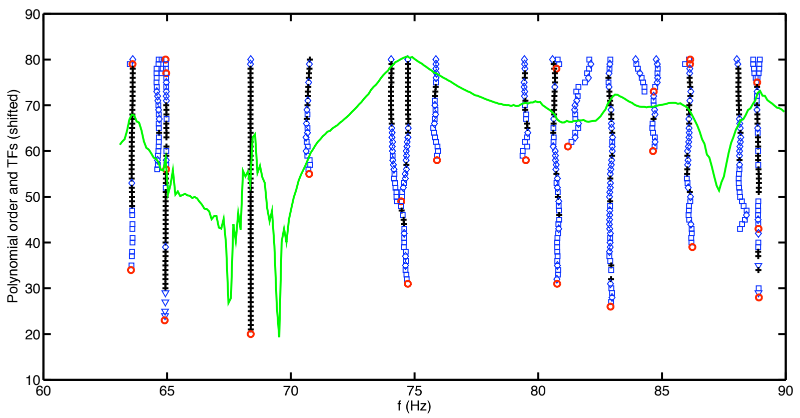

Figure 5.2: *Stabilization diagram* for BIG3 at high frequencies

Firstly, “middle“frequencies are observed (figure 5.1). Starting from the first flexible mode, all modes are easy to identify (they are stable for all polynomial orders) up to 48 Hz. Three unclear modes are found around this frequency. One could have set limit at 47 Hz, however, the following modes are easily identifiable and too much information would have been lost.

Analysis continues using figure 5.2. Unclear modes (around 64 and 71 Hz) are found in between clear modes, but they do not constitute a trend. A strong trend is observed over 75 Hz. From that point onwards, modes are mostly unstable either in damping ratio and/or in modal participation factor. Same trend has been observed for all configurations. Hence, the thesis results will be considered valid up to 75-77 Hz. The exact value depends on the configuration and the body. For instance, the mode at 74.73 Hz in BIG3 for the standard configuration corresponds to the mode at 76.11 Hz in BIG3 for the configuration without GOR and RB (correspondence is illustrated in figure 5.8).

5.2 MACOL study

Polynomial order (p) plays an important role in physical poles identification, especially for closely spaced modes. The method understanding obtained from programming allows studying the ins and outs of poles selection. The modal parameter extraction dependence on polynomial order arises the following questions:

- How sensible are the modal parameters to the polynomial order selection?
- Which modal parameters are more affected?
- Is it advisable choosing poles found for high or for low polynomial orders?

The questions will be answered using MACOL software. Results obtained cannot be directly extrapolated to LMS PolyMAX although same phenomena are likely to be found, as both programmes are based on p-LSCF algorithm.

The objective now is quantifying the influence of the selected polynomial order on the magnitudes of the modal parameters. Modes consistently found as stable for all polynomial orders are likely to show better results than those considered as unclear modes. Therefore, two extreme cases are investigated, an “easy-to-identify“mode and an unclear one. Poles selection was done using figure 3.4. Results are shown in tables 5.1 and 5.2. The last line in tables provides the maximum variance obtained for each modal parameter. The limits set for Δf_r, $\Delta \eta_r$ and $\Delta \| < L_r > \|$ when polynomial orders are consecutive can be checked in table 3.1.

Table 5.1: Poles selection dependence on polynomial order for an "easy-to-identify"mode

p	f_r	$\eta_r(\%)$	$< L_r >$
22	43.15	0.443	<-0.2826,-0.0731 + 0.0015i>
24	43.15	0.431	<-0.2761,-0.0686 - 0.0013i>
39	43.15	0.440	<0.2577,0.0669 + 0.0034i>
58	43.15	0.432	<0.2488,0.0651 + 0.0030i>
	$\Delta f_r(max) = 0.00\%$	$\Delta \eta_r(max) = 2.71\%$	$\Delta \| < L_r > \| \, (max) = 12.00\%$

Table 5.2: Poles selection dependence on polynomial order for an unclear mode

p	f_r	$\eta_r(\%)$	$< L_r >$
24	47.99	0.249	<0.0863 + 0.0068i,0.2406>
29	47.99	0.242	<0.0833 + 0.0215i,0.2256>
38	47.99	0.210	<0.0716 + 0.0277i,0.2041>
51	47.97	0.218	<0.0604 - 0.0072i,0.1989>
	$\Delta f_r(max) = 0.04\%$	$\Delta \eta_r(max) = 12.45\%$	$\Delta \| < L_r > \| \, (max) = 19.97\%$

Results are revealing. High accuracy in modes frequency is observed for both cases. Damping factors show different behavior in each case. In the "easy-to-identify"mode case, damping factors estimation is very consistent. Whereas for the unclear mode the maximum variation is over the double of the limit set for consecutive polynomial orders, 5%. The difference is not extreme but one should be aware of it.

Modal participation factors are not reliable in both cases. Its stability criterion for consecutive poles is 2%. A relative difference five times over the limit proves the lack of consistency. Modal participation factors relate to mode shapes (equation 3.16). Modal parameters sensibility to polynomial orders can be resumed as follows:

- Poles location in **frequency** is practically perfect.
- **Damping ratio** is not totally reliable for unclear modes.
- **Mode shapes** and **modal participation factors** are the most affected modal parameters. Their values should be considered as an orientation rather than an absolute number.

The difference between selecting poles estimated for high or low polynomial orders is analyzed. The extreme cases in figure 3.4 are taken, maximum and minimum polynomial orders available for each mode. In order to carry out the investigation, the error and the correlation between measured and synthesized FRFs are used.

Table 5.3: *Coherence* and *Normalized Error* for low and high polynomial order (p)

	Low p	**High p**
Correlation %	90.78	91.64
Normalized Error %	9.45	8.47

Table 5.3 shows insignificant differences between calculations, although results are slightly favorable to low polynomial order use. The correlation and the normalized error have been averaged over all frequency range. However, it should not be forgotten that fitting accuracy is mostly important at frequencies around resonance modes. Therefore, it is wise checking the synthesized and measured FRFs plot (figure 5.3). Figure observation does not reveal any trend. Indeed, some poles appear better fitted for high polynomial orders, and other poles for low polynomial orders. Hence, there is no advantage in selecting poles of high or low polynomial orders.

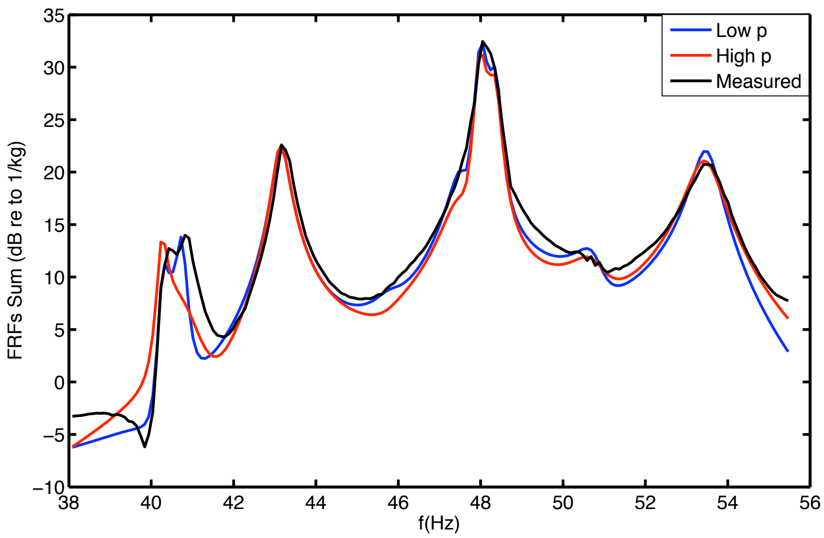

Figure 5.3: *Synthesized FRFs Summation Comparison*: low polynomial order, high polynomial order and measured FRFs

5.3 Brackets effect

The brackets implementation provides the best example to explain how to apply modal analysis on a BIG combined with FEM. In Volvo S80 development phase, measurements were done on a standard BIG, in which brackets had not been included yet.

Results discovered a resonance mode around 20 Hz. The mode was particularly disturbing because it was situated in the frequency range excited by the idling engine. The mode was related to GOR vibration. FEM was used to design some fixation able to damp the mode. Brackets were found as a good solution and were successfully implemented.

Figure 5.4 show the mentioned peak when brackets are ON and when they are OFF, from the data measured on BIG3 during the thesis.

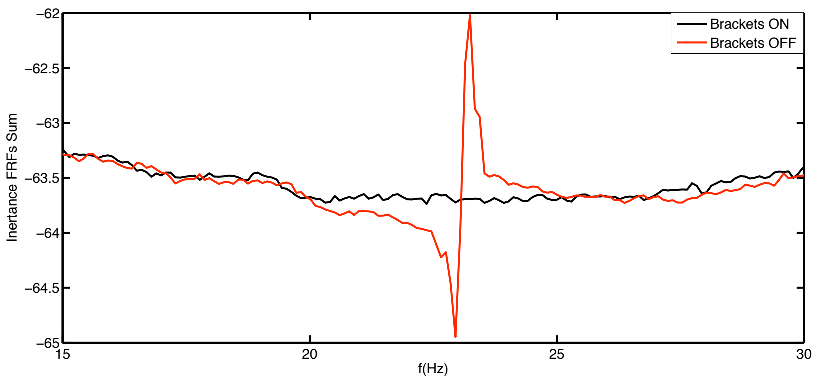

Figure 5.4: *FRFs Summation* with *brackets* ON and OFF

In Volvo GPDS project modal analysis was performed on BIG1, BIG2 and BIG3. Brackets were forgotten by mistake. GPDS results constitute the perfect benchmark to cross-check the thesis results. The aim is guaranteeing the quality of both, measuring process and modal analysis.

In figures 5.5 and 5.6, resonance frequencies and damping ratios are compared for the three bodies. V subindex relates to Volvo and T subindex relates to Thesis.

n	$f_T(1)$ (Hz)	$f_V(1)$ (Hz)	$\|\Delta f(1)\|_{rel}(\%)$	$f_T(2)$ (Hz)	$f_V(2)$ (Hz)	$\|\Delta f(2)\|_{rel}(\%)$	$f_T(3)$ (Hz)	$f_V(3)$ (Hz)	$\|\Delta f(3)\|_{rel}(\%)$
1	40.40	40.21	0.5	39.33	39.59	0.7	38.95	39.10	0.4
2	40.87	41.23	0.9	42.21	42.20	0.0	41.33	41.69	0.9
3	42.78	42.87	0.2	43.14	43.15	0.0	43.11	43.14	0.1
4	45.78	46.09	0.7	46.23	46.32	0.2	46.03	46.31	0.6
5	47.39	47.97	1.2	47.54	48.12	1.2	47.30	47.73	0.9
6	47.59	48.00	0.9	47.95	47.84	0.2	47.72	47.84	0.3
7	49.37	49.94	1.1	49.92	50.35	0.9	49.62	49.92	0.6
8	51.38	51.89	1.0	52.26	52.67	0.8	51.73	52.15	0.8
9	53.80	54.43	1.1	53.68	54.01	0.6	53.51	54.12	1.1
10	56.93	57.79	1.5	56.85	57.55	1.2	58.36	57.69	1.1
11	59.36	59.64	0.5	59.56	59.76	0.3	59.26	59.44	0.3
12	61.98	62.76	1.2	62.21	62.82	1.0	62.15	62.86	1.2
13	64.04	64.84	1.2	63.95	64.48	0.8	63.66	64.46	1.2
14	67.11	67.82	1.1	67.41	67.96	0.8	67.03	67.54	0.8
15	70.37	71.38	1.4	70.56	71.44	1.3	70.09	71.18	1.5

Figure 5.5: *Resonance frequencies for BIG1,BIG2,BIG3.* Volvo and Thesis results

Same resonance modes are found for both analysis. Differences in frequency are lower than 2%. However, damping ratios resemblance is poor for certain modes. The averaged difference is 20%, which could be considered as reasonable since damping ratio estimation is not highly accurate. The use of different set-ups might be the discrepances cause.

n	$\eta_T(1)$ (Hz)	$\eta_V(1)$ (Hz)	$\|\Delta\eta(1)\|_{rel}(\%)$	$\eta_T(2)$ (Hz)	$\eta_V(2)$ (Hz)	$\|\Delta\eta(2)\|_{rel}(\%)$	$\eta_T(3)$ (Hz)	$\eta_V(3)$ (Hz)	$\|\Delta\eta(3)\|_{rel}(\%)$
1	0.213	0.26	19.0	0.203	0.129	36.3	0.311	0.112	64.0
2	0.743	1.41	47.4	1.750	1.629	6.9	1.450	1.420	2.1
3	0.462	0.49	6.6	0.438	0.417	4.8	0.414	0.399	3.5
4	1.012	1.08	6.1	1.174	1.098	6.5	1.250	1.163	6.9
5	0.303	0.22	38.3	0.429	0.280	34.8	0.267	0.252	5.6
6	0.190	0.85	77.7	0.508	0.956	88.2	0.789	1.038	31.6
7	0.746	0.62	20.6	0.396	0.351	11.3	0.480	0.424	11.7
8	0.631	0.60	5.5	0.740	0.773	4.4	0.717	0.820	14.4
9	0.864	0.82	5.4	0.882	0.910	3.1	0.895	0.910	1.6
10	0.328	0.40	17.9	0.299	0.342	14.2	0.362	0.378	4.5
11	0.228	0.34	33.6	0.195	0.273	40.3	0.187	0.370	97.9
12	0.440	0.46	3.8	0.448	0.466	4.0	0.422	0.448	6.1
13	0.358	0.54	33.8	0.398	0.387	2.8	0.359	0.425	18.3
14	0.360	0.37	3.2	0.355	0.373	5.2	0.346	0.382	10.3
15	0.410	0.35	17.6	0.301	0.355	17.7	0.338	0.306	9.4

Figure 5.6: *Damping ratios for BIG1,BIG2,BIG3.* Volvo and Thesis results

5.4 Dispersion introduced by bolted items

Standard deviation (σ) is the variable selected to quantify the dispersion. Calculations could be done for all modal parameters although it has been considered sufficient to analyze the frequency deviation.

The standard deviation is defined as the square root of the variance. Therefore, it measures the data spread around the mean and it has same units as the data. In most cases, the standard deviation is estimated by examining a random sample from a entire population. Equation 5.1 was used to estimate the standard deviation. N is the number of samples (three in this case) and f_{mean} the averaged frequency of the mode.

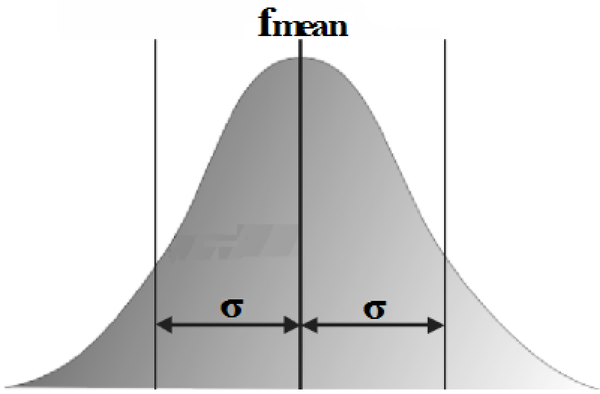

Figure 5.7: *Standard deviation definition*

$$
\begin{aligned}
f_{mean} - \sigma < f < f_{mean} + \sigma \\
\sigma = \sqrt{\frac{1}{N-1}\sum_{i=1}^{N}(f_i - f_{mean})}
\end{aligned}
\tag{5.1}
$$

One of the main objectives of the thesis is studying the inconsistency of the modal analysis results due to the bolted items inclusion. The inconsistency has been related to the results dispersion. This section intends to describe the dispersion added by each bolted item in order to possibly suggest the removal of any of them.

5.4.1 Tunnel brace

Table 5.4 presents the modes found for the configuration without GOR and RB of BIG1, BIG2 and BIG3. Frequencies are averaged and the standard deviation is estimated for each mode. Last line shows the mean deviation value. For instance, one can focus on the most deviated mode, number seven. Figure H.5 is used to check how easily can the mode be identified.

It is unexpected having an "easy-to-identify"mode with the highest dispersion. Opposite case is taken, one of the lowest deviation is found for mode number 2. However, this is one of the hardest modes to identify in figure H.5. Therefore, initial expectations are contradicted, dispersion is not proportional to the difficulties to identify a mode.

Table 5.4: *Modes for configuration without GOR and RB. Dispersion*

Index	f_r**(1)**	f_r**(2)**	f_r**(3)**	f_{mean}	σ_f
1	40.99	42.34	41.34	41.56	0.696
2	45.90	46.41	46.08	46.13	0.262
3	47.53	47.81	47.84	47.73	0.172
4	47.76	47.94	47.69	47.79	0.130
5	50.91	52.28	51.55	51.58	0.687
6	53.98	53.74	53.53	53.75	0.228
7	58.60	58.53	55.29	57.47	1.892
8	61.66	61.51	60.19	61.12	0.807
9	64.85	64.76	64.51	64.71	0.179
10	68.82	68.85	68.92	68.87	0.053
11	70.96	72.45	70.96	71.45	0.861
12	74.03	74.73	74.26	74.34	0.353
13	76.13	77.06	76.11	76.43	0.542
				$\sigma_f(avg)$	**0.528**

5.4.2 Radiator beam

The data shown in table 5.5 is taken from the configuration which contains both the radiator beam and the tunnel brace. The averaged deviation is decreased after adding the radiator beam on although it was expected the opposite trend. Joining this result to the ones for the tunnel brace, it can be stated that dispersion is not an indicator of the inconsistencies of modal analysis results.

Table 5.5: *Modes for configuration without GOR. Dispersion*

Index	f_r**(1)**	f_r**(2)**	f_r**(3)**	f_{mean}	σ_f
1	40.48	39.35	38.86	39.56	0.831
2	40.98	42.28	41.33	41.53	0.673
3	45.18	45.49	45.47	45.38	0.090
4	45.95	46.38	46.13	46.15	0.172
5	47.70	47.85	47.69	47.75	0.217
6	50.58	51.94	51.19	51.23	0.681

7	53.90	53.64	53.49	53.68	0.206
8	58.10	58.04	59.68	58.61	0.926
9	62.12	62.31	62.19	62.21	1.017
10	64.50	64.38	64.12	64.34	0.096
11	68.64	68.67	68.75	68.68	0.194
12	70.90	72.50	70.82	71.41	0.057
13	74.05	74.64	74.21	74.30	0.951
14	75.85	76.64	75.81	76.10	0.303
				$\sigma_f(avg)$	**0.458**

5.4.3 Grill over-hanging reinforcement

Table 5.6 corresponds to the standard configuration of the three BIG. According to the average deviation, the difference of having the GOR on and off is practically non-existent in terms of dispersion. Unclear modes (5,6,7,14,15) are of high interest. Figures 5.1 and 5.2 show the discontinuity of stable poles at these frequencies. In section 5.2 the results inconsistency for unclear modes were revealed. Nevertheless, the unclear modes deviation is very low in comparison with other modes. This reaffirms that dispersion is not proportional to inconsistency.

Table 5.6: *Modes for standard configuration. Dispersion*

Index	f_r**(1)**	f_r**(2)**	f_r**(3)**	f_{mean}	σ_f
1	40.29	39.34	38.94	39.52	0.693
2	40.82	42.20	41.35	41.46	0.694
3	43.15	43.45	43.45	43.35	0.135
4	45.78	46.22	46.05	46.02	0.174
5	47.53	47.76	47.67	47.65	0.225
6	47.98	48.09	47.91	47.99	0.114
7	48.50	48.74	48.52	48.59	0.089
8	50.74	51.96	51.36	51.35	0.610
9	53.46	53.34	53.33	53.37	0.074
10	56.23	56.12	54.39	55.58	1.033
11	61.11	60.82	58.02	59.98	1.709
12	61.91	62.07	62.03	62.01	0.083
13	63.97	63.85	63.58	63.80	0.200
14	64.90	65.00	64.61	64.84	0.203
15	65.15	65.14	64.94	65.08	0.121
16	68.21	68.30	68.38	68.29	0.085
17	70.59	72.36	70.69	71.21	0.993
18	73.82	74.40	74.06	74.09	0.290
19	74.63	75.49	74.74	74.95	0.471
				$\sigma_f(avg)$	**0.430**

5.5 Modes evolution. General results

The modes evolution study has been run over all configurations for BIG3. The aim is defining the effect of each bolted item on the body modes. To perform the modes evolution study MAC values were used. As explained in section 3.2.1, MAC values indicate the correlation between mode shapes.

MAC values were calculated between consecutive configurations, i.e. configurations differing on a single item. The starting point was the plain body (body where all bolted items are off), then one-by-one bolted items were added. Phenomena involved when two structures are joined are described in chapter 1.

A modes evolution diagram is shown in figure 5.8. MAC values used to develop the diagram can be found in appendix I. Reader must keep on mind that different structures are compared, therefore points which do not belong to both configurations are not taken into account to calculate MACs. However "usual"MAC values cannot be expected. Having attached an extra-item does influence a mode shape because body mass and damping are modified. Therefore, it is hard to find MAC values over 90% even if a couple of mode shapes resemble.

Different relations has been defined in the modes evolution diagram:

- **High correlation (**$MAC > 60\%$**)**: Modes highly correlated are joined by arrows.

- **Weak correlation (**$40\% < MAC < 60\%$**)**: Modes slightly correlated are joined by dotted arrows. The original mode, the one of the structure before the bolted item is added, suffers a strong modification.

- **New mode (**$MAC < 40\%$**)**: Modes not correlated to the ones from previous configuration. They are circled.

- **Swapped mode**: The modes order is modified due to a bolted item inclusion. They are surrounded by a polygon.

- **Unclear mode**: Hard-to-identify modes. They are marked by a sloping arrow.

In following subsections the influence of each bolted item is studied, to later summarize in the general results.

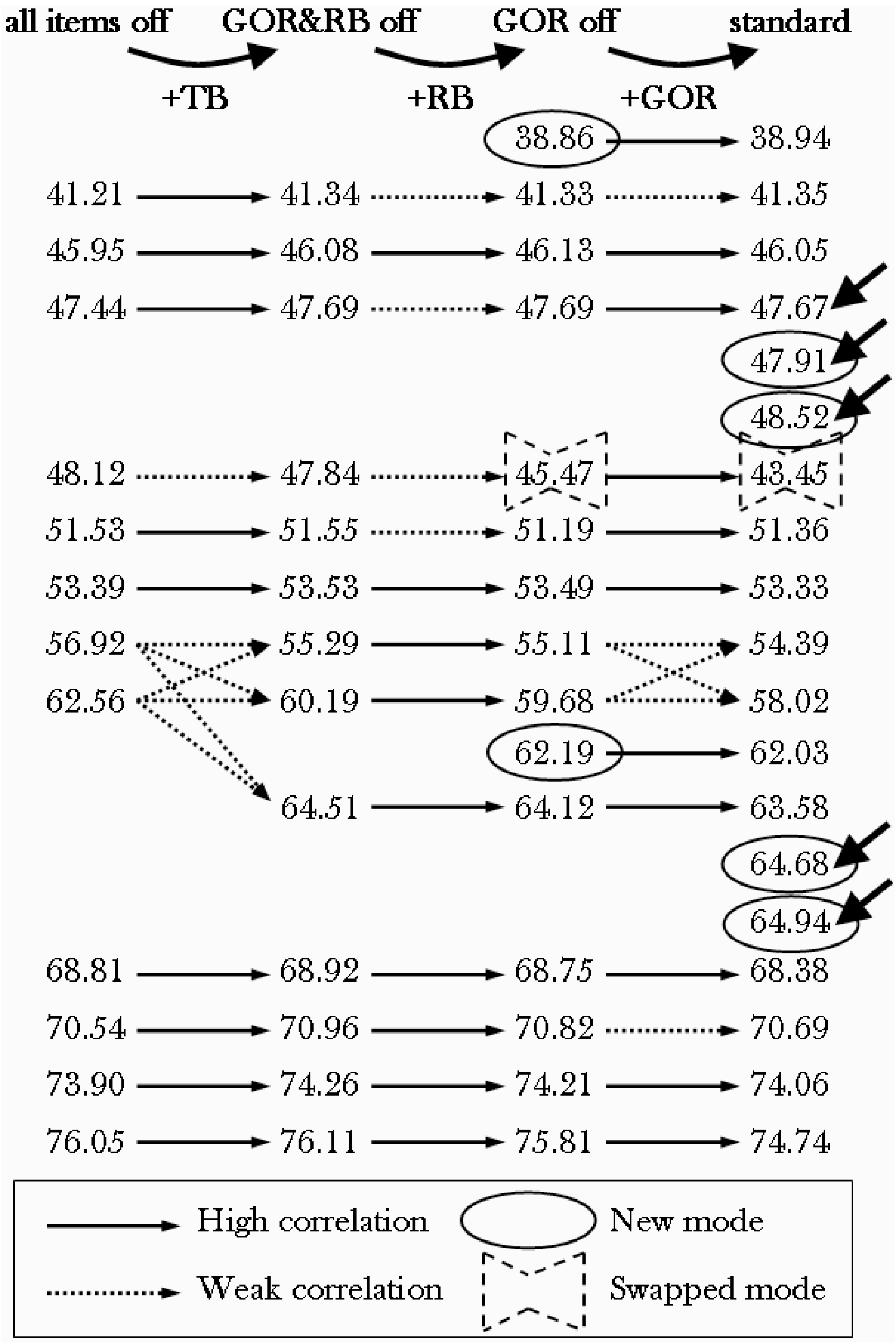

Figure 5.8: *Modes evolution diagram*

Tunnel brace influence

Tunnel brace (TB) is the bolted item less important. The modes evolution diagram highlights a higher contribution of the other items. Only three body modes, from the "all items off"configuration, are modified when TB is set on. Two body modes (56.92 and 62.56 Hz) experience coupling with a TB self-mode, yielding three body modes in the "GOR&RB off"configuration.

Radiator beam influence

Two modes (38.86 and 62.19 Hz) appear when the Radiator Beam (RB) is added. They are not correlated to any of the modes for the "GOR&RB off"configuration. In this case bolted item self-modes are not close (in frequency) to body modes. Therefore coupling phenomenon does not occur.

Four modes in the "GOR&RB off"configuration are strongly modified after adding the RB. It is of significance the case of the second one (47.84 Hz). One could think this mode is one of the unclear ones appearing in the standard configuration. However, modes evolution diagram shows how the mode is moved down in frequency due to RB effect. Indeed, it is swapped with the two previous modes (46.08 and 47.69 Hz) after setting the RB on.

Grill over-hanging reinforcement influence

The GOR is definitely the most influencing bolted item. Its heavier weight and its position might be the cause.

The addition of the GOR introduces four new body modes, probably GOR self-modes. It is also a matter of size, the bigger the bolted item is, the earlier its self-modes are found in frequency. Therefore, when a bigger bolted item is joined to the body, more new modes are found in the resulting structure. Additionally, four modes from the configuration without GOR are strongly modified.

General results

Modes evolution diagram is an optimal tool to track unclear modes. The sloping arrows in diagram mark them. They mainly appear for the standard configuration. As it was commented in section 5.4 they are situated in two different frequency areas, one around 48 Hz and the other one at 64 Hz.

Stabilization diagrams observation, together with the studies in section 5.2, discovered the key role of unclear modes in the inconsistency of modal analysis results. Avoiding them would probably improve the results accuracy, especially for the mode shapes estimation. The modes evolution diagram provides a straight answer to the problem.

Four of the five unclear modes appear when GOR is set on. Hence, modal analysis should be performed on BIGs excluding GOR. The other unclear mode, at 47.67 Hz, cannot be avoided as it comes from one of the modes from the plain body. Nevertheless this mode is not unclear when GOR is not on, as there is not coupling between itself and the modes introduced by the GOR.

The bolted items influence on body modes can be studied from another point of view. Chapter 1 explained the reason to include bolted items in the BIG concept. Their inclusion is meant to better account their influence on body stiffness. However, it was not clear whether the contribution to the stiffness is noticeable in the frequency range accessible for modal analysis. The modes evolution diagram can clarify this issue by the study of modes ”movement”when bolted items are included. In other words, by checking if modes are shifted up or down in frequency when bolted items are included. Damping factor variations have been studied as well.

Body modes are slightly shifted up in frequency when tunnel brace is attached. Damping ratio is also slightly increased. Therefore, it can be concluded that TB is adding stiffness to the body. Radiator beam effect is also moderate. In its case, modes are slimly shifted down in frequency and damping factors become lower. Hence, RB contributes mass rather than stiffness. Grill overhanging reinforcement is once again the most important bolted item.

From modes diagram can be clearly seen that GOR ”pushes down”body modes. Nevertheless, its influence on stiffness is small because damping factors are slightly decreased. Both characteristics determine a mass behavior. In short, bolted items contribution to stiffness cannot be considered important for the frequency range of interest. Therefore, it is not a concern to remove any of the bolted items to obtain more accurate results.

Chapter 6

Conclusions

MACOL programme has been successfully compared with PolyMAX software. Its operational capabilities has been proved although mode shapes could not be totally validated.

According to the results, modes can be consistently identified up to 75-77 Hz for all configurations. Nevertheless, a few modes, called unclear modes, do not yield consistent results in damping factors and mode shapes.

The dispersion of modes in frequency has been found as an innappropriate tool to study body modes influence. Therefore, conclusions are based on modes evolution observation. Modal analysis results stand out grill over-hanging reinforcement (GOR) as the most important bolted item. Its exclusion is suggested for further Modal Analysis tests in order to improve results consistency. Exclusion of both, tunnel brace (TB) and radiator beam (RB), is considered unnecessary.

Additionally, bolted items contribution to body stiffness has been analyzed. Radiator beam and tunnel brace seem to have slight effect on stiffness. The grill over-hanging reinforcement has some more influence although it is mass rather than spring behavior. In any case, the bolted items contribution to stiffness is very low to be an obstacle to remove any of the items.

Chapter 7

Future work

MACOL programme is left to be improved in several aspects. Mode shapes animation would complete the programme and provide the information necessary to fully validate its operation. Complex residuals should be implemented to improve synthesized FRFs fitting. In addition, programme development could be extended to shorten calculation time and to offer a "nicer"interface.

Further studies could be done related to results dispersion. The dispersion of modal assurance criterion (MAC) values could be calculated to better investigate the mode shapes relation to the inconsistency of modal analysis results.

Grill over-hanging reinforcement removal has been suggested for future modal analysis tests. It is advisable to quantify the advance obtained in results consistency due to grill over-hanging reinforcement removal. The variation of body performance in terms of stiffness should be quantified as well, in order to analyze its effect more deeply.

References

[1] Ewins, D.J.: *Modal testing: Theory and Practice* 2º ed., Research Studies Press Ltd., England, 2000

[2] Heylen, W., Lammens, S. and Sas, P.: *Modal Analysis Theory and Testing*, Katholieke Universiteit Leuven, Belgium, 1998

[3] Anderson, P.: *Signal Analysis*, Sound and vibration measurement lab instructions, Chalmers Tekniska Högskola, Göteborg, Sweden, 2005.

[4] Allemang, R.J.: *Vibrations: Experimental Modal Analysis*, Lecture notes, University of Cincinnati, Ohio, USA, 1999.

[5] Avitabile, P.: *Modal Analysis*, Lecture notes, University of Massachusetts Lowell

[6] Van der Auweraer, H., Guillaume, P., Verboven, P., Vanlanduit S.: *Application of a Fast-Stabilizing Frequency Domain Parameter Estimation Method*, ASME Journal of Dynamic Systems, Measurement, and Control, 651-658, 2001.

[7] Peeters, B., Guillaume, P., Van der Auweraer, H., Cauberghe, B., Verboven, P., Leuridan, J.: *Automotive and aerospace applications of the PolyMAX modal parameter estimation method*, in Proceedings of IMAC 22, Dearborn, USA, 2004.

[8] Guillaume, P., Verboven, P., Vanlanduit, S., Van der Auweraer, H., Peeters, B.: *A poly-reference implementation of the least-squares complex frequency-domain estimator*, in Proceedings of IMAC 21, Kissimmee, USA, 2003.

[9] LMS International: *LMS Polymax: A revolution in modal parameter estimation*, Leuven, Belgium, 2003.

[10] Williams, R., Crowley, J., Vold, H.: *The multivariate mode indicator function in Modal Analysis*, in Proceedings of IMAC 3, Orlando, USA, 1985.

[11] Verboven, P.: *Frequency-domain system identification for Modal Analysis*

[12] Schwarz, B.J., Richardson, M.H.: *Experimental Modal Analysis*, CSI Reliability Week, Orlando, USA, 1999.

[13] Andersson, P.: *Vibroacoustic measurement equipment at applied acoustics*, Lab instructions, Chalmers Tekniska Högskola, Göteborg, Sweden, 2004.

Appendix A

MACOL code structure

```
%%%%%%%%%%%%%%%%%%%%%%%%%%%%%%%%%%%%%%%%%%%%%%%%%%%%%%%%%%%%%%%%%%%%%%%%%%%
%%% MODAL ANALYSIS PROGRAMME: MACOL
%%% POLY-REFERENCE LEAST SQUARES COMPLEX FREQUENCY METHOD (p-LSCF == PolyMAX)
% Author: Miguel Colomo
% Project start date: 28-06-2007

% p-LSCF method is based on the right matrix-fraction model:
                                               % [H_calc(f)] = [B(f)]/[A(f)]
% p-LSCF fits the TFs by using the division of two matrices:
% - denominator matrix polynomial: [A(f)] = sum(capital_omega(f,r)*alfa(r))
% - numerator matrix polynomial: [B(f,o)] = sum(capital_omega(f,r)*beta(o,r))
%                      capital_omega(f,r) = exp(-j*2*pi*f*dt*r); (z-domain)

clear all; close all; clc;
global n_fig

disp('*****************************************************************')
disp('MACOL PROGRAMME')
disp('*****************************************************************')

% loading of: - measured H, transfer matrix: H = H(nf,i,o)
                             % (nf: frequency, i:input, o:output) ((m/s^2)/N)
%             - coherence matrix: coherence = coherence(nf,o)
%             - fa: frequency vector (Hz)
file_loading                          % script to load file from explorer
eval(['load ',matfilepath,matfile])

df = fa(2)-fa(1);                     % frequency step
No = size(H,3);                       % number of output signals
Ni = size(H,2);                       % number of input signals
nd = 25;                              % mean number of averages (in measurements)

% functions to show data in general:
% Multivariate Mode Indicator Function (MMIF) and Sum of the TFs (H_sum)
[MMIF,H_sum] = calc_MMIF_and_H_sum(H);% funtion to calculate MMIF and H sum

% modal analysis frequency range
disp('   ')
```

```
disp('--------------------------------------------------------------------')
disp('SELECTION OF FREQUENCY RANGE')
disp('   ')
% measurements data
disp('Choose the data to display select the frequency range:')
disp('   ')
disp('1. Single DOF')
disp('2. FRFs sum')
disp('3. MMIF')
data_display = input('Data chosen: ');
general_data_display                 % script to display general data
disp('   ')
f_min = input('Minimum frequency: ');
f_max = input('Maximum frequency: ');

% avoid first frequency component (f = 0)
if f_min == 0
   f_min = f_min + df;
end

% set of the variables according to the frequency range
i_f = find(fa>=f_min & fa<=f_max);
H = H(i_f,:,:); fa = fa(i_f); MMIF = MMIF(i_f);
coherence = coherence(i_f,:); H_sum = H_sum(i_f);

Nf = length(fa);                     % number of frequency components
dt = 1/(2*Nf*df);                    % sampling time
omega = 2*pi*fa;                     % (rad/s)

%%%%%%%%%%%%%%%%%%%%%%%%%%%%%%%%%%%%%%%%%%%%%%%%%%%%%%%%%%%%%%%%%%%%%%%%%%%
% MACOL (Part1): CALCULATION OF DENOMINATOR POLYNOMIAL,
%                  POLES AND MODAL PARTICIPATION FACTORS
% select range of polynomial order
clc
disp('--------------------------------------------------------------------')
disp('MACOL (Part1): CALCULATION OF POLES AND MODAL PARTICIPATION FACTORS')
disp('   ')
p_min = input('Minimum polynomial order: ');     % minimum polinomial order
p_max = input('Maximum polynomial order: ');     % maximum polinomial order
% polynomial basis functions (capital_omega)
r = 0:p_max;
capital_omega = zeros(Nf,p_max+1);
for k = 1:p_max+1
    capital_omega(:,k) = exp(-j*dt*(omega-omega(1))*r(k));
end
% weighting factor calculation (w)
    % 1. No weighting
    % 2. Depending on coherence
weighting = 1;
if weighting == 2
   w = weighting_func(Nf,nd,No,H,coherence);     % function to calculate w
else w = ones(length(fa),No);
end
```

```
% building up the reduced normal equations matrix (intermediate calculations)
M = red_normal_eq(Nf,Ni,No,H,w,capital_omega,p_max);
% red_normal_eq: function to estimate reduced normal equations matrix

% calculation of the denominator-matrix coefficients and poles for different
% modal orders
figure(2)
fig2 = gcf;
set(fig2,'position',[0 200 1280 600]);
[lambda_matrix,L_matrix,n_poles] = sys_poles(M,Ni,No,p_max,p_min,f_max,f_min,dt);
% sys_poles: function to calculate system poles for different polynomial
% orders and to plot stabilization diagrams
% lambda_matrix: poles calculated for each polynomial orders
% L_matrix: modal participation factors calculated for each polynomial orders
% n_poles: number of poles found for each polynomial order

% stabilization diagram background
% - 1. Single DOF
% - 2. FRFs sum
% - 3. MMIF
background = 2;                     % default background
background_display                  % script to plot background

% select the stable poles by using the stabilization diagram
lambdas = []; Ls = [];
disp('   ')
disp('---------------------------------------------------------------------')
disp('SELECTION OF STABLE POLES')
disp('   ')
disp('Note: Press just enter in case all the poles are already introduced')
disp('   ')
fr = input('Pole frequency (X-component): ');
p = input('Polynomail order (Y-component): ');
while length(p) == 1
      [f_diff2,i_f_pole] =  ...
          min(abs(imag(lambda_matrix(1:n_poles(p_max-p+1),p_max-p+1)) ...
          /(2*pi)-fr*ones(n_poles(p_max-p+1),1)));
      lambdas = [lambdas lambda_matrix(i_f_pole,p_max-p+1)]; % laplace poles
      Ls = [Ls L_matrix(:,i_f_pole,p_max-p+1)]; % modal participation factor
      disp('   ')
      fr = input('Pole frequency (X-component): ');
      p = input('Polynomail order (Y-component): ');
end
frs = imag(lambdas)/(2*pi);           % resonance frequencies
etas = -real(lambdas)./abs(lambdas);  % resonance damping ratios
n = length(lambdas);                  % number of resonance frequencies

% list of poles display
clc
poles_display                       % script to display the poles on screen
pause

%%%%%%%%%%%%%%%%%%%%%%%%%%%%%%%%%%%%%%%%%%%%%%%%%%%%%%%%%%%%%%%%%%%%%%%%%%%%
% MACOL (Part2):  MODAL PARAMETER EXTRATION AND RESULTS
```

```
[mode_shapes,UR,LR,H_synt] = modal_extra(H,fa,lambdas,Ls,Nf,Ni,No,n);
% modal_extra: function to extract modal parameters
% mode_shapes
% UR,LR: upper and lower residuals
% H_synt: synthesized FRFs

% plot transfer functions
n_fig = 3;
results_display                      % script to display the results
% list of poles display
clc
poles_display
% modal assurance criterion (MAC)
MAC = calc_MAC(mode_shapes,mode_shapes,n,n_fig) % function to calculate auto-MAC
n_fig = n_fig+1;
% correlation and normalised error
[corr,norm_error] = calc_corr_and_norm_error(H,H_synt,No,Ni);
% calc_corr_and_norm_error: function to calculate correlation and error
disp('   ')
disp('-------------------------------------------------------------------')
disp('ACCURACY OF THE SYNTHESIZED VTF')
disp('   ')
disp(['Correlation: ' num2str(mean(mean(corr,2)))])
disp(['Normalized error: ' num2str(mean(mean(norm_error,2)))])
% modal phase collinearity
MPC = calc_MPC(mode_shapes,n,No);
% calc_MPC: function to calculate MPC values

% re-calculation
disp('   ')
disp('-------------------------------------------------------------------')
disp('RE-CALCULATION')
disp('   ')
recalculation = input('Press 1 if you would like to change some poles: ');
while recalculation == 1
      disp('   ')
      poles_display
      remove_pole = input('Press 1 if you would like to remove some poles: ');
      while remove_pole == 1
            n_pole = input('Pole number you would like to remove: ');
            lambdas(n_pole) = []; Ls(:,n_pole) = [];
            remove_pole = input('Press 1 if you want to remove more poles: ');
      end
      frs = imag(lambdas)/(2*pi);           % resonance frequencies
      etas = -real(lambdas)./abs(lambdas);  % resonance damping ratios
      n = length(lambdas);                  % number of resonance frequencies
      disp('   ')
      poles_display
      one_more_pole = input('Press 1 if you would like to change some poles: ');
      while one_more_pole == 1
            disp('   ')
            n_pole = input('Introduce pole number you would like to change: ');
            disp('   ')
            disp('Introduce new data')
```

```
            disp('   ')
            fr = input('Pole frequency (X-component): ');
            p = input('Polynomail order (Y-component): ');
            [f_diff,i_f_pole] = ...
                min(abs(imag(lambda_matrix(1:n_poles(p_max-p+1),p_max-p+1))/ ...
                (2*pi)-fr));
            lambdas(n_pole) = lambda_matrix(i_f_pole,p_max-p+1);
            Ls(:,n_pole) = L_matrix(:,i_f_pole,p_max-p+1);
            one_more_pole = input('Press 1 if you want to change more poles: ');
      end
    frs = imag(lambdas)/(2*pi);           % resonance frequencies
    etas = -real(lambdas)./abs(lambdas);  % resonance damping ratios
    n = length(lambdas);                  % number of resonance frequencies
    % modal parameter extration re-calculation
    [mode_shapes,UR,LR,H_synt] = modal_extra(H,fa,lambdas,Ls,Nf,Ni,No,n);
    results_display
    % list of poles display
    clc
    poles_display
    % modal assurance criterion (MAC)
    MAC = calc_MAC(mode_shapes,mode_shapes,n,n_fig)
    n_fig = n_fig + 1;
    % modal phase collinearity
    MPC = calc_MPC(mode_shapes,n,No);
    % correlation and normalised error
    [corr,norm_error] = calc_corr_and_norm_error(H,H_synt,No,Ni);
    disp('   ')
    disp('-------------------------------------------------------------------')
    disp('ACCURACY OF THE SYNTHESIZED VTF')
    disp('   ')
    disp(['Correlation: ' num2str(mean(mean(corr,2)))])
    disp(['Normalized error: ' num2str(mean(mean(norm_error,2)))])
    disp('   ')
    recalculation = input('Press 1 if you would like to calculate once again: ');
end

save Modal_Analysis_Results UR LR H_synt corr norm_error frs etas MAC MPC mode_shapes

clear all;
```

Appendix B

Mode shapes validation

Mode shapes amplitude for mode at 47.79 Hz, according to LMS, and at 47.69 Hz, according to MACOL. Results extracted for the configuration without GOR and RB from BIG3. Mode shapes units can be derived from equation 3.16, where modal participation factors have same units as mode shapes. Therefore, mode shapes units are $\sqrt{\frac{s}{kg}}$.

	LMS	PolyMAX	Error (%)		LMS	PolyMAX	Error (%)
Body:111:+X	1,73E-06	1,51E-06	12,7	**Body:121:+Z**	4,08E-06	1,51E-06	12,7
Body:111:+Y	9,78E-06	7,73E-06	20,9	**Body:122:+X**	5,82E-07	7,73E-06	20,9
Body:111:+Z	5,11E-06	4,23E-06	17,2	**Body:122:+Y**	1,29E-06	4,23E-06	17,2
Body:112:+X	9,99E-07	9,53E-07	4,6	**Body:122:+Z**	2,70E-06	9,53E-07	4,6
Body:112:+Y	1,05E-05	8,31E-06	20,8	**Body:123:+X**	1,06E-06	8,31E-06	20,8
Body:112:+Z	2,29E-06	1,88E-06	17,8	**Body:123:+Y**	5,25E-07	1,88E-06	17,8
Body:113:+X	1,09E-06	9,96E-07	8,3	**Body:123:+Z**	2,14E-06	9,96E-07	8,3
Body:113:+Y	5,48E-06	4,29E-06	21,6	**Body:124:+X**	7,58E-07	4,29E-06	21,6
Body:113:+Z	3,75E-06	3,27E-06	12,9	**Body:124:+Y**	1,53E-06	3,27E-06	12,9
Body:114:+X	1,33E-06	1,21E-06	9,1	**Body:124:+Z**	2,92E-06	1,21E-06	9,1
Body:114:+Y	1,85E-06	1,35E-06	27,1	**Body:125:+X**	1,30E-06	1,35E-06	27,1
Body:114:+Z	2,46E-06	2,26E-06	8,2	**Body:125:+Y**	5,99E-06	2,26E-06	8,2
Body:115:+X	9,48E-07	9,20E-07	3,0	**Body:125:+Z**	1,67E-06	9,20E-07	3,0
Body:115:+Y	1,19E-06	9,31E-07	21,9	**Body:126:+X**	9,45E-07	9,31E-07	21,9
Body:115:+Z	2,03E-06	2,14E-06	5,6	**Body:126:+Y**	1,46E-06	2,14E-06	5,6
Body:116:+X	1,56E-06	1,25E-06	20,1	**Body:126:+Z**	2,37E-06	1,25E-06	20,1
Body:116:+Y	4,43E-06	3,32E-06	25,0	**Body:127:+X**	1,30E-06	3,32E-06	25,0
Body:116:+Z	3,52E-06	3,03E-06	13,8	**Body:127:+Y**	1,10E-06	3,03E-06	13,8
Body:117:+X	1,02E-06	8,36E-07	18,3	**Body:127:+Z**	1,37E-06	8,36E-07	18,3
Body:117:+Y	4,44E-07	3,41E-07	23,2	**Body:128:+X**	1,44E-06	3,41E-07	23,2
Body:117:+Z	2,39E-06	2,49E-06	4,3	**Body:128:+Y**	1,14E-06	2,49E-06	4,3
Body:118:+X	1,02E-06	9,43E-07	7,2	**Body:128:+Z**	2,28E-06	9,43E-07	7,2
Body:118:+Y	4,09E-07	3,19E-07	22,2	**Body:129:+X**	1,64E-06	3,19E-07	22,2
Body:118:+Z	2,09E-06	2,20E-06	5,3	**Body:129:+Y**	1,17E-06	2,20E-06	5,3
Body:119:+X	3,26E-07	3,15E-07	3,6	**Body:129:+Z**	3,58E-06	3,15E-07	3,6
Body:119:+Y	8,08E-07	6,61E-07	18,1	**Body:130:+X**	1,15E-06	6,61E-07	18,1
Body:119:+Z	2,39E-06	2,51E-06	4,9	**Body:130:+Y**	1,04E-06	2,51E-06	4,9
Body:120:+X	1,16E-06	1,21E-06	4,5	**Body:130:+Z**	3,57E-06	1,21E-06	4,5
Body:120:+Y	3,73E-06	3,53E-06	5,3	**Body:131:+X**	1,33E-06	3,53E-06	5,3
Body:120:+Z	3,43E-06	3,70E-06	8,0	**Body:131:+Y**	1,04E-06	3,70E-06	8,0
Body:121:+X	1,51E-06	1,59E-06	5,2	**Body:131:+Z**	5,27E-06	1,59E-06	5,2
Body:121:+Y	4,66E-06	4,46E-06	4,4	**Body:132:+X**	6,66E-06	4,46E-06	4,4
Body:121:+Z	4,08E-06	4,42E-06	8,2	**Body:132:+Y**	2,98E-06	4,42E-06	8,2

Body:216:+Y	4,09E-06	3,09E-06	24,3	**Body:312:+Z**	6,18E-06	6,80E-06	10,0
Body:216:+Z	2,67E-06	2,18E-06	18,3	**Body:313:+X**	1,56E-06	1,53E-06	1,9
Body:217:+X	7,15E-07	6,26E-07	12,4	**Body:313:+Y**	9,63E-07	9,96E-07	3,4
Body:217:+Y	2,09E-07	1,46E-07	30,2	**Body:313:+Z**	4,26E-06	4,68E-06	9,9
Body:217:+Z	1,55E-06	1,30E-06	16,2	**Body:314:+X**	2,45E-07	2,64E-07	8,0
Body:218:+X	1,05E-06	9,28E-07	11,4	**Body:314:+Y**	4,86E-06	4,98E-06	2,4
Body:218:+Y	3,71E-07	2,48E-07	33,3	**Body:314:+Z**	2,34E-06	1,78E-06	23,9
Body:218:+Z	1,74E-06	1,77E-06	1,4	**Body:315:+X**	7,36E-06	7,60E-06	3,2
Body:219:+X	2,08E-07	1,00E-07	51,7	**Body:315:+Y**	3,11E-06	3,19E-06	2,5
Body:219:+Y	7,61E-07	5,38E-07	29,2	**Body:315:+Z**	2,93E-05	3,05E-05	4,1
Body:219:+Z	1,59E-06	1,26E-06	20,4	**Body:316:+X**	8,40E-06	8,84E-06	5,2
Body:220:+X	1,23E-06	1,07E-06	12,8	**Body:316:+Y**	4,41E-07	4,69E-07	6,3
Body:220:+Y	3,04E-06	2,86E-06	6,1	**Body:316:+Z**	3,83E-06	3,61E-06	5,8
Body:220:+Z	3,16E-06	2,98E-06	5,8	**Body:317:+X**	6,08E-07	5,63E-07	7,4
Body:221:+X	1,44E-06	1,37E-06	4,9	**Body:317:+Y**	2,10E-07	1,99E-07	5,0
Body:221:+Y	4,16E-06	4,12E-06	0,9	**Body:317:+Z**	6,27E-06	6,78E-06	8,2
Body:221:+Z	3,80E-06	3,85E-06	1,3	**Body:318:+X**	1,18E-06	1,25E-06	6,2
Body:222:+X	8,98E-07	8,45E-07	5,8	**Body:318:+Y**	1,57E-06	1,59E-06	1,0
Body:222:+Y	9,50E-07	5,12E-07	46,2	**Body:318:+Z**	2,46E-06	2,45E-06	0,3
Body:222:+Z	2,60E-06	2,68E-06	2,9	**Body:319:+X**	8,02E-07	8,22E-07	2,5
Body:223:+X	1,02E-06	9,33E-07	8,7	**Body:319:+Y**	3,48E-06	3,76E-06	8,1
Body:223:+Y	5,70E-07	4,52E-07	20,7	**Body:319:+Z**	2,59E-06	2,19E-06	15,5
Body:223:+Z	1,30E-06	1,12E-06	13,1	**Body:320:+X**	2,83E-06	3,18E-06	12,4
Body:224:+X	6,34E-07	7,75E-07	22,4	**Body:320:+Y**	6,53E-06	7,06E-06	8,1
Body:224:+Y	1,56E-06	1,22E-06	21,7	**Body:320:+Z**	8,17E-06	8,82E-06	8,0
Body:224:+Z	2,15E-06	1,77E-06	17,4	**Body:321:+X**	1,59E-06	1,63E-06	2,6
Body:213:+Y	5,74E-06	4,39E-06	23,4	**Body:233:+Z**	3,95E-06	4,38E-06	10,9
Body:213:+Z	3,58E-06	2,90E-06	18,9	**Body:241:+X**	7,57E-07	7,54E-07	0,3
Body:214:+X	8,71E-07	8,39E-07	3,6	**Body:241:+Y**	1,44E-06	1,17E-06	18,7
Body:214:+Y	2,20E-06	1,66E-06	24,8	**Body:241:+Z**	1,73E-06	1,38E-06	20,0
Body:214:+Z	2,17E-06	1,75E-06	19,2	**Body:311:+X**	2,11E-06	2,19E-06	3,7
Body:215:+X	8,46E-07	8,41E-07	0,6	**Body:311:+Y**	6,69E-07	6,38E-07	4,6
Body:215:+Y	1,21E-06	1,02E-06	15,8	**Body:311:+Z**	5,91E-06	6,46E-06	9,3
Body:215:+Z	1,32E-06	1,17E-06	11,3	**Body:312:+X**	1,25E-06	1,22E-06	2,0
Body:216:+X	1,17E-06	1,01E-06	13,3	**Body:312:+Y**	1,64E-07	1,92E-07	17,0
Body:216:+Y	4,09E-06	3,09E-06	24,3	**Body:312:+Z**	6,18E-06	6,80E-06	10,0
Body:216:+Z	2,67E-06	2,18E-06	18,3	**Body:313:+X**	1,56E-06	1,53E-06	1,9
Body:217:+X	7,15E-07	6,26E-07	12,4	**Body:313:+Y**	9,63E-07	9,96E-07	3,4
Body:217:+Y	2,09E-07	1,46E-07	30,2	**Body:313:+Z**	4,26E-06	4,68E-06	9,9
Body:217:+Z	1,55E-06	1,30E-06	16,2	**Body:314:+X**	2,45E-07	2,64E-07	8,0
Body:218:+X	1,05E-06	9,28E-07	11,4	**Body:314:+Y**	4,86E-06	4,98E-06	2,4
Body:218:+Y	3,71E-07	2,48E-07	33,3	**Body:314:+Z**	2,34E-06	1,78E-06	23,9
Body:218:+Z	1,74E-06	1,77E-06	1,4	**Body:315:+X**	7,36E-06	7,60E-06	3,2
Body:219:+X	2,08E-07	1,00E-07	51,7	**Body:315:+Y**	3,11E-06	3,19E-06	2,5
Body:219:+Y	7,61E-07	5,38E-07	29,2	**Body:315:+Z**	2,93E-05	3,05E-05	4,1
Body:219:+Z	1,59E-06	1,26E-06	20,4	**Body:316:+X**	8,40E-06	8,84E-06	5,2
Body:220:+X	1,23E-06	1,07E-06	12,8	**Body:316:+Y**	4,41E-07	4,69E-07	6,3
Body:220:+Y	3,04E-06	2,86E-06	6,1	**Body:316:+Z**	3,83E-06	3,61E-06	5,8
Body:220:+Z	3,16E-06	2,98E-06	5,8	**Body:317:+X**	6,08E-07	5,63E-07	7,4
Body:221:+X	1,44E-06	1,37E-06	4,9	**Body:317:+Y**	2,10E-07	1,99E-07	5,0
Body:221:+Y	4,16E-06	4,12E-06	0,9	**Body:317:+Z**	6,27E-06	6,78E-06	8,2
Body:221:+Z	3,80E-06	3,85E-06	1,3	**Body:318:+X**	1,18E-06	1,25E-06	6,2
Body:222:+X	8,98E-07	8,45E-07	5,8	**Body:318:+Y**	1,57E-06	1,59E-06	1,0
Body:222:+Y	9,50E-07	5,12E-07	46,2	**Body:318:+Z**	2,46E-06	2,45E-06	0,3
Body:222:+Z	2,60E-06	2,68E-06	2,9	**Body:319:+X**	8,02E-07	8,22E-07	2,5
Body:223:+X	1,02E-06	9,33E-07	8,7	**Body:319:+Y**	3,48E-06	3,76E-06	8,1
Body:223:+Y	5,70E-07	4,52E-07	20,7	**Body:319:+Z**	2,59E-06	2,19E-06	15,5
Body:223:+Z	1,30E-06	1,12E-06	13,1	**Body:320:+X**	2,83E-06	3,18E-06	12,4
Body:224:+X	6,34E-07	7,75E-07	22,4	**Body:320:+Y**	6,53E-06	7,06E-06	8,1
Body:224:+Y	1,56E-06	1,22E-06	21,7	**Body:320:+Z**	8,17E-06	8,82E-06	8,0
Body:224:+Z	2,15E-06	1,77E-06	17,4	**Body:321:+X**	1,59E-06	1,63E-06	2,6

Body:321:+Y	6,96E-07	6,50E-07	6,6	**Body:419:+X**	8,63E-07	7,29E-07	15,5
Body:321:+Z	6,02E-06	6,58E-06	9,3	**Body:419:+Y**	4,17E-06	4,51E-06	8,1
Body:322:+X	1,68E-06	1,71E-06	2,1	**Body:419:+Z**	3,71E-06	4,05E-06	9,0
Body:322:+Y	1,13E-06	8,06E-07	28,6	**Body:420:+X**	2,84E-06	3,29E-06	15,6
Body:322:+Z	2,94E-06	3,15E-06	7,3	**Body:420:+Y**	6,65E-06	7,24E-06	8,9
Body:323:+X	1,20E-06	1,13E-06	6,1	**Body:420:+Z**	1,00E-05	1,11E-05	10,5
Body:323:+Y	2,40E-06	1,87E-06	21,9	**Body:418:+Z**	1,78E-06	1,56E-06	12,5
Body:323:+Z	6,45E-06	6,83E-06	5,9	**Body:421:+X**	1,70E-06	1,71E-06	0,9
Body:324:+X	2,58E-06	2,82E-06	9,4	**Body:421:+Y**	8,24E-07	8,61E-07	4,4
Body:324:+Y	9,58E-07	8,95E-07	6,6	**Body:421:+Z**	5,11E-06	5,21E-06	2,0
Body:324:+Z	7,92E-06	9,08E-06	14,6	**Body:422:+X**	1,51E-06	1,44E-06	4,7
Body:325:+X	1,30E-05	1,45E-05	11,7	**Body:422:+Y**	1,02E-06	6,71E-07	34,1
Body:325:+Y	3,27E-07	2,78E-07	14,9	**Body:422:+Z**	2,03E-06	1,61E-06	20,3
Body:325:+Z	4,41E-06	4,76E-06	8,0	**Body:423:+X**	1,14E-06	8,17E-07	28,1
Body:326:+X	5,37E-06	6,17E-06	14,9	**Body:423:+Y**	2,32E-06	1,75E-06	24,6
Body:326:+Y	1,71E-06	1,57E-06	8,1	**Body:423:+Z**	8,92E-06	9,83E-06	10,1
Body:326:+Z	1,36E-05	1,48E-05	9,4	**Body:424:+X**	2,17E-06	2,58E-06	18,9
Body:327:+X	7,77E-07	9,43E-07	21,4	**Body:424:+Y**	1,03E-06	9,08E-07	11,6
Body:327:+Y	3,71E-06	3,84E-06	3,4	**Body:424:+Z**	9,83E-06	1,08E-05	9,4
Body:327:+Z	1,45E-05	1,68E-05	15,6	**Body:425:+X**	6,85E-07	8,95E-07	30,8
Body:328:+X	1,57E-06	7,00E-07	55,4	**Body:425:+Y**	1,03E-05	1,14E-05	10,3
Body:328:+Y	6,70E-07	9,92E-06	1381,1	**Body:425:+Z**	8,08E-06	8,85E-06	9,5
Body:328:+Z	3,73E-06	6,65E-06	78,5	**Fwin:601:+X**	3,23E-07	8,22E-06	2442,8
Body:411:+X	2,01E-06	2,04E-06	1,8	**Fwin:601:+Y**	8,95E-07	5,36E-07	40,1
Body:411:+Y	6,28E-07	5,84E-07	7,0	**Fwin:601:+Z**	7,67E-06	3,57E-05	366,2
Body:411:+Z	5,40E-06	5,82E-06	7,8	**Fwin:602:+X**	3,37E-07	2,31E-07	31,5
Body:412:+X	8,60E-07	6,87E-07	20,0	**Fwin:602:+Y**	1,07E-06	6,48E-07	39,6
Body:412:+Y	2,59E-08	7,17E-08	176,6	**Fwin:602:+Z**	7,60E-06	7,59E-06	0,1
Body:412:+Z	5,30E-06	5,33E-06	0,7	**Fwin:603:+X**	1,04E-06	2,65E-07	74,4
Body:413:+X	1,57E-06	1,50E-06	4,8	**Fwin:603:+Y**	1,34E-06	9,20E-07	31,4
Body:413:+Y	6,70E-07	7,39E-07	10,5	**Fwin:603:+Z**	1,50E-05	7,82E-06	48,0
Body:413:+Z	3,73E-06	3,64E-06	2,3	**Fwin:604:+X**	9,91E-07	9,50E-07	4,1
Body:414:+X	3,11E-07	3,46E-07	11,5	**Fwin:604:+Y**	1,18E-06	1,17E-06	0,6
Body:414:+Y	6,64E-06	6,88E-06	3,7	**Fwin:604:+Z**	1,42E-05	1,51E-05	6,0
Body:414:+Z	3,39E-06	3,42E-06	0,8	**Pshe:642:+X**	7,69E-06	9,20E-07	88,0
Body:415:+X	7,09E-06	7,21E-06	1,7	**Pshe:642:+Y**	5,28E-07	1,04E-06	97,7
Body:415:+Y	2,55E-06	2,67E-06	4,6	**Pshe:642:+Z**	3,39E-05	1,45E-05	57,2
Body:415:+Z	2,88E-05	2,94E-05	1,9	**Rwin:621:+X**	2,27E-06	2,28E-06	0,5
Body:416:+X	8,27E-06	8,85E-06	7,0	**Rwin:621:+Y**	3,82E-07	4,31E-07	12,9
Body:416:+Y	8,44E-07	9,28E-07	9,9	**Rwin:621:+Z**	9,94E-06	1,03E-05	3,5
Body:416:+Z	5,04E-06	5,50E-06	9,2	**Rwin:622:+X**	1,81E-06	1,89E-06	4,1
Body:417:+X	9,28E-07	8,35E-07	10,0	**Rwin:622:+Y**	1,20E-06	1,24E-06	2,7
Body:417:+Y	4,46E-07	5,04E-07	12,9	**Rwin:622:+Z**	9,91E-06	9,90E-06	0,1
Body:417:+Z	5,34E-06	5,51E-06	3,1	**Rwin:627:+X**	2,28E-06	2,34E-06	2,7
Body:418:+X	1,38E-06	1,37E-06	0,9	**Rwin:627:+Y**	8,02E-07	8,18E-07	1,9
Body:418:+Y	2,80E-06	2,84E-06	1,4	**Rwin:627:+Z**	1,83E-06	1,61E-06	12,1
						Avg Error	**19,8**

Figure B.1: *PolyMAX and MACOL comparison of mode shapes amplitudes*

Appendix C

Response points

The response points are labeled by four characters and three numbers. The characters represent the body part the point belongs to. There are seven different parts: Gorf (Grill Over-Hanging Reinforcement), Bbar (Bunny bar = radiator beam), Body (main structure), Pshe (Parcel Shelf), Fwin (Front Window), Rwin (Rear window) and Roof (top part of the roof). The first figure of the number is different depending on the body part: 1 (left front half), 2 (right front half), 3 (left rear half), 4 (left rear half), 5 (Gorf & Bbar) and 6 (Pshe & Roof). No number is coincident.

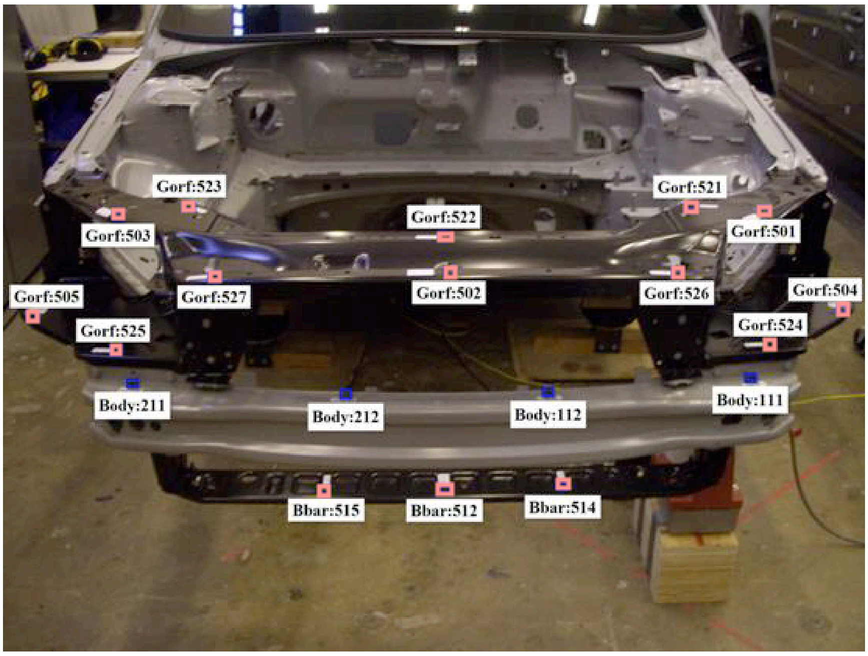

Figure C.1: *GOR&RB points*

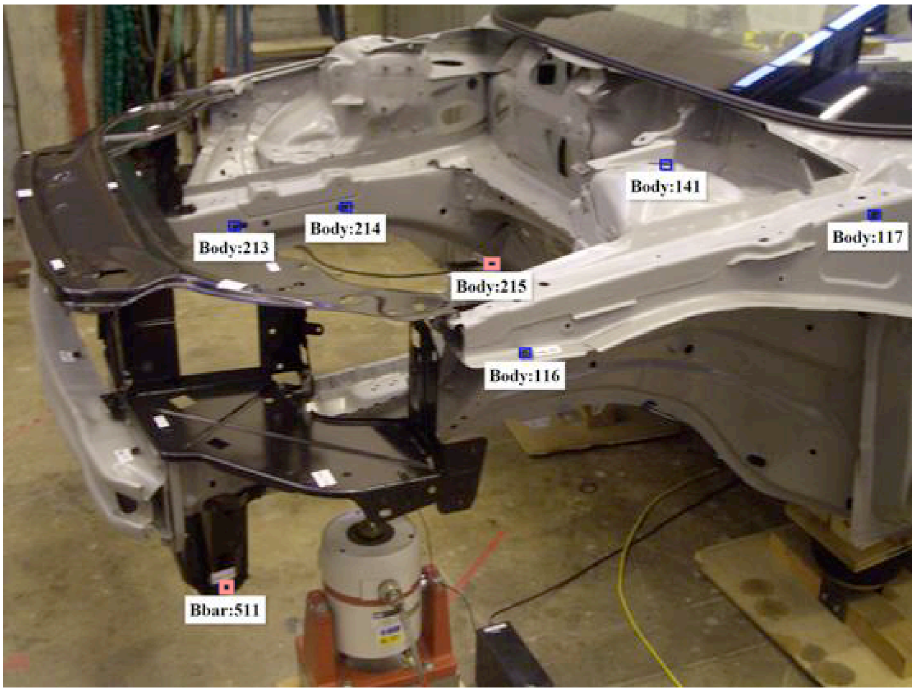

Figure C.2: *Left front side points*

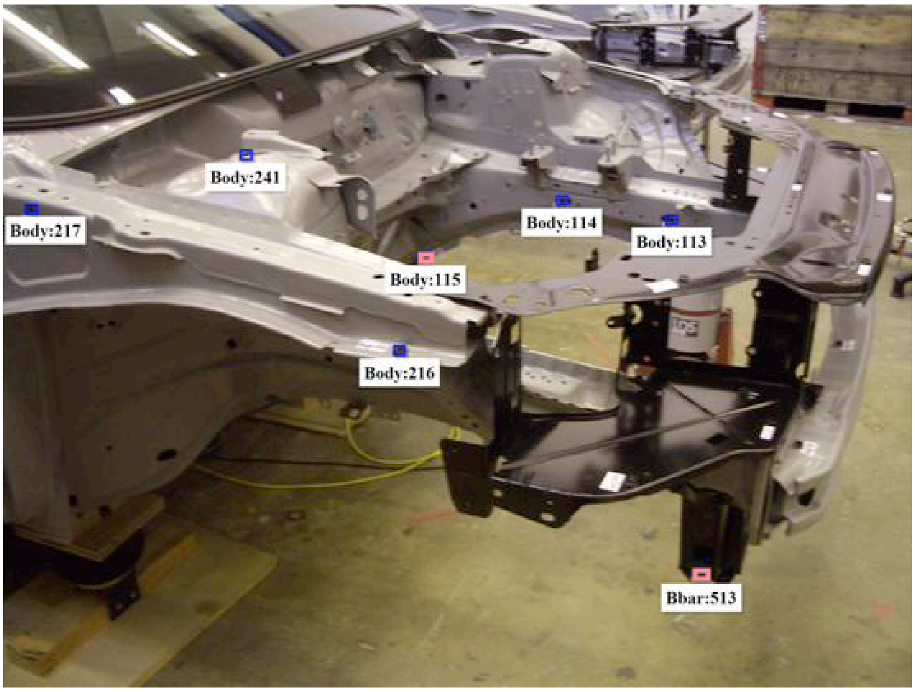

Figure C.3: *Right front side points*

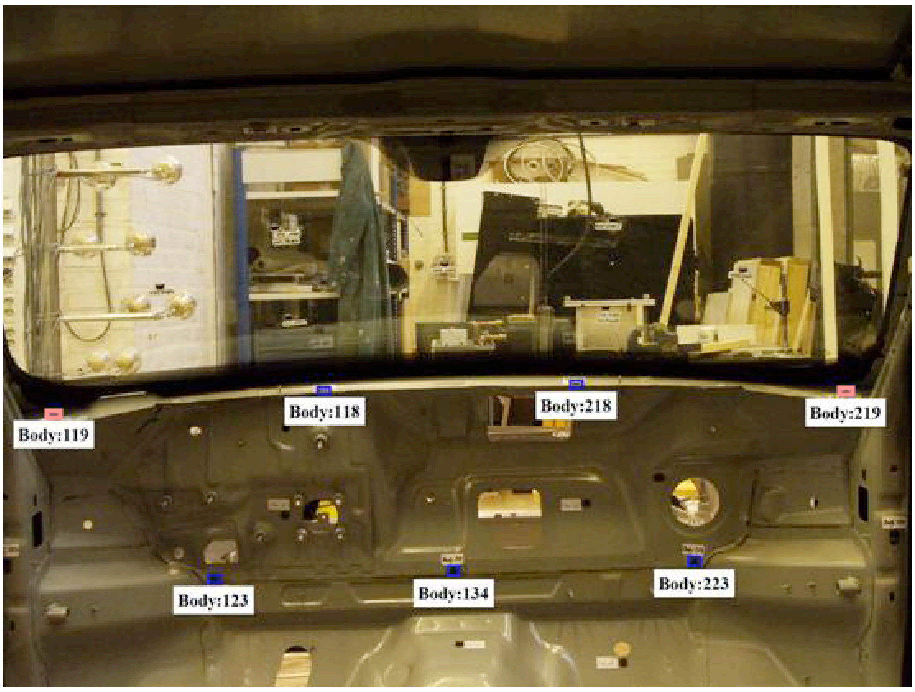

Figure C.4: *Firewall points*

Figure C.5: *Front roof points*

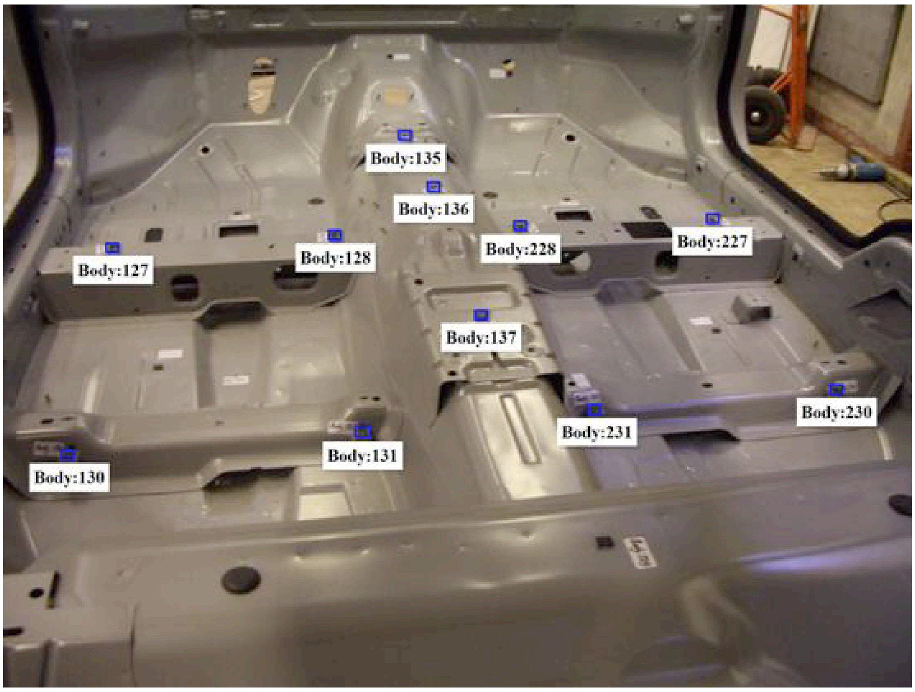

Figure C.6: *Front floor points*

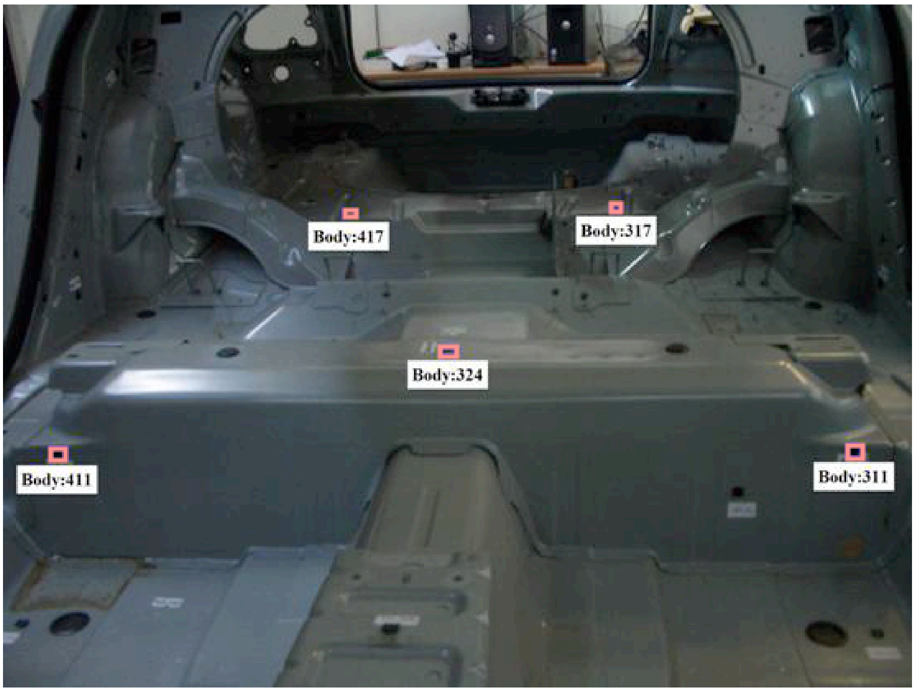

Figure C.7: *Rear floor points*

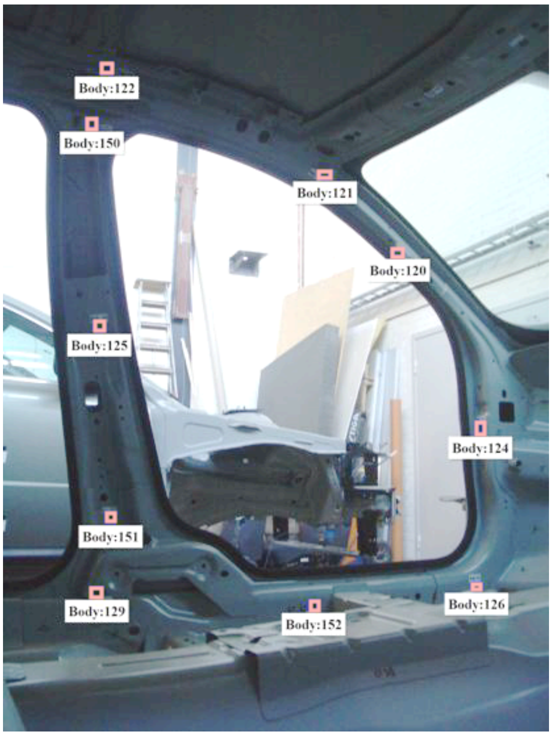

Figure C.8: *Left front door points*

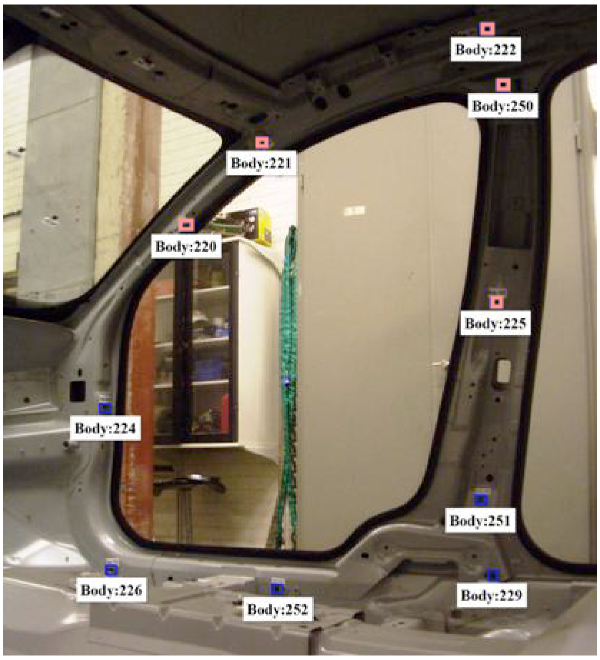

Figure C.9: *Right front door points*

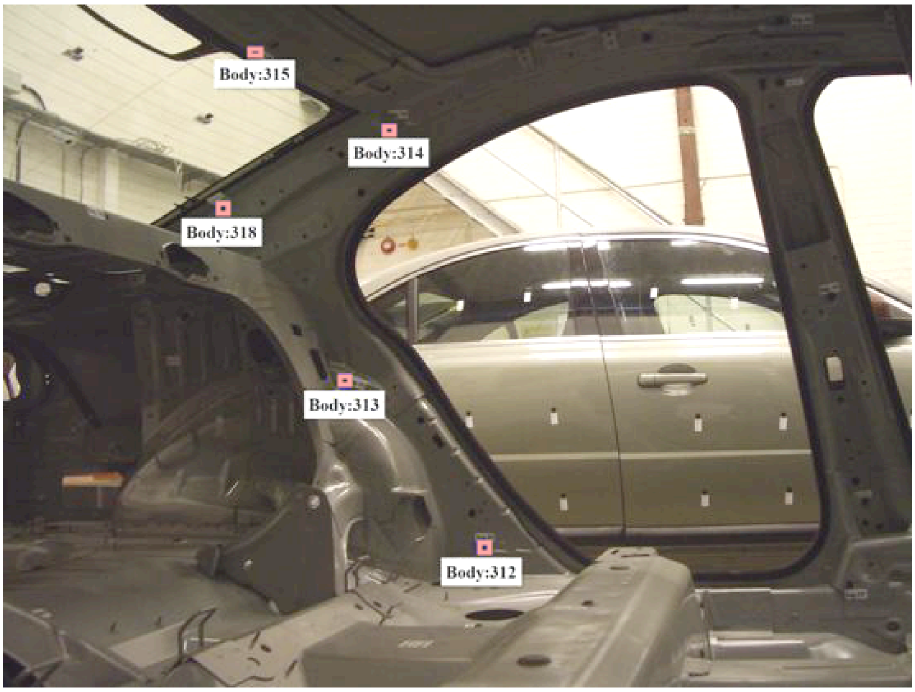

Figure C.10: *Left rear door points*

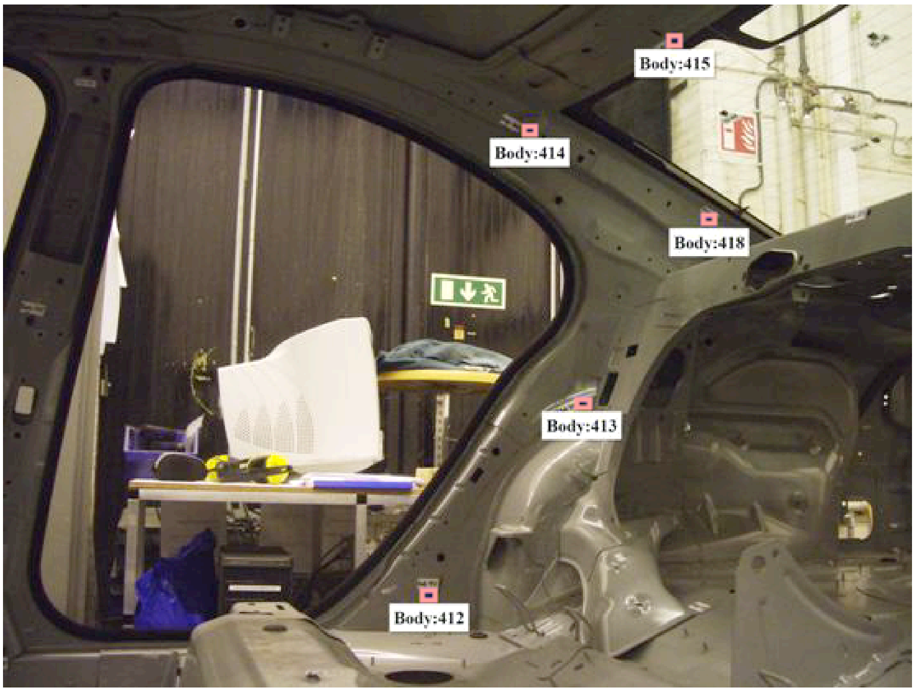

Figure C.11: *Right rear door points*

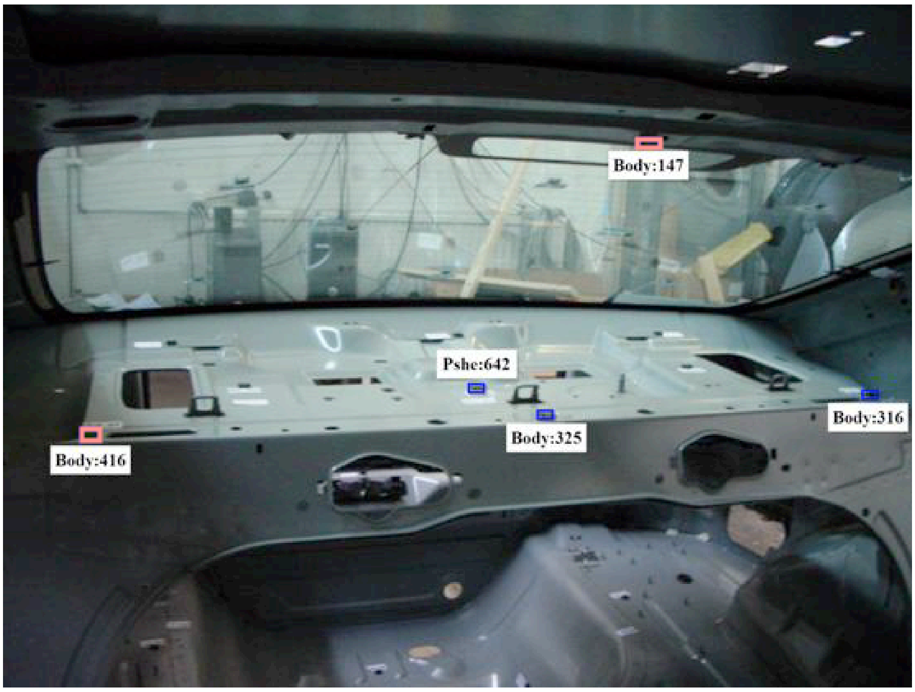

Figure C.12: *Cabin back points*

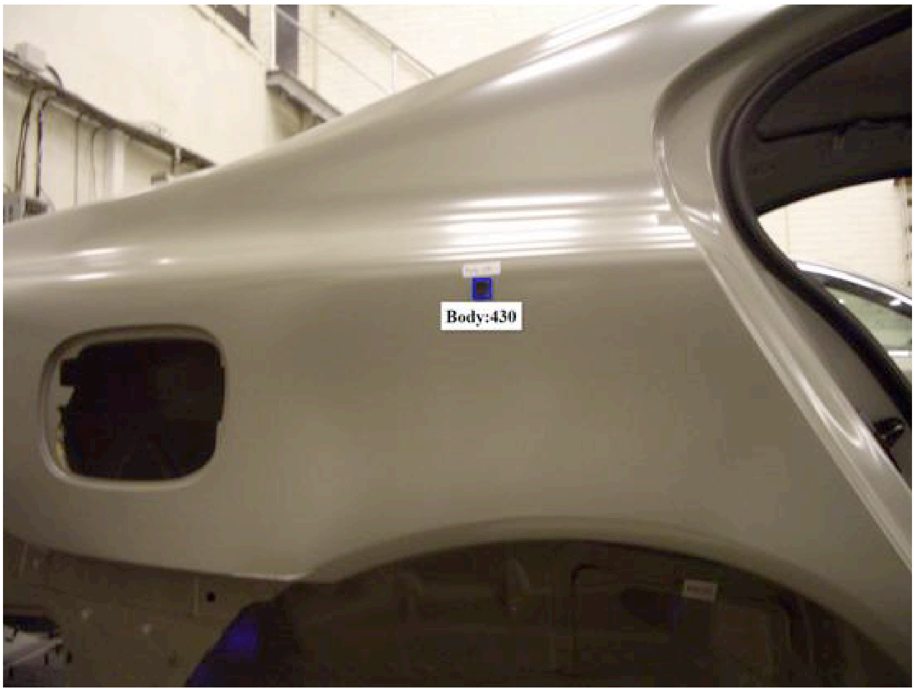

Figure C.13: *Fuel hole point*

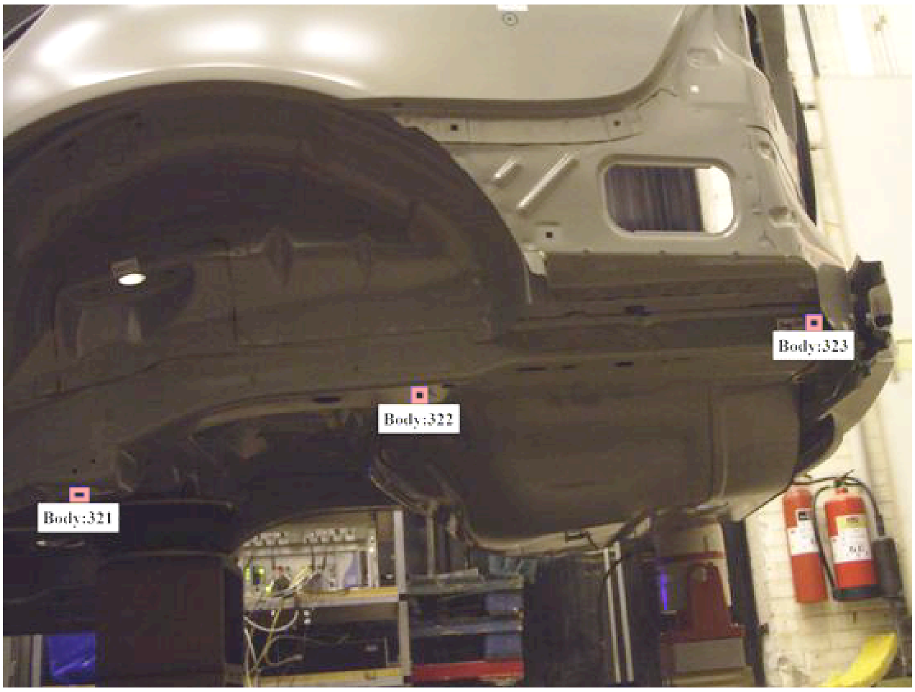

Figure C.14: *Body left back points*

Figure C.15: *Body right back points*

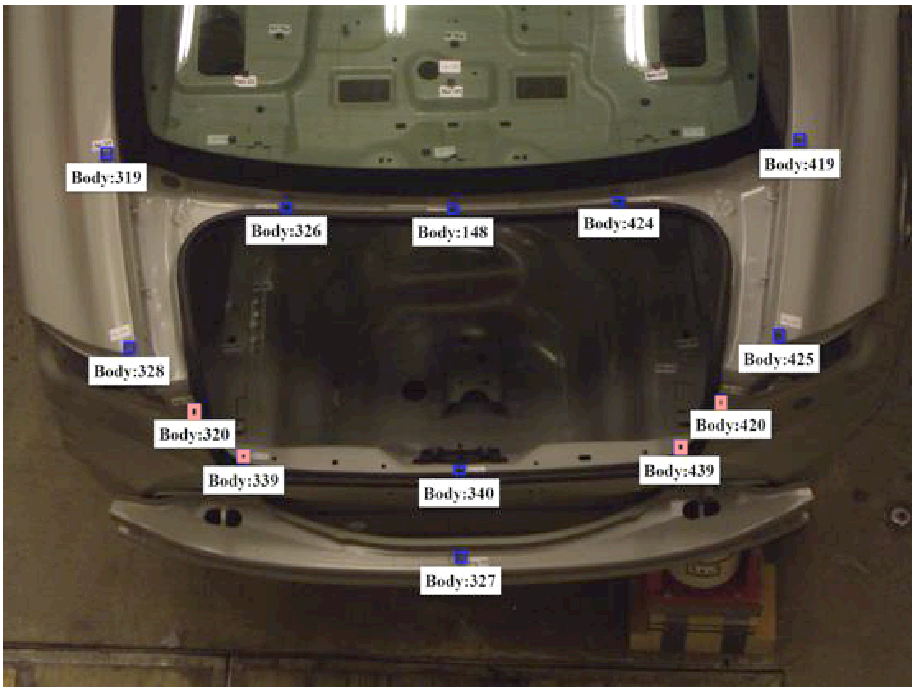

Figure C.16: *Trunk points*

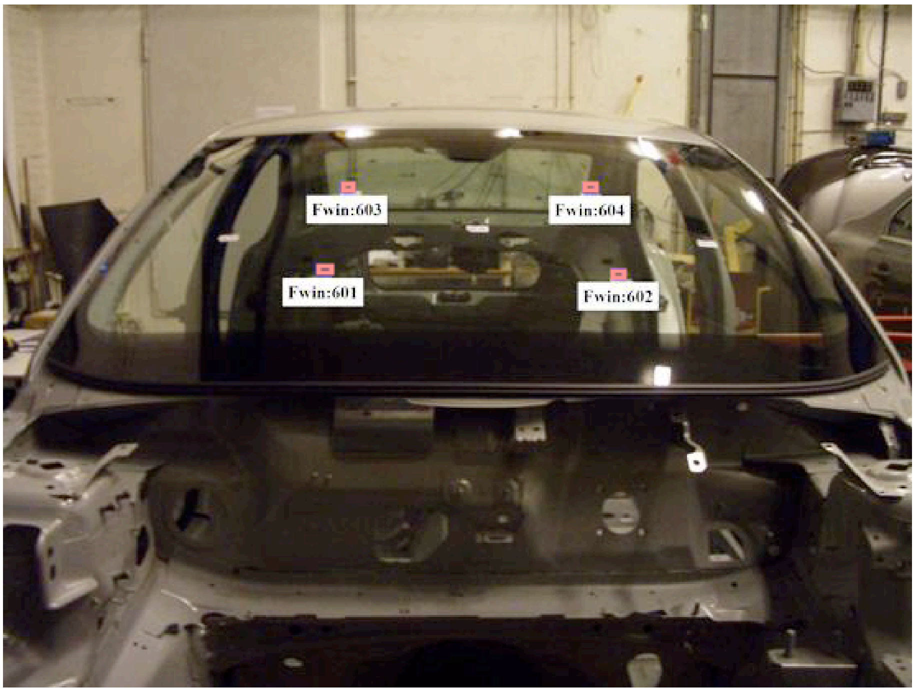

Figure C.17: *Front window points*

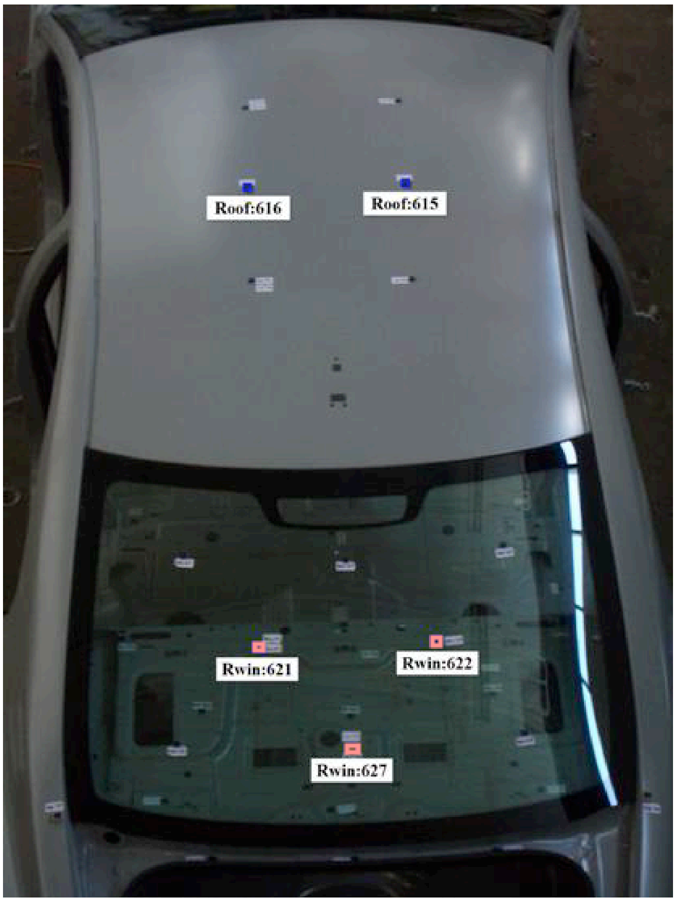

Figure C.18: *Rear window and roof top points*

In table C.1 the coordinates of the response points are shown. Please notice that axis directions are different to the ones used along the thesis. The origin is on the floor, at the body front. x and z-axis are pointing the body, therefore they are always positive. y-axis is positive in the opposite direction to the driver.

Table C.1: Response points coordinates (mm)

Point	X	Y	Z	Point	X	Y	Z
BBAR:511	1045.2	-543.7	418.5	**BODY:141**	1741.8	-616.3	1039.8
BBAR:512	1023.2	0	384.2	**BODY:145**	2772	0	1498
BBAR:513	1045.2	543.1	418.5	**BODY:146**	3445	56	1602
BBAR:514	1030	-226	388	**BODY:147**	4285	17	1520
BBAR:515	1030	226	388	**BODY:148**	5110	0	1196
GORF:501	1109.1	-579.8	910.9	**BODY:150**	3413	-598	1464
GORF:502	842.6	0	901.6	**BODY:151**	3288	-755	654
GORF:503	1109.1	579.8	910.9	**BODY:152**	2848	-692	450
GORF:504	1134.0	-782.3	714.0	**BODY:211**	937.8	522.6	668.1
GORF:505	1134.0	782.3	714.0	**BODY:212**	901.8	160.6	668.3
GORF:521	1170	-452	904.7	**BODY:213**	1321.9	465.0	646.9
GORF:522	1001.8	0	889.7	**BODY:214**	1590.8	465.9	663.9
GORF:523	1170	452	904.7	**BODY:215**	1966.8	440.0	480.3
GORF:524	969.5	-568.6	714	**BODY:216**	1404.4	809.1	865.5
GORF:525	969.5	568.6	714	**BODY:217**	1979.0	812.7	997.6
GORF:526	877.4	-350.7	889.1	**BODY:218**	2075.8	220.8	1112.1
GORF:527	877.4	350.7	889.1	**BODY:219**	2146.4	683.5	1090.5
BODY:111	940.5	-534.6	669.1	**BODY:220**	2598.5	663.1	1309.3
BODY:112	900.7	-169.3	668.3	**BODY:221**	2849.8	589.1	1449.1
BODY:113	1324.6	-473.6	647.5	**BODY:222**	3397.5	520.3	1552.0
BODY:114	1601.4	-473.3	665.2	**BODY:223**	1993.1	442.9	763.7
BODY:115	1969.1	-446.2	482.2	**BODY:224**	2307.0	719.0	868.1
BODY:116	1409.0	-815.7	866.9	**BODY:225**	3334.8	740.3	1054.8
BODY:117	1986.3	-817.8	999.7	**BODY:226**	2366.5	684.8	450.3
BODY:118	2078.1	- 224.1	1113.2	**BODY:227**	2701.5	572.2	466.4
BODY:119	2150.6	-679.9	1091.7	**BODY:228**	2702.7	174.4	466.1
BODY:120	2595.9	-663.1	1312.2	**BODY:229**	3333.0	695.9	500.2
BODY:121	2855.0	-585.6	1454.1	**BODY:230**	3227.1	574.3	383.5
BODY:122	3396.7	-516.8	1557.1	**BODY:231**	3223.7	172.2	390.1
BODY:123	1990.8	-445.4	761.9	**BODY:232**	2816.4	225.3	1499.1
BODY:124	2308.3	-724.2	869.1	**BODY:233**	3440.3	251.0	1588.1
BODY:125	3334.2	-738.9	1058.1	**BODY:241**	1738.8	611.1	1038.1
BODY:126	2369.3	-689.5	453.5	**BODY:250**	3413	598	1464
BODY:127	2703.9	-574.7	469.9	**BODY:251**	3288	755	654
BODY:128	2701.4	-178.4	468.2	**BODY:252**	2848	692	450
BODY:129	3338.4	-698.0	502.9	**BODY:311**	3614.3	-541.3	502.4
BODY:130	3227.3	-579.4	387.9	**BODY:312**	4072.6	-714.1	592.6
BODY:131	3226.1	-173.0	390.3	**BODY:313**	4370.0	-714.2	959.4
BODY:132	2811.2	-228.3	1500.5	**BODY:314**	4187.7	-569.4	1470.9
BODY:133	3442.1	-250.2	1589.5	**BODY:315**	4306.2	-214.0	1519.4
BODY:134	1990.2	-3.2	764.7	**BODY:316**	4506.6	-495.4	1207.8
BODY:135	2375.2	-2.9	545.9	**BODY:317**	4369.7	-301.9	631.8

Point	X	Y	Z	Point	X	Y	Z
BODY:136	2704.5	8.4	549.6	**BODY:417**	4368.4	303.3	628.8
BODY:137	3181.7	3.0	537.3	**BODY:418**	4606.7	616.6	1342.1
BODY:318	4613.6	-611.2	1345.9	**BODY:419**	5002.6	627.5	1254.7
BODY:319	5003.9	-620.3	1257.6	**BODY:420**	5413.5	471.8	1029.0
BODY:320	5414.8	-465.4	1030.6	**BODY:421**	4285.4	478.3	448.9
BODY:321	4272.1	-457.1	451.3	**BODY:422**	4787.1	497.5	562.1
BODY:322	4788.7	-498.2	567.8	**BODY:423**	5370.8	580.1	609.8
BODY:323	5370.0	-570.9	620.5	**BODY:424**	5100.7	298.3	1186.4
BODY:324	3729.8	1.5	602.2	**BODY:425**	5373.5	568.4	1197.9
BODY:325	4490.0	2.9	1206.8	**BODY:430**	4608	856	1075
BODY:326	5100.7	-298.3	1186.4	**BODY:439**	5388	392	796
BODY:327	5534.1	2.3	651.6	**FWIN:601**	2195.0	262.7	1248.2
BODY:328	5373.5	-568.4	1197.9	**FWIN:602**	2196.8	-267.7	1249.6
BODY:339	5388	-392	796	**FWIN:603**	2460.6	223.0	1390.5
BODY:340	5430	0	798	**FWIN:604**	2458.6	-230.4	1390.3
BODY:411	3612.2	544.7	494.3	**RWIN:621**	4691.4	-189.6	1399.0
BODY:412	4069.5	714.0	586.6	**RWIN:622**	4689.6	197.3	1398.7
BODY:413	4375.5	716.5	962.6	**RWIN:627**	4904.7	3.4	1313.2
BODY:414	4189.3	573.8	1466.8	**PSHE:642**	4720.4	8.1	1176.6
BODY:415	4304.5	224.2	1509.1	**ROOF:615**	3488	189	1626
BODY:416	4501.7	499.4	1204.3	**ROOF:616**	3488	-189	1626

Appendix D

Excitation points

The excitation points are shown in figure 4.9. Table D.1 contains their coordinates:

Table D.1: Excitation points coordinates (mm)

Point	X	Y	Z
BODY:001	1283.8	-576.7	551
BODY:003	5336.7	473	566.5

Appendix E

Equipment pictures

Some of the equipment was already shown during the report. An air-mount appears in figure 4.5. In addition two shakers and a charge amplifier can be found in figure 4.9. Other important elements of the equipment are shown below:

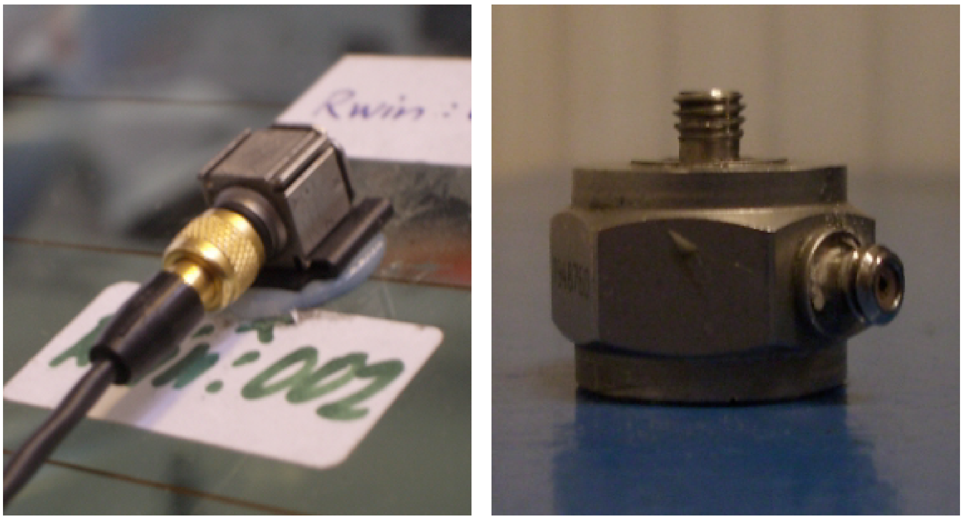

Figure E.1: *Accelerometer on a mounting clip and Force transducer*

Figure E.2: *Power amplifier*

Figure E.3: *Acquisition system and computer station*

Appendix F

Trigger Happy code updated for MIMO testing

```
% ***********************************************************************
% Script for real-time frequency anaysis of time signals acquired
%   with TriggerHappy/VXI
% Patrik Andersson 2005
% ***********************************************************************
%
% ***********************************************************************
% Comments
% ***********************************************************************
%   NB! This algorithm uses a Hanning window on all time data as default.
%   Variable names have changed compared to previous versions (see below).
%   The single sided spectra are only calculated for the components in-
%       significanlty affected by the anti-alias filter.
%
% ***********************************************************************
% Variables from TriggerHappy/XVI
% ***********************************************************************
%   X       - Matrix of time data of the last acquired block. NB!
%               Time data! (# channels x # samples)
%
%   Span    - The upper frequency limit as specified in TriggerHappy. It is
%               the maximum frequency insignificantly affected by the
%               anti-aliasing lowpass filter. The sampling frequency is
%               2.56 times this frequency (i.e. fs=2,56*Span) (scalar)
%
%   C       - Vector of calibration factors as specified in TriggerHappy
%               (1 x # channels)
%
%   N       - Number of blocks acquired since the aquisition started (scalar)
%
% ***********************************************************************
% Variables calculated in this algorithm
% ***********************************************************************
%   Nf       - number of samples in the block = components in the
%               double-sided spectra (scalar)
```

```
%   Na        - number of components in the single sided spectra
%                insignificantly affected by the anti-alias filter (scalar)
%
%   t        - Time vector (1 x # samples)
%
%   f        - Frequency vector for the double-sided spectra (ASxy)
%                (1 x # samples)
%
%   fa       - Frequency vector for the components insignificantly affected
%                by the anti-alias filter. For the single sided-spectra (AGxy)
%                (1 x Na)
%
%   ASxy(:,i,j) - Matrix of the averaged double sided auto- and cross-spectra.
%                ASxy(:,i,i) gives the autospectrum of channel i.
%                ASxy(:,i,j) gives the cross-spectrum between channel i and j.
%                It contains the squared top-amplitudes.
%                (blocksize x # channels x # channels)
%
%   AGxy(:,i,j) - Matrix of the averaged single sided spectra. Same
%                structure as ASxy. It contains the squared rms-amplitudes.
%                (Na x # channels x # channels)
%
%   Hxy(:,i,j) - Matrix of all H1 estimate of the frequency response
%                functions. Hxy(:,i,j) gives the transfer function between
%                channel i and j, i.e. the autospectrum of channel i is in
%                the denominator. (Na x # channels x # channels)
%
%   MIMO_updated
%   multi_gamma2xy(:,j) - Matrix of coherence functions. multi_gamma2xy(:,i,j)
%                gives the multi-coherence function of output j over input i.
%                (Na x # channels x # channels)
%
% ************************************************************************

% ************************************************************************
% Select number of inputs (MIMO_updated)
% ************************************************************************
Ni = 2;    % Number of input channels (situate them in the first channels)
           % DETERMINED BY USER!!

% ************************************************************************
% ************************************************************************
%  Start of algoritm
% ************************************************************************
% ************************************************************************

global ASxy;
if N==1
   clear X1 Sx AGxy Hxy multi_gamma2xy
end

% ************************************************************************
% Initial setup
% ************************************************************************
```

```
Na = size(X,1)/2.56 + 1;  % Compute # of alias protected f components
df = Span/(Na-1);    % Frequncy resolution
[Nf,M]=size(X);     % Nf = # of frequency components
                                % M= # of active channels
t=(1:length(X))/Nf/df;    % Building time axis
f=(0:Nf-1)*df;     % Building frequency axis

% **********************************************************************
% Windowing and calibration
% **********************************************************************
wind=hanning(Nf);    % Hanning window
w_fact=sqrt(sum(wind.^2)/Nf); % Compenstion factor for the energy lost
                                % when applying the window
X1=X.*wind(:,ones(1,M))/w_fact; % Windowing and compensation on the time signal

for m = 1:M
    X1(:,m) = X1(:,m).*C(m);  % Calibration accoriding to the factors
                                % specified in Bullerby
end

% **********************************************************************
% Fourier transform
% **********************************************************************
Sx = fft(X1)/Nf;  % fft has to be divided by block size to get the right
                    % scale for a double sided top-amplitude spectrum


% **********************************************************************
% Autospectra and cross spectra
% **********************************************************************

% Calculating instantainous double-sided auto- and corss-spectra
% **********************************************************************
for i1=1:M
for i2=1:M
  Sxy(:,i1,i2)=conj(Sx(:,i1)).*Sx(:,i2);
end
end

% Averaging double sided auto- and corss-spectra
% **********************************************************************
if N==1
  ASxy = zeros(Na-1,M,M);
  ASxy = Sxy;
else
   ASxy = ASxy - (ASxy - Sxy)/N;
end

% Calculating the corresponding single sided rms spectra and its f vector
% **********************************************************************
AGxy(1,:,:)=ASxy(1,:,:);
AGxy(2:Na,:,:)=2*ASxy(2:Na,:,:);
fa=f(1:Na);
```

```
% Calculating frequency response functions (MIMO_updated)
% ***********************************************************************
for nf = 1:Na
    Hxy_prev = (squeeze(AGxy(nf,1:Ni,Ni+1:M)))'* ...
        ((squeeze(AGxy(nf,1:Ni,1:Ni)))')^-1;
    Hxy(nf,:,:) = ctranspose(Hxy_prev); % Hxy = Hxy(nf,ni,no)
                                        % nf: frequency component
                                        % ni: input index
                                        % no: output index
end

% Calculating multi-coherence functions (MIMO_updated)
% ***********************************************************************
multi_gamma2xy = zeros(Na,M-Ni);
for no=Ni+1:M
    for i1=1:Ni
        for i2=1:Ni
            multi_gamma2xy(:,no-Ni) = multi_gamma2xy(:,no-Ni) + ...
                Hxy(:,i1,no-Ni).*conj(Hxy(:,i2,no-Ni)).*AGxy(1:Na,i2,i1)...
                ./AGxy(1:Na,no,no);
        end
    end
end

% ***********************************************************************
% Presentation (MIMO_updated) (display for 2 inputs signals)
% ***********************************************************************
% setting up the collours used for plotting
collar=['rbgkmcyrbgkmcyrbgkmcy'];

if N==1
close all
figure(1)
h1=gcf;
set(h1,'position',[140 400 400 266]);
figure(2)
h2=gcf;
set(h2,'position',[550 400 400 266])
figure(3)
h3=gcf;
set(h3,'position',[140 59 400 266])
figure(4)
h4=gcf;
set(h4,'position',[550 59 400 266])
end

   for nm=1:M-Ni;

      % single sided autospectra
      figure(1)
      eval(['plot(fa,10*log10(abs(AGxy(1:Na,nm+2,nm+2))),''',collar(nm),''')'])
      hold on
```

```
      % frequency response functions over 1st signal
      figure(2)
      eval(['plot(fa,20*log10(abs(Hxy(:,1,nm))),''',collar(nm),''')'])
      hold on


      % frequency response functions over 2nd signal
      figure(3)
      eval(['plot(fa,20*log10(abs(Hxy(:,2,nm))),''',collar(nm),''')'])
      hold on


      % coherence functions
      figure(4)
      eval(['plot(fa,abs(multi_gamma2xy(:,nm)),''',collar(nm),''')'])
      hold on


   end

      % setting up a legend text for the time signal window
      leg_text=['''ch 3'''];
      for nm=2:M-Ni;
          leg_text=[leg_text,',''ch ',num2str(nm+Ni),'''']
      end

      figure(1)
      hold off
      title('Single sided autospectra')
      eval(['legend(',leg_text,')'])
      drawnow

   figure(2)
   hold off
   title('Frequency response function over 1st input')
   drawnow

   figure(3)
   hold off
   title('Frequency response function over 2nd input')
   drawnow

   figure(4)
   hold off
   title('Multi-coherence function')
   drawnow

% ************************************************************************
%   End of script
% ************************************************************************
```

Appendix G

Data structure

Figure G provides the list of sets followed in the measurements and the correspondence of each point to one of the four available accelerometers. Please notice that each accelerometer has three channels which are actually the space directions, x-y-z. Sometimes the response points location does not allow accelerometers to face global coordinates. Therefore, channels correspondence is defined.

The global coordinate is written as w_r, and the accelerometer one as w_m. These characteristics must be taken into account when looking to the data from sets. For instance, if one wants to check the global y-direction for point Body:124, one would have to check the second accelerometer and out of it the third channel (z_r), and notice that it was taken in opposite direction. After measurements, data from sets was gathered and reorganiced to build up the FRFs and coherence matrices. The matrices components is related to the outputs measured as shown in figure G.

Point	N°Acc	Set	x_r	y_r	z_r	Point	N° Acc	Set	x_r	y_r	z_r	Point	N°Acc	Set	x_r	y_r	z_r
Gorf:501	1	1	GLO	BAL	COO	Body:136	3	11	GLO	BAL	COO	Body:316	4	22	-x_m	-y_m	z_m
Gorf:502	2	1	GLO	BAL	COO	Body:137	4	11	GLO	BAL	COO	Body:317	3	22	GLO	BAL	COO
Gorf:503	3	1	GLO	BAL	COO	Body:141	1	12	GLO	BAL	COO	Body:318	2	22	-x_m	-y_m	z_m
Gorf:504	4	1	GLO	BAL	COO	Body:145	2	12	GLO	BAL	COO	Body:319	1	22	GLO	BAL	COO
Gorf:505	4	2	GLO	BAL	COO	Body:146	3	12	GLO	BAL	COO	Body:320	1	23	y_m	-z_m	-x_m
Gorf:521	1	2	GLO	BAL	COO	Body:147	4	12	GLO	BAL	COO	Body:321	3	23	GLO	BAL	COO
Gorf:522	2	2	GLO	BAL	COO	Body:148	4	13	y_m	-x_m	z_m	Body:322	4	23	GLO	BAL	COO
Gorf:523	3	2	GLO	BAL	COO	Body:150	3	13	GLO	BAL	COO	Body:323	2	23	-x_m	-y_m	z_m
Gorf:524	1	3	GLO	BAL	COO	Body:151	2	13	GLO	BAL	COO	Body:324	3	24	GLO	BAL	COO
Gorf:525	4	3	GLO	BAL	COO	Body:152	1	13	GLO	BAL	COO	Body:325	4	24	-x_m	-y_m	z_m
Gorf:526	2	3	GLO	BAL	COO	Body:211	1	14	-x_m	-y_m	z_m	Body:326	2	24	y_m	-x_m	z_m
Gorf:527	3	3	GLO	BAL	COO	Body:212	2	14	GLO	BAL	COO	Body:327	1	24	GLO	BAL	COO
Bbar:511	1	4	GLO	BAL	COO	Body:213	3	14	GLO	BAL	COO	Body:328	1	25	GLO	BAL	COO
Bbar:512	2	4	GLO	BAL	COO	Body:214	4	14	GLO	BAL	COO	Body:339	1	26	y_m	-x_m	z_m
Bbar:513	4	4	GLO	BAL	COO	Body:215	4	15	GLO	BAL	COO	Body:340	2	25	y_m	-x_m	z_m
Bbar:514	3	4	GLO	BAL	COO	Body:216	2	15	GLO	BAL	COO	Body:411	3	25	y_m	z_m	x_m
Bbar:515	2	5	GLO	BAL	COO	Body:217	3	15	GLO	BAL	COO	Body:412	4	25	-x_m	-y_m	z_m
Body:111	1	5	-x_m	-y_m	z_m	Body:218	1	15	GLO	BAL	COO	Body:413	2	26	-x_m	-y_m	z_m
Body:112	3	5	GLO	BAL	COO	Body:219	1	16	GLO	BAL	COO	Body:414	4	26	-x_m	-y_m	z_m
Body:113	4	5	GLO	BAL	COO	Body:220	2	16	GLO	BAL	COO	Body:415	3	26	-x_m	-y_m	z_m
Body:114	2	6	GLO	BAL	COO	Body:221	3	16	GLO	BAL	COO	Body:416	3	27	-x_m	-y_m	z_m
Body:115	1	6	-x_m	-y_m	z_m	Body:222	4	16	GLO	BAL	COO	Body:417	4	27	GLO	BAL	COO
Body:116	3	6	GLO	BAL	COO	Body:223	1	17	y_m	-z_m	-x_m	Body:418	2	27	-x_m	-y_m	z_m
Body:117	4	6	GLO	BAL	COO	Body:224	2	17	y_m	-z_m	-x_m	Body:419	1	27	GLO	BAL	COO
Body:118	1	7	GLO	BAL	COO	Body:225	3	17	GLO	BAL	COO	Body:420	1	28	y_m	-z_m	-x_m
Body:119	2	7	GLO	BAL	COO	Body:226	4	17	GLO	BAL	COO	Body:421	3	28	GLO	BAL	C.
Body:120	3	7	GLO	BAL	COO	Body:227	1	18	GLO	BAL	COO	Body:422	4	28	GLO	BAL	COO
Body:121	4	7	GLO	BAL	COO	Body:228	2	18	GLO	BAL	COO	Body:423	2	28	-x_m	-y_m	z_m
Body:122	4	8	GLO	BAL	COO	Body:229	3	18	GLO	BAL	COO	Body:424	4	29	y_m	-x_m	z_m
Body:123	1	8	y_m	-z_m	-x_m	Body:230	4	18	GLO	BAL	COO	Body:425	2	29	GLO	BAL	COO
Body:124	2	8	y_m	-z_m	-x_m	Body:231	2	19	GLO	BAL	COO	Body:430	3	29	GLO	BAL	COO
Body:125	3	8	GLO	BAL	COO	Body:232	3	19	GLO	BAL	COO	Body:439	1	29	y_m	x_m	-z_m
Body:126	1	9	GLO	BAL	COO	Body:233	1	19	GLO	BAL	COO	Fwin:601	1	31	GLO	BAL	COO
Body:127	2	9	GLO	BAL	COO	Body:241	4	19	GLO	BAL	COO	Fwin:602	2	31	GLO	BAL	COO
Body:128	3	9	GLO	BAL	COO	Body:250	1	20	GLO	BAL	COO	Fwin:603	3	31	GLO	BAL	COO
Body:129	4	9	GLO	BAL	COO	Body:251	2	20	GLO	BAL	COO	Fwin:604	4	31	GLO	BAL	COO
Body:130	1	10	GLO	BAL	COO	Body:252	3	20	GLO	BAL	COO	Rwin:621	1	30	GLO	BAL	COO
Body:131	2	10	GLO	BAL	COO	Body:311	4	20	y_m	z_m	x_m	Rwin:622	4	30	GLO	BAL	COO
Body:132	3	10	GLO	BAL	COO	Body:312	1	21	-x_m	-y_m	z_m	Rwin:627	2	30	GLO	BAL	COO
Body:133	4	10	GLO	BAL	COO	Body:313	2	21	-x_m	-y_m	z_m	Pshe:642	3	30	-x_m	-y_m	z_m
Body:134	1	11	y_m	-z_m	-x_m	Body:314	3	21	-x_m	-y_m	z_m	Roof:615	1	32	GLO	BAL	COO
Body:135	2	11	GLO	BAL	COO	Body:315	4	21	-x_m	-y_m	z_m	Roof:616	2	32	GLO	BAL	COO

Figure G.1: *Channel set-ups*

Number	Output	Number	Output	Number	Output	Number	Output
1	Gorf:501 +X	43	Bbar:513 +X	85	Body:122 +X	127	Body:136 -X
2	Gorf:501 +Y	44	Bbar:513 +Y	86	Body:122 +Y	128	Body:136 -Y
3	Gorf:501 +Z	45	Bbar:513 +Z	87	Body:122 +Z	129	Body:136 +Z
4	Gorf:502 +X	46	Bbar:514 +X	88	Body:123 +X	130	Body:137 +X
5	Gorf:502 +Y	47	Bbar:514 +Y	89	Body:123 -Y	131	Body:137 +Y
6	Gorf:502 +Z	48	Bbar:514 +Z	90	Body:123 -Z	132	Body:137 +Z
7	Gorf:503 +X	49	Bbar:515 +X	91	Body:124 +X	133	Body:141 +X
8	Gorf:503 +Y	50	Bbar:515 +Y	92	Body:124 -Y	134	Body:141 +Y
9	Gorf:503 +Z	51	Bbar:515 +Z	93	Body:124 -Z	135	Body:141 +Z
10	Gorf:504 +X	52	Body:111 -X	94	Body:125 +X	136	Body:145 +X
11	Gorf:504 +Y	53	Body:111 -Y	95	Body:125 +Y	137	Body:145 +Y
12	Gorf:504 +Z	54	Body:111 +Z	96	Body:125 +Z	138	Body:145 +Z
13	Gorf:505 +X	55	Body:112 +X	97	Body:126 +X	139	Body:146 +X
14	Gorf:505 +Y	56	Body:112 +Y	98	Body:126 +Y	140	Body:146 +Y
15	Gorf:505 +Z	57	Body:112 +Z	99	Body:126 +Z	141	Body:146 +Z
16	Gorf:521 +X	58	Body:113 +X	100	Body:127 +X	142	Body:147 +Z
17	Gorf:521 +Y	59	Body:113 +Y	101	Body:127 +Y	143	Body:147 +Y
18	Gorf:521 +Z	60	Body:113 +Z	102	Body:127 +Z	144	Body:147 +X
19	Gorf:522 +X	61	Body:114 +X	103	Body:128 +X	145	Body:148 +X
20	Gorf:522 +Y	62	Body:114 +Y	104	Body:128 +Y	146	Body:148 -Y
21	Gorf:522 +Z	63	Body:114 +Z	105	Body:128 +Z	147	Body:148 +Z
22	Gorf:523 +X	64	Body:115 +X	106	Body:129 +X	148	Body:150 +X
23	Gorf:523 +Y	65	Body:115 +Y	107	Body:129 +Y	149	Body:150 +Y
24	Gorf:523 +Z	66	Body:115 +Z	108	Body:129 +Z	150	Body:150 +Z
25	Gorf:524 +X	67	Body:116 +X	109	Body:130 +X	151	Body:151 +X
26	Gorf:524 +Y	68	Body:116 +Y	110	Body:130 +Y	152	Body:151 +Y
27	Gorf:524 +Z	69	Body:116 +Z	111	Body:130 +Z	153	Body:151 +Z
28	Gorf:525 +X	70	Body:117 +X	112	Body:131 +X	154	Body:152 +X
29	Gorf:525 +Y	71	Body:117 +Y	113	Body:131 +Y	155	Body:152 +Y
30	Gorf:525 +Z	72	Body:117 +Z	114	Body:131 +Z	156	Body:152 +Z
31	Gorf:526 +X	73	Body:118 +X	115	Body:132 +X	157	Body:211 -X
32	Gorf:526 +Y	74	Body:118 +Y	116	Body:132 +Y	158	Body:211 -Y
33	Gorf:526 +Z	75	Body:118 +Z	117	Body:132 +Z	159	Body:211 +Z
34	Gorf:527 +X	76	Body:119 +X	118	Body:133 +X	160	Body:212 +X
35	Gorf:527 +Y	77	Body:119 +Y	119	Body:133 +Y	161	Body:212 +Y
36	Gorf:527 +Z	78	Body:119 +Z	120	Body:133 +Z	162	Body:212 +Z
37	Bbar:511 +X	79	Body:120 +X	121	Body:134 +X	163	Body:213 +X
38	Bbar:511 +Y	80	Body:120 +Y	122	Body:134 -Y	164	Body:213 +Y
39	Bbar:511 +Z	81	Body:120 +Z	123	Body:134 -Z	165	Body:213 +Z
40	Bbar:512 +X	82	Body:121 +X	124	Body:135 +X	166	Body:214 +X
41	Bbar:512 +Y	83	Body:121 +Y	125	Body:135 +Y	167	Body:214 +Y
42	Bbar:512 +Z	84	Body:121 +Z	126	Body:135 +Z	168	Body:214 +Z

Figure G.2: *Outputs list*

Number	Output	Number	Output	Number	Output	Number	Output
169	Body:215 +X	211	Body:229 +X	253	Body:316 -X	295	Body:340 +X
170	Body:215 +Y	212	Body:229 +Y	254	Body:316 -Y	296	Body:340 -Y
171	Body:215 +Z	213	Body:229 +Z	255	Body:316 +Z	297	Body:340 +Z
172	Body:216 +X	214	Body:230 +X	256	Body:317 +X	298	Body:411 +X
173	Body:216 +Y	215	Body:230 +Y	257	Body:317 +Y	299	Body:411 +Y
174	Body:216 +Z	216	Body:230 +Z	258	Body:317 +Z	300	Body:411 +Z
175	Body:217 +X	217	Body:231 +X	259	Body:318 -X	301	Body:412 -X
176	Body:217 +Y	218	Body:231 +Y	260	Body:318 -Y	302	Body:412 -Y
177	Body:217 +Z	219	Body:231 +Z	261	Body:318 +Z	303	Body:412 +Z
178	Body:218 +X	220	Body:232 +X	262	Body:319 +X	304	Body:413 -X
179	Body:218 +Y	221	Body:232 +Y	263	Body:319 +Y	305	Body:413 -Y
180	Body:218 +Z	222	Body:232 +Z	264	Body:319 +Z	306	Body:413 +Z
181	Body:219 +X	223	Body:233 +X	265	Body:320 +X	307	Body:414 -X
182	Body:219 +Y	224	Body:233 +Y	266	Body:320 -Y	308	Body:414 -Y
183	Body:219 +Z	225	Body:233 +Z	267	Body:320 -Z	309	Body:414 +Z
184	Body:220 +X	226	Body:241 +X	268	Body:321 +X	310	Body:415 -X
185	Body:220 +Y	227	Body:241 +Y	269	Body:321 +Y	311	Body:415 -Y
186	Body:220 +Z	228	Body:241 +Z	270	Body:321 +Z	312	Body:415 +Z
187	Body:221 +X	229	Body:250 +X	271	Body:322 +X	313	Body:416 -X
188	Body:221 +Y	230	Body:250 +Y	272	Body:322 +Y	314	Body:416 -Y
189	Body:221 +Z	231	Body:250 +Z	273	Body:322 +Z	315	Body:416 +Z
190	Body:222 +X	232	Body:251 +X	274	Body:323 -X	316	Body:417 +X
191	Body:222 +Y	233	Body:251 +Y	275	Body:323 -Y	317	Body:417 +Y
192	Body:222 +Z	234	Body:251 +Z	276	Body:323 +Z	318	Body:417 +Z
193	Body:223 +X	235	Body:252 +X	277	Body:324 +X	319	Body:418 -X
194	Body:223 -Y	236	Body:252 +Y	278	Body:324 +Y	320	Body:418 -Y
195	Body:223 -Z	237	Body:252 +Z	279	Body:324 +Z	321	Body:418 +Z
196	Body:224 +X	238	Body:311 +X	280	Body:325 -X	322	Body:419 +X
197	Body:224 -Y	239	Body:311 +Y	281	Body:325 -Y	323	Body:419 +Y
198	Body:224 -Z	240	Body:311 +Z	282	Body:325 +Z	324	Body:419 +Z
199	Body:225 +X	241	Body:312 -X	283	Body:326 +X	325	Body:420 +X
200	Body:225 +Y	242	Body:312 -Y	284	Body:326 -Y	326	Body:420 -Y
201	Body:225 +Z	243	Body:312 +Z	285	Body:326 +Z	327	Body:420 -Z
202	Body:226 +X	244	Body:313 -X	286	Body:327 +X	328	Body:421 +X
203	Body:226 +Y	245	Body:313 -Y	287	Body:327 +Y	329	Body:421 +Y
204	Body:226 +Z	246	Body:313 +Z	288	Body:327 +Z	330	Body:421 +Z
205	Body:227 +X	247	Body:314 -X	289	Body:328 +X	331	Body:422 +X
206	Body:227 +Y	248	Body:314 -Y	290	Body:328 +Y	332	Body:422 +Y
207	Body:227 +Z	249	Body:314 +Z	291	Body:328 +Z	333	Body:422 +Z
208	Body:228 +X	250	Body:315 -X	292	Body:339 +X	334	Body:423 -X
209	Body:228 +Y	251	Body:315 -Y	293	Body:339 -Y	335	Body:423 -Y
210	Body:228 +Z	252	Body:315 +Z	294	Body:339 +Z	336	Body:423 +Z

Number	Output
337	Body:424 +X
338	Body:424 -Y
339	Body:424 +Z
340	Body:425 +X
341	Body:425 +Y
342	Body:425 +Z
343	Body:430 +X
344	Body:430 +Y
345	Body:430 +Z
346	Body:439 +X
347	Body:439 +Y
348	Body:439 -Z
349	Fwin:601 +X
350	Fwin:601 +Y
351	Fwin:601 +Z
352	Fwin:602 +X
353	Fwin:602 +Y
354	Fwin:602 +Z
355	Fwin:603 +X
356	Fwin:603 +Y
357	Fwin:603 +Z
358	Fwin:604 +X
359	Fwin:604 +Y
360	Fwin:604 +Z
361	Rwin:621 +X
362	Rwin:621 +Y
363	Rwin:621 +Z
364	Rwin:622 +X
365	Rwin:622 +Y
366	Rwin:622 +Z
367	Rwin:627 +X
368	Rwin:627 +Y
369	Rwin:627 +Z
370	Pshe:642 -X
371	Pshe:642 -Y
372	Pshe:642 +Z
373	Roof:615 +X
374	Roof:615 +Y
375	Roof:615 +Z
376	Roof:616 +X
377	Roof:616 +Y
378	Roof:616 +Z

Appendix H

Stabilization diagrams for frequency limit study

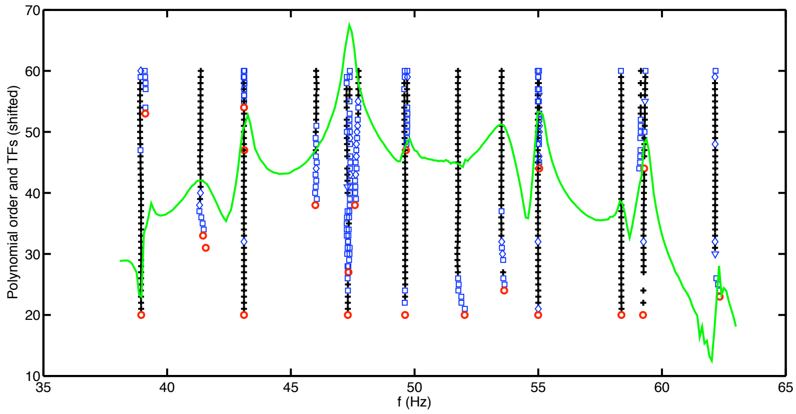

Figure H.1: *Stabilization diagram* for BIG3 without brackets at “middle“frequencies

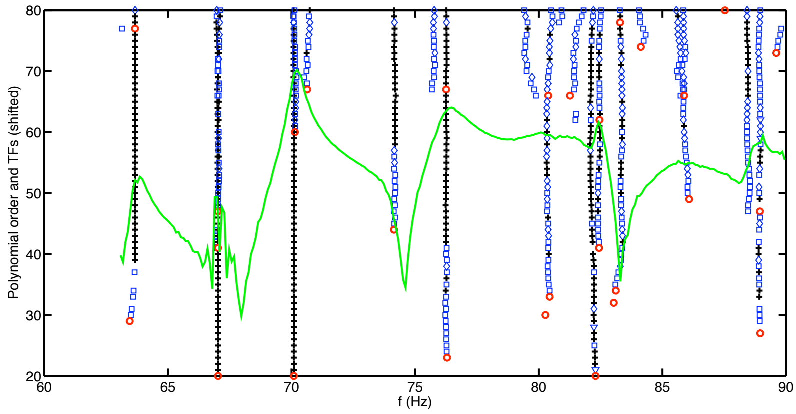

Figure H.2: *Stabilization diagram* for BIG3 without brackets at high frequencies

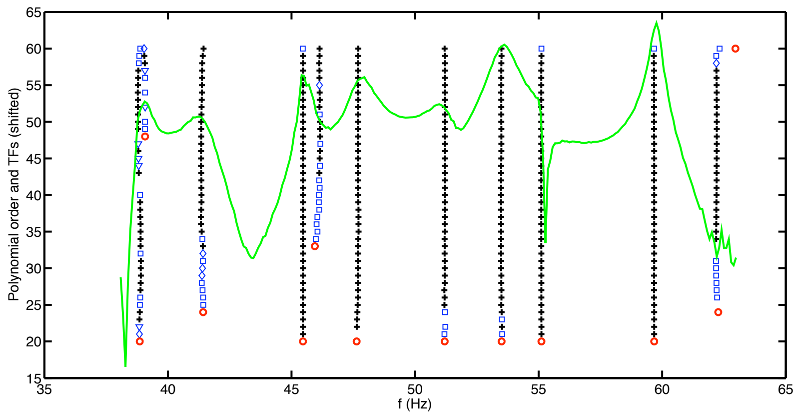

Figure H.3: *Stabilization diagram* for BIG3 without GOR at "middle"frequencies

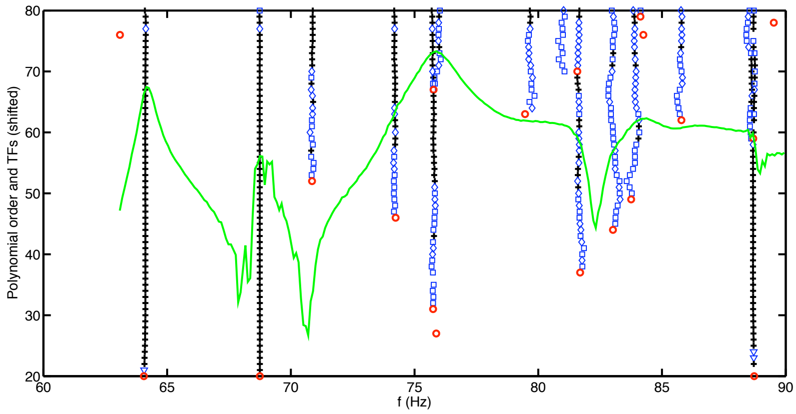

Figure H.4: *Stabilization diagram* for BIG3 without GOR at high frequencies

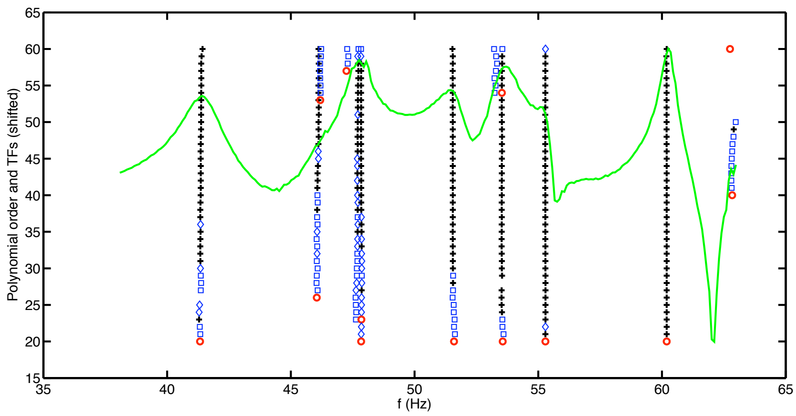

Figure H.5: *Stabilization diagram* for BIG3 without GOR and RB at "middle"frequencies

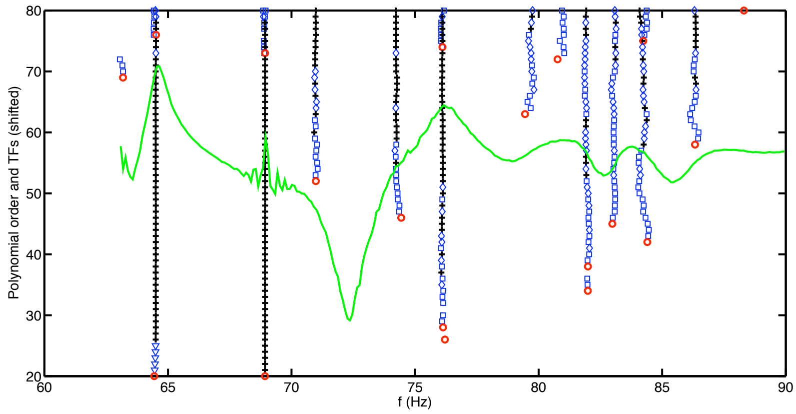

Figure H.6: *Stabilization diagram* for BIG3 without GOR and RB at high frequencies

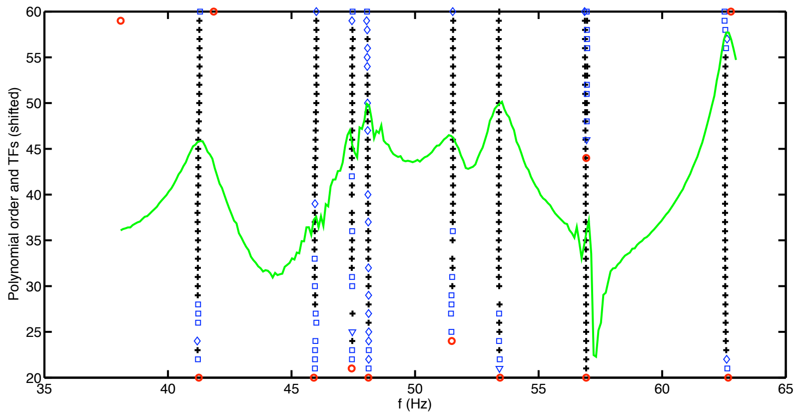

Figure H.7: *Stabilization diagram* for BIG3 without GOR, RB and TB at “middle“frequencies

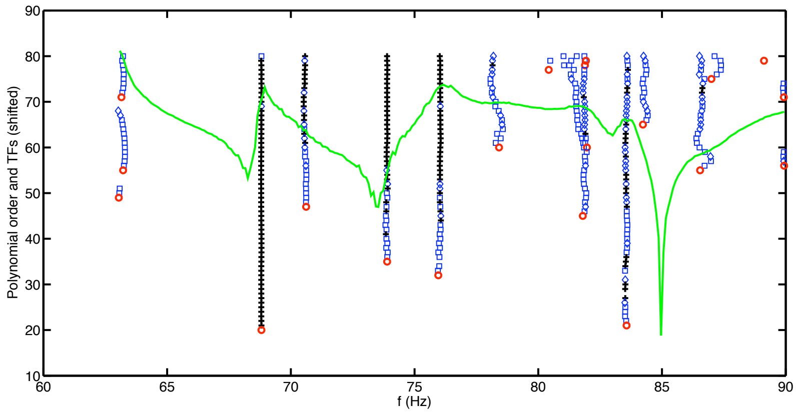

Figure H.8: *Stabilization diagram* for BIG3 without GOR, RB and TB at high frequencies

Appendix I

MAC values used to build up modes evolution

Index		1	2	3	4	5	6	7	8	9	10	11	12	13
	MAC	41.34	46.08	47.69	47.84	51.55	53.53	55.29	60.19	64.51	68.92	70.96	74.26	76.11
1	41.21	93.8	4.4	6.5	1.6	0.3	0.9	0.0	0.6	0.1	0.5	1.5	3.0	2.0
2	45.95	1.7	79.7	8.7	3.8	1.3	3.7	1.9	1.1	4.4	0.4	0.1	3.9	1.2
3	47.44	6.2	7.0	72.4	5.0	2.1	6.9	1.0	3.8	1.8	0.1	0.9	0.3	1.0
4	48.12	2.6	0.4	31.6	53.1	0.4	5.8	2.0	1.0	0.1	0.5	0.1	0.2	0.9
5	51.53	1.2	0.9	8.0	1.2	71.4	13.3	3.4	2.6	0.2	4.8	0.2	0.1	0.5
6	53.39	1.2	0.5	8.7	2.4	3.5	91.2	51.5	7.2	1.0	0.2	0.1	1.5	0.4
7	56.92	1.1	1.0	0.7	0.4	0.0	4.8	35.9	51.6	13.5	0.0	0.0	0.7	0.4
8	62.56	0.1	2.2	4.4	0.7	0.2	5.0	0.7	22.7	37.8	0.0	0.6	2.1	1.0
9	68.81	0.3	0.3	0.1	0.9	4.7	0.2	0.0	0.7	0.5	88.5	21.1	1.6	0.2
10	70.54	0.6	0.3	1.3	0.3	0.2	0.1	0.0	2.0	4.8	9.1	91.5	3.0	0.5
11	73.90	3.6	3.0	0.1	0.0	0.1	0.7	2.4	0.9	2.3	4.4	19.8	87.5	7.4
12	76.05	1.1	1.5	1.1	0.4	0.4	0.1	0.7	0.6	0.0	0.2	0.6	7.3	88.3

Figure I.1: *MAC matrix* for BIG3. Configurations: GOR&RB&TB off (rows) and GOR&RB off (columns)

Index		1	2	3	4	5	6	7	8	9	10	11	12	13	14	15
	MAC	38.86	41.33	45.47	46.13	47.69	51.19	53.49	55.11	59.68	62.19	64.12	68.75	70.82	74.21	75.81
1	41.34	8.1	53.9	0.0	1.3	0.7	0.3	0.0	0.4	0.1	1.2	0.2	0.7	0.2	0.9	0.2
2	46.08	0.3	1.7	0.8	63.7	1.1	0.9	2.6	0.7	1.4	0.1	4.6	0.2	0.3	2.1	0.3
3	47.69	8.3	0.7	2.1	0.8	58.8	0.6	5.9	1.3	4.3	0.4	4.6	0.4	0.3	2.0	0.0
4	47.84	9.8	0.4	30.9	1.1	14.1	0.3	1.9	1.0	0.5	0.1	0.6	0.4	0.1	0.6	0.0
5	51.55	2.7	0.4	2.5	0.9	0.6	57.6	2.5	0.8	0.1	3.7	0.0	4.2	0.8	0.0	0.7
6	53.53	14.0	0.0	0.0	2.3	8.6	3.2	84.4	45.5	5.8	0.3	3.2	0.3	0.3	0.7	1.0
7	55.29	19.0	0.3	0.4	1.2	2.1	1.1	57.6	76.3	6.3	0.1	1.5	0.0	0.1	3.0	0.9
8	60.19	2.2	0.2	0.6	0.5	3.3	0.2	1.9	17.2	72.3	0.8	0.1	0.4	2.0	1.5	0.2
9	64.51	7.9	0.1	0.8	3.5	5.0	0.0	2.2	0.0	1.8	3.2	65.5	0.1	0.6	1.1	0.0
10	68.92	4.1	1.1	0.5	0.2	0.2	3.4	0.4	0.0	0.5	0.6	0.1	76.3	12.1	3.0	0.9
11	70.96	3.6	0.2	0.3	0.5	0.2	0.8	0.3	0.1	1.6	0.0	1.5	13.6	89.9	7.7	0.5
12	74.26	2.5	1.0	0.0	1.8	2.4	0.0	1.0	3.6	1.1	0.4	0.9	2.6	6.2	89.7	9.2
13	76.11	1.5	0.1	0.2	0.0	0.0	1.4	1.2	1.2	0.2	1.5	0.0	0.1	0.0	5.5	68.2

Figure I.2: *MAC matrix* for BIG3. Configurations: GOR&RB off (rows) and GOR off (columns)

Index		1	2	3	4	5	6	7	8	9	10	11	12	13	14	15	16	17	18	19
	MAC	38.94	41.35	43.45	46.05	47.67	47.91	48.52	51.36	53.33	54.39	58.02	62.03	63.58	64.68	64.94	68.38	70.69	74.06	74.74
1	38.86	96.1	1.4	0.0	0.1	1.0	9.4	8.0	0.2	1.0	9.2	2.3	0.0	0.1	0.4	0.4	0.1	0.1	0.0	0.1
2	41.33	1.9	44.9	0.2	1.3	2.1	0.9	0.4	0.7	0.0	0.0	0.1	0.3	0.3	0.2	0.3	1.5	4.2	4.0	0.9
3	45.47	0.0	0.1	94.1	1.6	0.6	1.5	18.0	0.4	0.0	0.2	0.2	2.1	0.1	0.7	0.8	0.2	0.2	0.0	0.1
4	46.13	0.1	1.2	4.6	60.3	0.7	5.5	1.0	0.1	1.6	0.1	1.7	0.2	5.1	0.9	2.9	0.1	2.9	0.7	0.2
5	47.69	0.0	1.3	0.4	2.4	60.5	19.7	6.0	0.6	4.8	6.3	6.8	0.3	1.9	0.0	0.2	0.0	0.3	3.6	0.5
6	51.19	0.0	0.6	1.6	0.6	0.2	2.9	15.6	76.0	1.3	0.0	0.1	1.2	0.2	3.6	3.1	3.7	1.7	0.0	3.4
7	53.49	0.5	0.1	0.1	2.5	5.7	19.7	10.0	0.1	91.0	0.9	24.7	0.3	1.5	0.5	0.1	0.2	0.4	0.7	0.0
8	55.11	7.0	0.1	0.0	1.0	9.7	52.4	38.1	0.5	61.4	49.5	1.7	0.1	1.0	0.0	0.8	0.1	0.3	1.6	0.1
9	59.68	3.9	0.3	0.1	0.6	9.6	24.6	21.8	0.2	0.3	76.1	71.8	0.1	0.3	0.3	1.1	0.0	0.3	0.1	0.0
10	62.19	0.0	0.3	2.8	0.5	0.2	0.0	0.1	2.0	0.1	1.0	0.2	86.3	0.3	19.1	13.2	0.7	0.0	0.6	0.4
11	64.12	0.4	0.1	0.0	5.7	5.1	7.2	6.1	0.1	0.5	7.2	9.5	0.6	67.0	2.6	8.2	0.0	0.4	1.3	0.5
12	68.75	0.0	1.6	0.0	0.4	0.2	0.5	0.6	5.6	0.1	0.0	0.0	0.1	1.5	50.1	46.2	75.3	15.5	0.6	1.5
13	70.82	0.1	4.6	0.1	3.2	0.0	2.0	1.8	1.2	0.9	0.6	0.2	0.1	1.6	1.0	2.2	6.3	44.3	0.0	0.0
14	74.21	0.0	4.2	0.0	0.6	3.5	1.7	0.7	0.1	0.5	0.4	0.1	0.8	0.8	0.2	0.2	1.7	3.4	69.2	15.7
15	75.81	0.0	0.5	0.0	0.0	0.0	0.6	0.8	2.6	0.6	0.3	0.1	2.2	0.6	0.1	0.2	0.0	0.0	3.5	68.2

Figure I.3: *MAC matrix* for BIG3. Configurations: GOR off (rows) and standard (columns)